Turbulent flows of superfluid helium-4: an experimentalist view

Marco LA MANTIA

Department of Low Temperature Physics
Faculty of Mathematics and Physics
Charles University, Prague, Czech Republic

superfluid.cz

Support from the Czech Science Foundation is acknowledged

Liquid helium

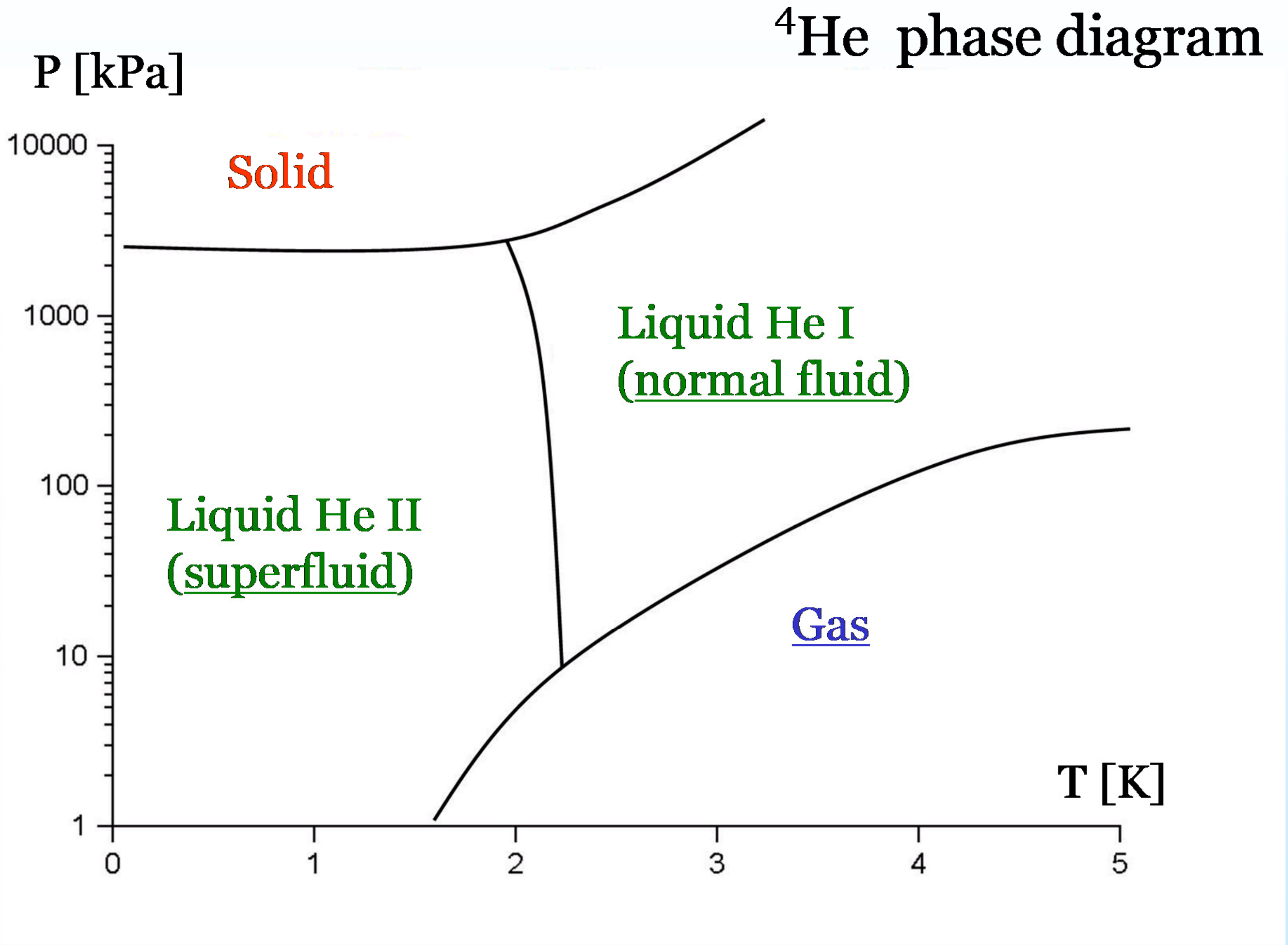

Helium II

He II is often described by using the two-fluid model

- Normal fluid: viscous, carries entropy
- Superfluid: inviscid, does not carry entropy

$$\rho = \rho_n + \rho_s$$

ρ_n / ρ and ρ_s / ρ depend on temperature (more than ρ)

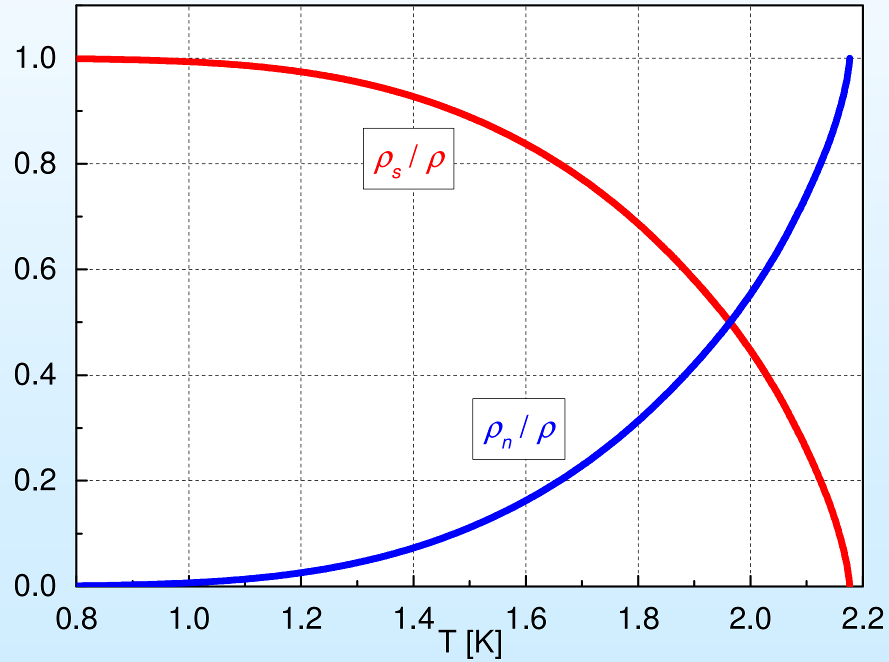

RJ Donnelly, CF Barenghi **J Phys Chem Ref Data** 27, 1217 (1998)
RJ Donnelly **Phys Today** 62, 10, 34 (2009)
MS Mongiovì, D Jou, M Sciacca **Phys Rep** 726, 1 (2018)

Helium II

Kinematic viscosity
$\nu = \mu_n/\rho$

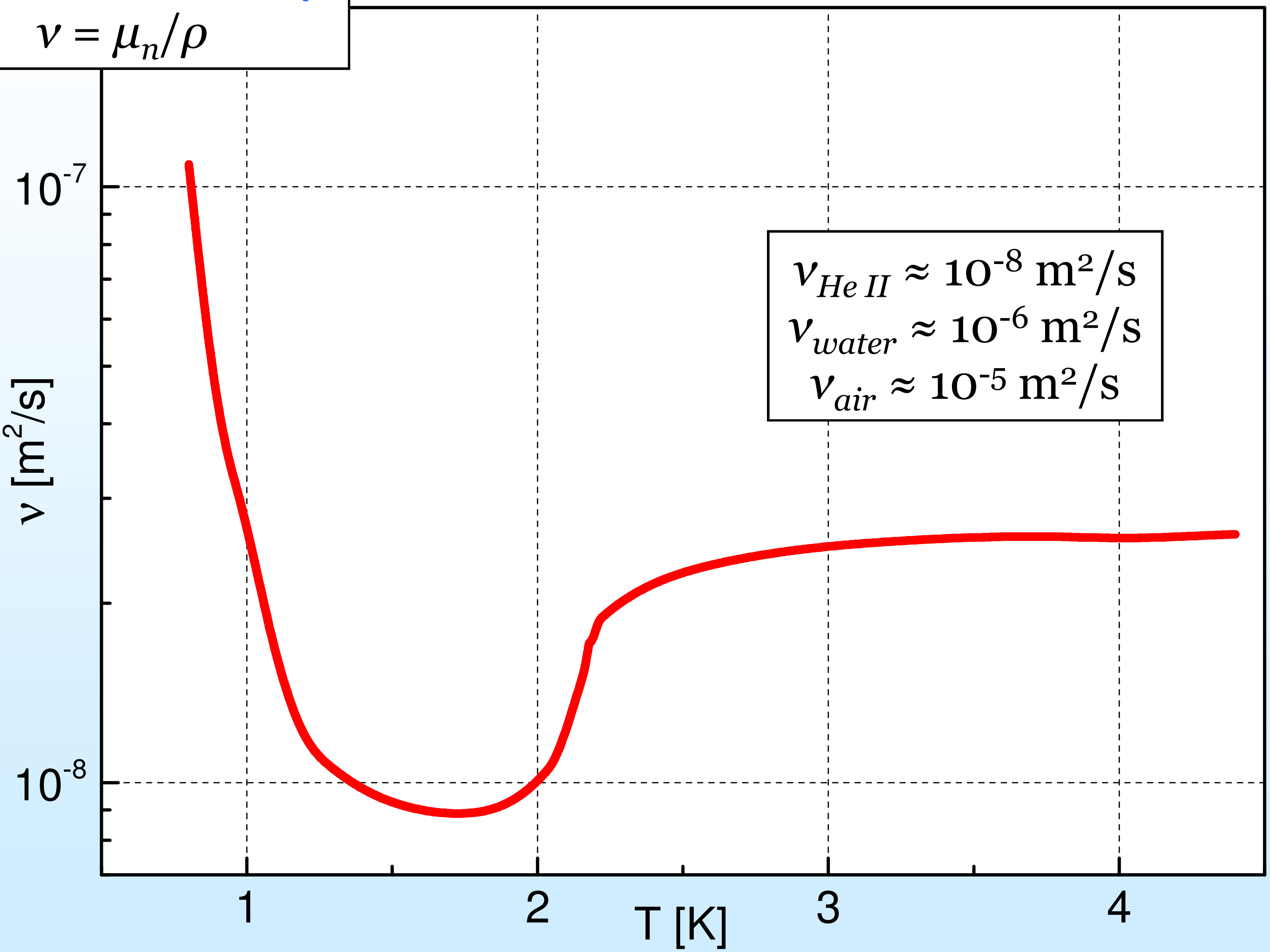

$\nu_{He\ II} \approx 10^{-8}\ \mathrm{m^2/s}$
$\nu_{water} \approx 10^{-6}\ \mathrm{m^2/s}$
$\nu_{air} \approx 10^{-5}\ \mathrm{m^2/s}$

RJ Donnelly, CF Barenghi **J Phys Chem Ref Data** 27, 1217 (1998)

Helium II

The second sound can be seen as a temperature (entropy) wave, while the first (ordinary) sound is due to density (pressure) fluctuations

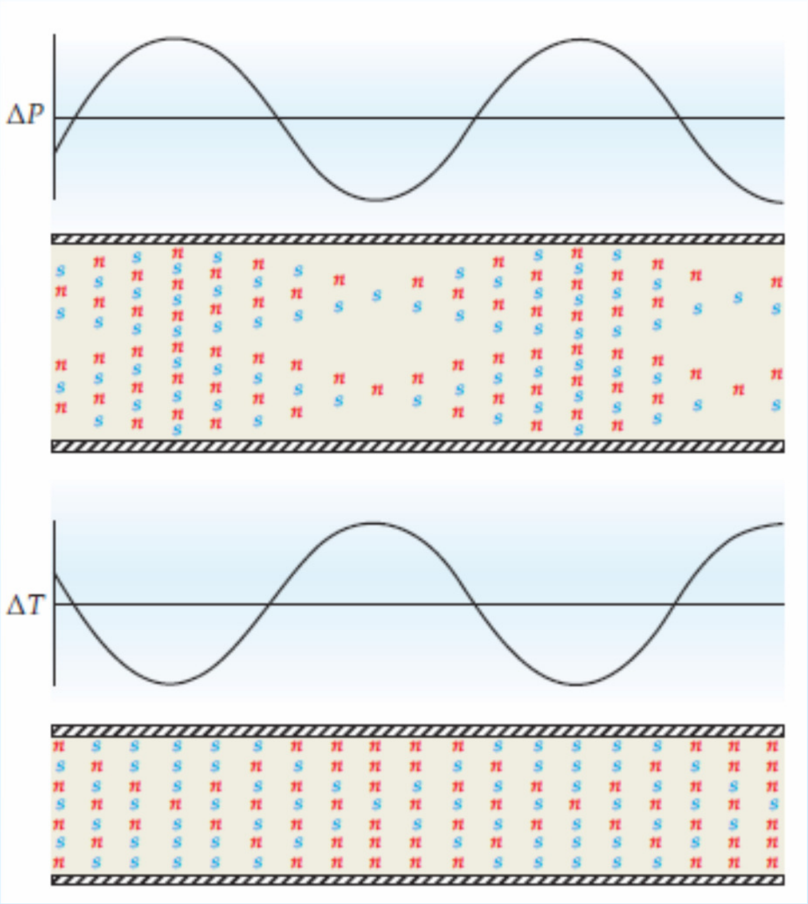

Symbols *n* and *s* on any vertical line represent the relative portion of normal and superfluid components (the number of symbols on each vertical line denotes the total fluid density)

Second sound can be seen as a spatial variation of the component relative densities, while the fluid density and pressure do not change, to a first approximation

RJ Donnelly **Phys Today** 62, 10, 34 (2009)

Helium II

The second sound can be seen as a temperature (entropy) wave, while the first (ordinary) sound is due to density (pressure) fluctuations

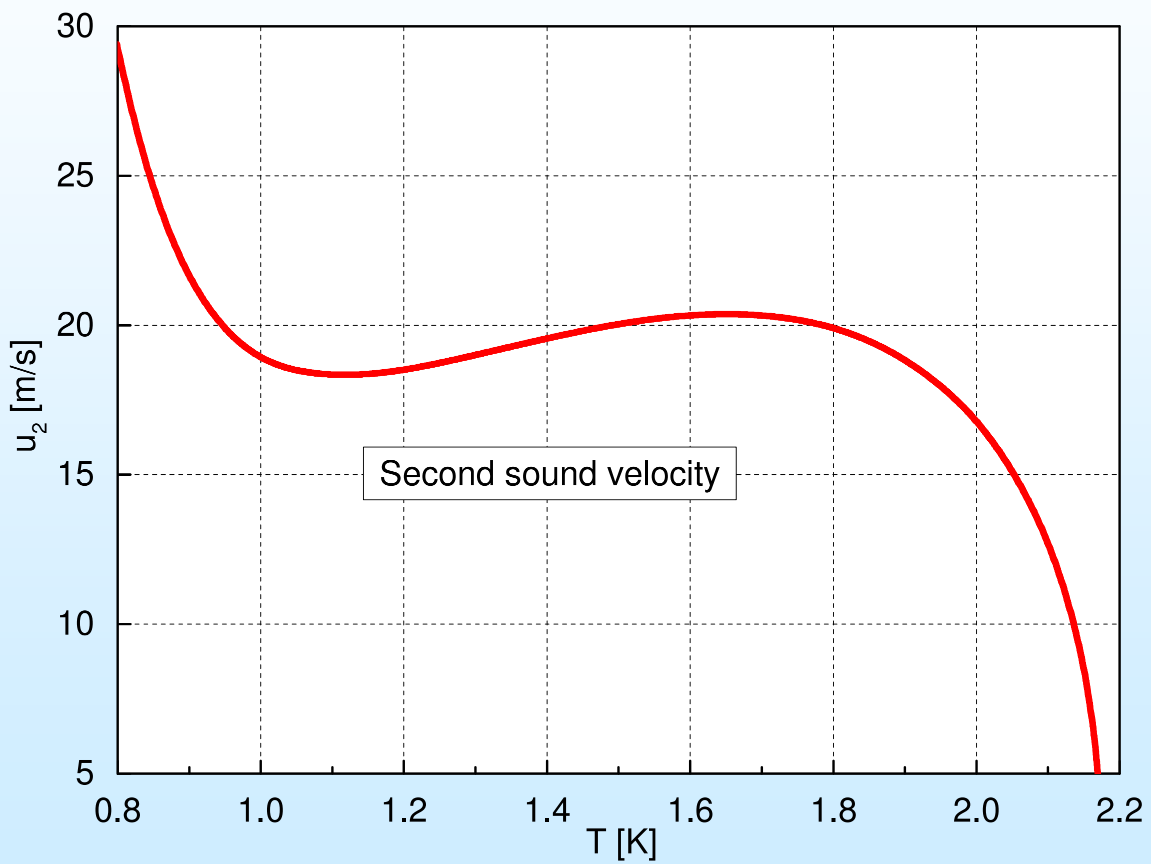

RJ Donnelly, CF Barenghi **J Phys Chem Ref Data** 27, 1217 (1998)
RJ Donnelly **Phys Today** 62, 10, 34 (2009)

Helium II

The superfluid component of He II can be described as a quantum fluid, by using a macroscopic wave function

$$\Psi = \Psi_0 \, e^{iS} = \sqrt{\left(\rho_s / m_4\right)} \, e^{iS} \qquad v_s = \frac{\hbar}{m_4} \nabla S \qquad \omega = curl\left(v_s\right) = 0$$

Multiply connected fluid region, circulation $\Gamma \neq 0$

$$\Gamma = \oint v_s dl = \frac{\hbar}{m_4} \oint \nabla S \, dl = n \, \kappa$$

quantum of circulation

$\kappa = h / m_4 \approx 10^{-7}$ m²/s

quantized vortex core $\approx 10^{-10}$ m

Quantum turbulence: tangle of quantized vortices interacting with the fluid flow

Quantum fluids

- Liquid helium
  ^{4}He (boson)
  ^{3}He (fermion)
- Bose-Einstein condensates

March 25, 2014 | vol. 111 | suppl. 1

PNAS

Proceedings of the National Academy of Sciences of the United States of America www.pnas.org

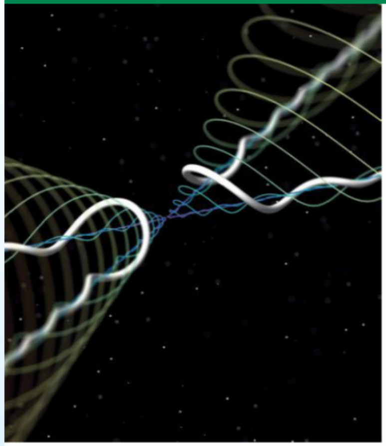

Cover image: Pictured are Kelvin waves following quantized vortex reconnection. Quantum fluids such as superfluid helium show vortical motion through topological defects known as quantized vortices. These line-like quantum objects cross, exchange tails, and separate, exciting helical waves that propagate along their retracting lengths. This phenomenon has been recently observed using frozen tracers in superfluid helium. See the article by Fonda et al., a part of the Quantum Turbulence Special Feature, on pages 4707–4710. Image courtesy of Enrico Fonda.

Quantum Turbulence Special Feature

Contents

Superfluidity and quantized vorticity: *macroscopic manifestations of quantum mechanics*

Quantum flows

may also be relevant for
neutron stars and cosmology

VOLUME 28, NUMBER 16 PHYSICAL REVIEW LETTERS 17 APRIL 1972

Pulsar Speedups Related to Metastability of the Superfluid Neutron-Star Core

Richard E. Packard
Physics Department, University of California, Berkeley, California 94720
(Received 13 March 1972)

The sudden speed changes observed in the Vela and Crab pulsars may be caused by transitions between metastable flow states in the superfluid interior of the star.

A mathematical description of glitches in neutron stars

Maria Stella Mongiovì,[1★] Francesco G. Russo[2★] and Michele Sciacca[3,4★]
[1]*Dipartimento di Innovazione Industriale e Digitale, Università degli Studi di Palermo, Viale Delle Scienze, Edificio 8, I-90128 Palermo, Italy*
[2]*Department of Mathematics and Applied Mathematics, University of Cape Town, Private Bag X1, 7701, Rondebosch, Cape Town, South Africa*
[3]*Dipartimento di Scienze Agrarie e Forestali, Università degli Studi di Palermo, Viale Delle Scienze, Edificio 4, I-90128 Palermo, Italy*
[4]*Istituto Nazionale di Alta Matematica, Piazzale Aldo Moro, I-00185 Roma, Italy*

Monthly Notices of the ROYAL ASTRONOMICAL SOCIETY
MNRAS **469**, 2141–2150 (2017)

Accepted 2017 March 31. Received 2017 March 24; in original form 2016 June 30

ABSTRACT
In a pulsar, there are gaps and difficulties in our knowledge of glitches, mainly because of the absence of information about the physics of the matter of the star. This has motivated several authors to suggest dynamical models that interpret most of the astronomical data. Many predictions are based on the assumption that the inner part is analogous to the structure of matter of superfluids. Here, we illustrate a new mathematical model, partially inspired by the dynamics of superfluid helium. We obtain two evolution equations for the angular velocities (of the crust and of superfluid), which are supported by another evolution equation for the average vortex line length per unit volume. This third equation is more delicate from an analytical perspective and is probably at the origin of glitches. We identify two stationary solutions, corresponding to the straight vortex regime and the turbulent regime.

Key words: turbulence – pulsars: general – stars: neutron – stars: rotation.

26 JULY 2013 VOL 341 **SCIENCE**

Holographic Vortex Liquids and Superfluid Turbulence

Paul M. Chesler,* Hong Liu,* Allan Adams*

Superfluid turbulence is a fascinating phenomenon for which a satisfactory theoretical framework is lacking. Holographic duality provides a systematic approach to studying such quantum turbulence by mapping the dynamics of a strongly interacting quantum liquid into the dynamics of classical gravity. We use this gravitational description to numerically construct turbulent flows in a holographic superfluid in two spatial dimensions. We find that the superfluid kinetic energy spectrum obeys the Kolmogorov $-5/3$ scaling law, with energy injected at long wavelengths undergoing a direct cascade to short wavelengths where dissipation by vortex annihilation and vortex drag becomes efficient. This dissipation has a simple gravitational interpretation as energy flux across a black hole event horizon.

NATURE · VOL 368 · 24 MARCH 1994

Generation of defects in superfluid ^{4}He as an analogue of the formation of cosmic strings

P. C. Hendry*, N. S. Lawson*, R. A. M. Lee*, P. V. E. McClintock* & C. D. H. Williams†

* School of Physics and Materials, Lancaster University, Lancaster LA1 4YB, UK
† Department of Physics, University of Exeter, Exeter EX4 4QL, UK

ALTHOUGH the birth of the Universe is inaccessible to experimental study, aspects of cosmological theories can nonetheless be explored in the laboratory. Tiny inhomogeneities in the mix of particles and radiation produced in the Big Bang grew into the clusters of galaxies that we see today, but how those inhomogeneities arose and grew is still unclear. Cosmologies based on grand unified theories suggest that a symmetry-breaking phase transition occurred via the Higgs mechanism about 10^{-34} s after the Big Bang as the Universe cooled through a critical temperature of 10^{27} K. It has been proposed by Kibble[1] that this transition may have generated defects in the geometry of space-time (such as cosmic strings), which provided the inhomogeneities on which galaxies subsequently condensed. Zurek[2–4] has suggested that it might be possible to model this cosmological phase transition by a laboratory analogue, the superfluid transition of liquid ^{4}He induced by fast adiabatic expansion through the critical density. Here we report the results of such an experiment. We observe copious production of quantized vortices[5], the superfluid analogue of cosmic strings. These results support Kibble's contention that such defects were available in the early Universe to seed galaxy formation.

Helium II flows

$$j = \rho_n v_n + \rho_s v_s$$

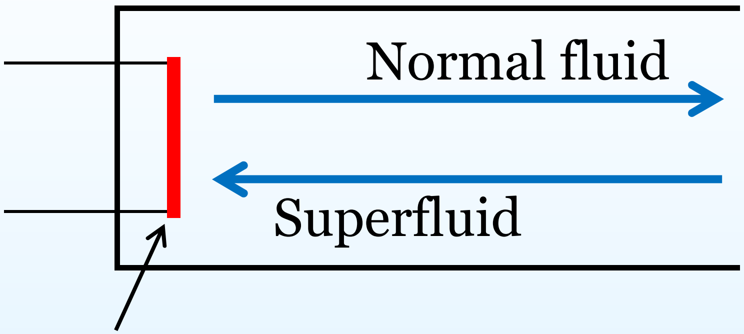

thermally driven flow
(e.g. heater)

Counterflow: $j = 0$

$$\rho_n v_n = -\rho_s v_s$$

(on average, at large scales)

Counterflow velocity v_{ns}

$$v_{ns} = v_n - v_s = \frac{q}{\rho S T}\left(1 + \frac{\rho_n}{\rho_s}\right) = \frac{q}{\rho_s S T}$$

mechanically driven flow
(e.g. piston)

Coflow: $j \neq 0$

$$v_n = v_s$$

(on average, at large scales)

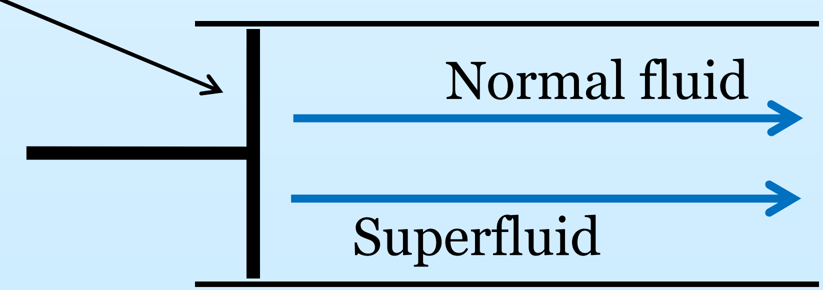

Experimental and physical scales

Physical (quantum) scales

- Quantum vortex core ≈ 10^{-10} m
- Mean distance between quantized vortices ≈ 10^{-4} m
(loosely related to the Kolmogorov dissipative scale of classical turbulent flows of viscous fluids)
- Outer flow scale ≈ 10^{-1} m
(of the order of the experimental volume size)

Experimental scales

- Probe size ≈ 10^{-5} m
(it is often larger and can be tuned, i.e. increased)

Physical questions

1) Are He II turbulent flows different from classical turbulent flows of viscous fluids?

The answer *depends on the probed scale*, if it is smaller or larger than the mean distance between quantized vortices

To date, *quantum features have been clearly detected solely at sufficiently small scales*, while *at large enough scales a classical-like picture is observed in most cases*

2) Do large-scale quantum features of He II turbulent flows exist?

Experimental answers

2) Do large-scale quantum features
of He II turbulent flows exist?

Which are the available experimental tools?

At large scales
pressure probes, thermometers,
quartz tuning forks, *second sound sensors*,
visualization with flow-probing particles
and with excimer molecules, ...

At small scales
visualization with flow-probing particles, ...

Large scales

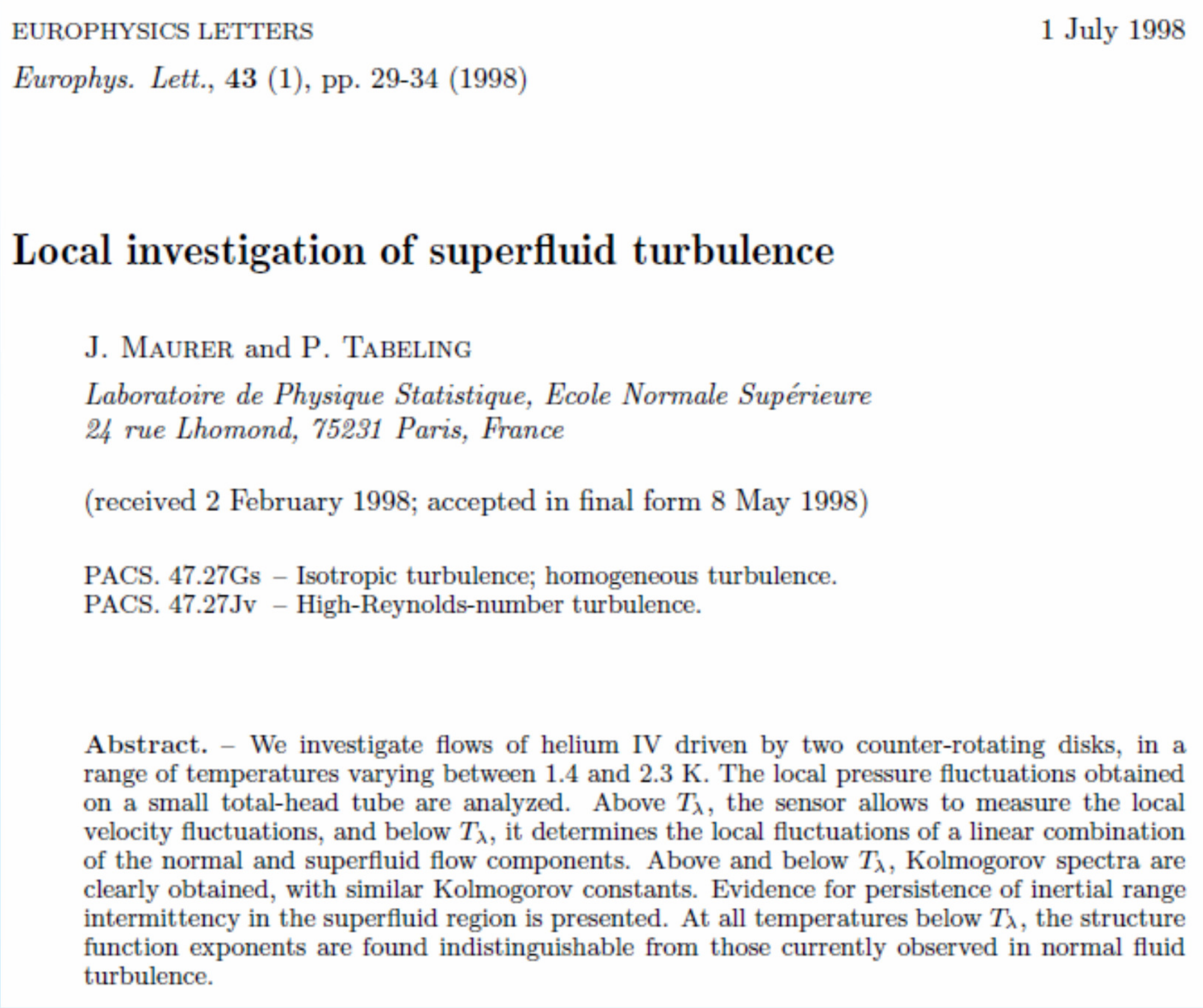
EUROPHYSICS LETTERS 1 July 1998

Europhys. Lett., **43** (1), pp. 29-34 (1998)

Local investigation of superfluid turbulence

J. MAURER and P. TABELING

Laboratoire de Physique Statistique, Ecole Normale Supérieure
24 rue Lhomond, 75231 Paris, France

(received 2 February 1998; accepted in final form 8 May 1998)

PACS. 47.27Gs – Isotropic turbulence; homogeneous turbulence.
PACS. 47.27Jv – High-Reynolds-number turbulence.

Abstract. – We investigate flows of helium IV driven by two counter-rotating disks, in a range of temperatures varying between 1.4 and 2.3 K. The local pressure fluctuations obtained on a small total-head tube are analyzed. Above T_λ, the sensor allows to measure the local velocity fluctuations, and below T_λ, it determines the local fluctuations of a linear combination of the normal and superfluid flow components. Above and below T_λ, Kolmogorov spectra are clearly obtained, with similar Kolmogorov constants. Evidence for persistence of inertial range intermittency in the superfluid region is presented. At all temperatures below T_λ, the structure function exponents are found indistinguishable from those currently observed in normal fluid turbulence.

Large scales

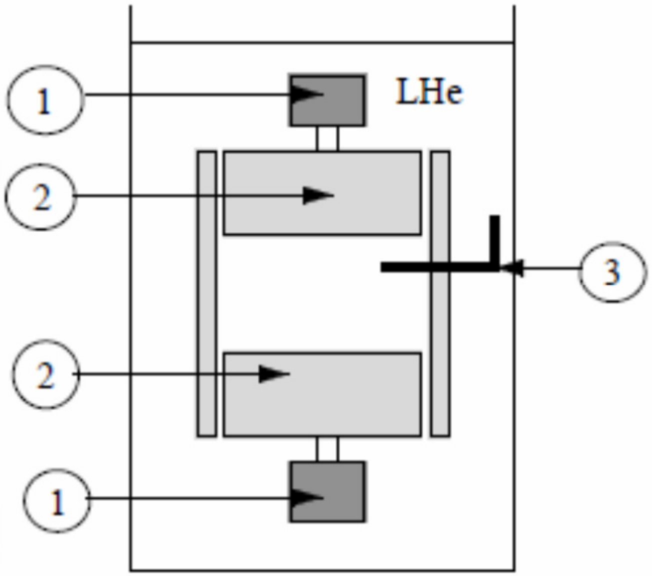

Fig. 1

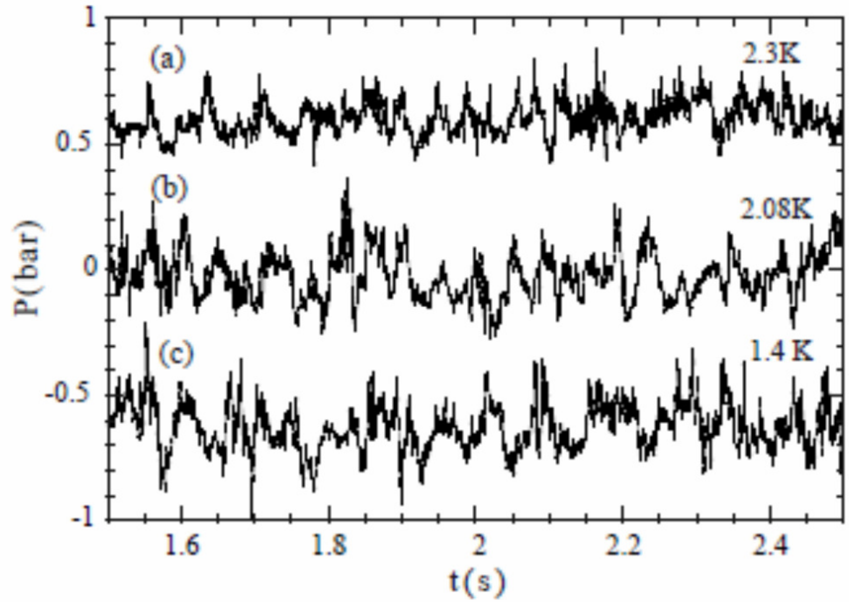

Fig. 2

Fig. 1. – Sketch of the experiment; 1: DC Motor, 2: propellor, 3: probe.

Fig. 2. – Time series obtained for a frequency rotation of 6 Hz, at three different temperatures: (a) 2.3 K (at a 1 bar pressure); (b) 2.08 K; (c) 1.4 K. The time series have been shifted vertically so as to make their representation clear.

J Maurer, P Tabeling **EPL** 43, 29 (1998)

Large scales

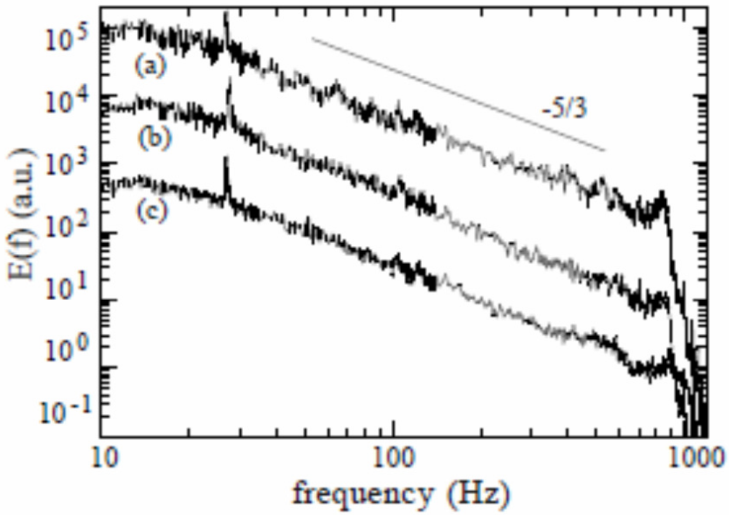

Fig. 3

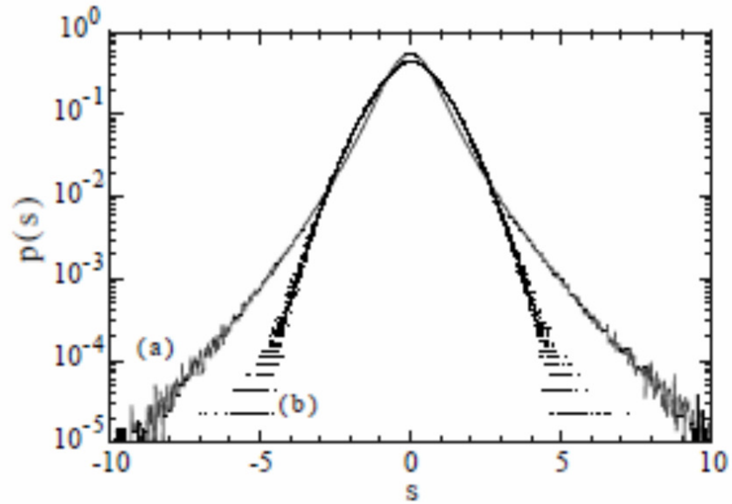

Fig. 4

Fig. 3. – Energy spectra obtained in the same conditions, but at different temperatures: (a) 2.3 K; (b) 2.08 K; (c) 1.4 K. The spectra have been shifted vertically so as to make their representation clear.

Fig. 4. – pdf of the velocity increments obtained for time separations equal to (a) $\delta t = 1$ ms (corresponding to the smallest scale we can resolve) and (b) $\delta t = 100$ ms (which is representative of a large scale), at $T = 1.4$ K; the abcissa s is rescaled so as the variances of the distributions are equal to one.

J Maurer, P Tabeling **EPL** 43, 29 (1998)

Large scales

$$\boxed{\mathrm{Re} = \frac{UD}{\nu}}$$ Reynolds number

$$\boxed{\varepsilon \sim \frac{U^3}{D}}$$ energy dissipation (injection) rate

$$\boxed{\eta = \left(\frac{\nu^3}{\varepsilon}\right)^{1/4}}$$ Kolmogorov length scale

$$\boxed{\frac{\eta}{D} \sim \mathrm{Re}^{-3/4}}$$

$$\boxed{\tau = \left(\frac{\nu}{\varepsilon}\right)^{1/2}}$$ Kolmogorov time scale

$$\boxed{\frac{\tau U}{D} \sim \mathrm{Re}^{-1/2}}$$

J Maurer, P Tabeling
EPL 43, 29 (1998)

$$\nu \sim 2\times10^{-8}\ \mathrm{m^2/s}$$
$$D \sim 0.1\ \mathrm{m}$$
$$U \sim 0.8\ \mathrm{m/s}$$
$$\mathrm{Re} \sim 4\times10^{6}$$

$\longrightarrow$

$$\eta \sim 1\times10^{-6}\ \mathrm{m}$$
$$\tau \sim 6\times10^{-5}\ \mathrm{s}$$

Large scales

PHYSICS OF FLUIDS **22**, 125102 (2010)

Turbulent velocity spectra in superfluid flows

J. Salort,[1] C. Baudet,[2] B. Castaing,[3] B. Chabaud,[1] F. Daviaud,[4] T. Didelot,[1] P. Diribarne,[1,3,4,5] B. Dubrulle,[4] Y. Gagne,[2] F. Gauthier,[1] A. Girard,[5] B. Hébral,[1] B. Rousset,[5] P. Thibault,[1,5] and P.-E. Roche[1]
[1]*Institut Néel, CNRS/UJF, 25 rue des Martyrs, BP 166, F-38042 Grenoble Cedex 9, France*
[2]*Laboratoire des Écoulements Géophysiques et Industriels, CNRS/UJF/INPG, F-38041 Grenoble Cedex 9, France*
[3]*École Normale Supérieure de Lyon, 46 Allée d'Italie, F-69364 Lyon Cedex 7, France*
[4]*DSM/IRAMIS/SPEC, CEA Saclay and CNRS (URA 2464), F-91191 Gif sur Yvette Cedex, France*
[5]*CEA-Grenoble/UJF, SBT, 17 rue des Martyrs, BP166, F-38054 Grenoble Cedex 9, France*

(Received 26 April 2010; accepted 17 September 2010; published online 13 December 2010)

We present velocity spectra measured in three cryogenic liquid ^{4}He steady flows: grid and wake flows in a pressurized wind tunnel capable of achieving mean velocities up to 5 m/s at temperatures above and below the superfluid transition, down to 1.7 K, and a "chunk" turbulence flow at 1.55 K, capable of sustaining mean superfluid velocities up to 1.3 m/s. Depending on the flows, the stagnation pressure probes used for anemometry are resolving from one to two decades of the inertial regime of the turbulent cascade. We do not find any evidence that the second-order statistics of turbulence below the superfluid transition differ from the ones of classical turbulence, above the transition. [doi:10.1063/1.3504375]

Large scales

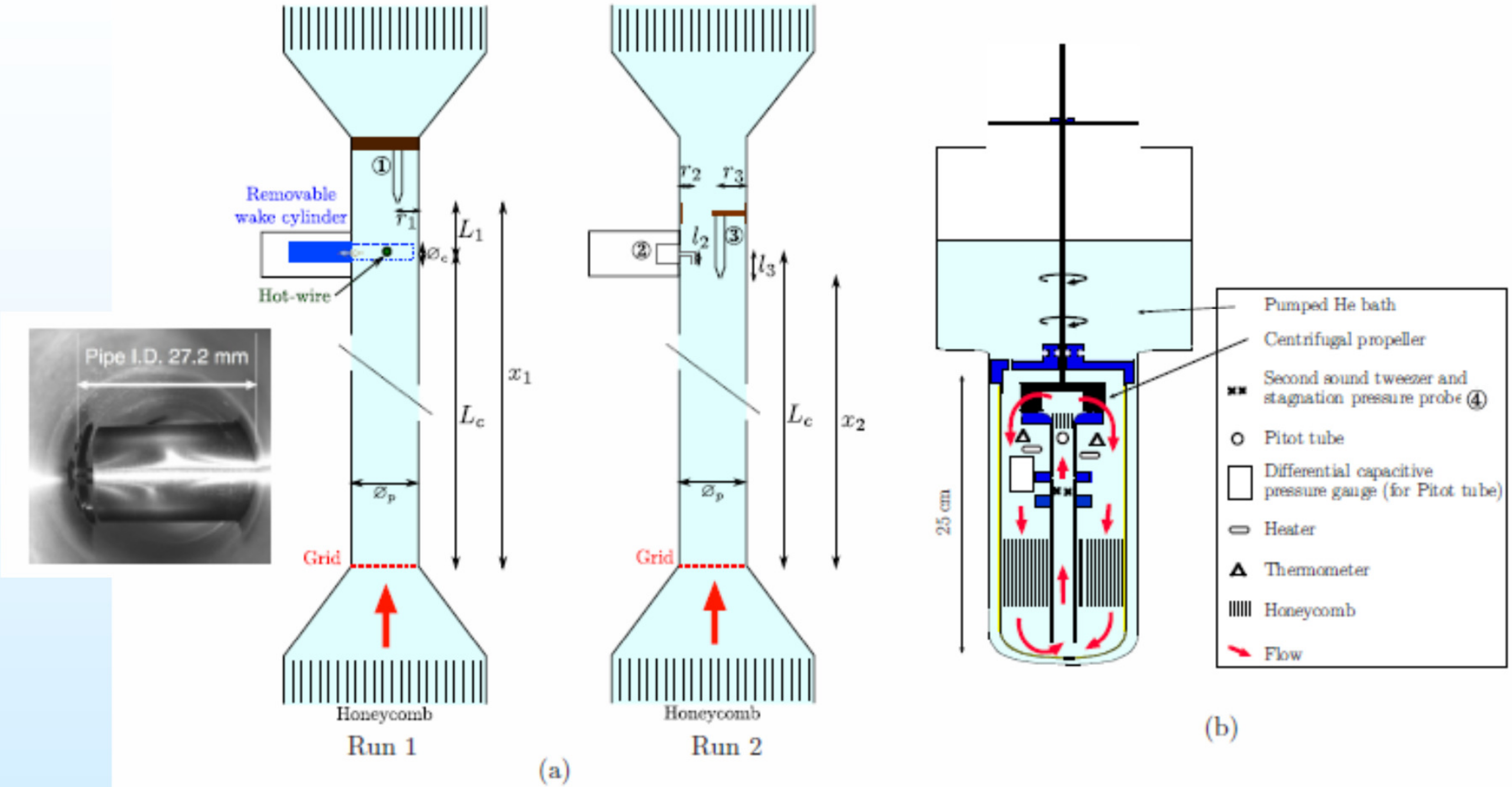

FIG. 3. (Color online) (a) *TSF wind tunnel*: Schematics of the test section and the probe locations for runs 1 and 2. For run 1, a removable cylinder can be inserted across the flow at a distance L_c downstream the grid. It was originally designed to protect a hot-wire during the transient of the system. The stagnation pressure probe ①, located at a distance L_c+L_1 downstream the grid can either measure grid turbulence when the cylinder is removed or wake turbulence when the cylinder is inserted in the flow. Probe ① was not positioned on the pipe axis to avoid the wake of the hot-wire. For run 2, two stagnation pressure probes (② and ③) are available. (b) *Néel wind tunnel*: Schematics and picture of the test section and location of stagnation pressure probe ④.

J Salort *et al*. **Phys Fluids** 22, 125102 (2010)

Large scales

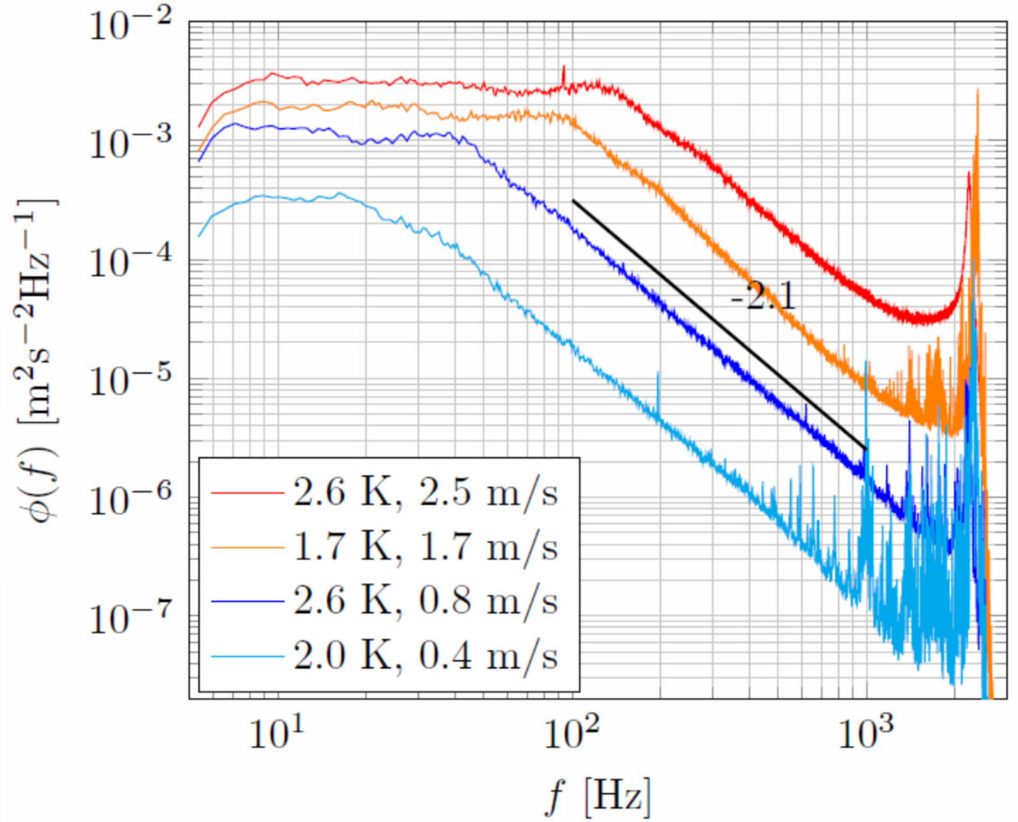

FIG. 7. (Color online) Velocity spectra in the near wake of a cylinder in the TSF wind tunnel both above and below the superfluid transition with mean velocity increasing from bottom to top. The high-frequency peak near 2 kHz is the sensor Helmholtz frequency.

J Salort *et al*. **Phys Fluids** 22, 125102 (2010)

Large scales

A LETTERS JOURNAL EXPLORING THE FRONTIERS OF PHYSICS

February 2012

EPL, **97** (2012) 34006
doi: 10.1209/0295-5075/97/34006

www.epljournal.org

Energy cascade and the four-fifths law in superfluid turbulence

J. SALORT[1], B. CHABAUD[1], E. LÉVÊQUE[2] and P.-E. ROCHE[1]

[1] *Institut Néel, CNRS/UJF - BP 166, F-38042 Grenoble cedex 9, France, EU*
[2] *Laboratoire de Physique de l'ENS de Lyon, CNRS/Université Lyon - F-69364 Lyon cedex 7, France, EU*

received 2 August 2011; accepted in final form 14 December 2011
published online 2 February 2012

PACS 47.37.+q – Hydrodynamic aspects of superfluidity; quantum fluids
PACS 67.30.hb – Transport, hydrodynamics, and superflow
PACS 67.25.dk – Vortices and turbulence

Abstract – The 4/5-law of turbulence, which characterizes the energy cascade from large to small-sized eddies at high Reynolds numbers in classical fluids, is verified experimentally in a superfluid ^{4}He wind tunnel, operated down to 1.56 K and up to $R_\lambda \approx 1640$. The result is corroborated by high-resolution simulations of Landau-Tisza's two-fluid model down to 1.15 K, corresponding to a residual normal fluid concentration below 3% but with a lower Reynolds number of order $R_\lambda \approx 100$. Although the Kármán-Howarth equation (including a viscous term) is not valid *a priori* in a superfluid, it is found that it provides an empirical description of the deviation from the ideal 4/5-law at small scales and allows us to identify an effective viscosity for the superfluid, whose value matches the kinematic viscosity of the normal fluid regardless of its concentration.

Large scales

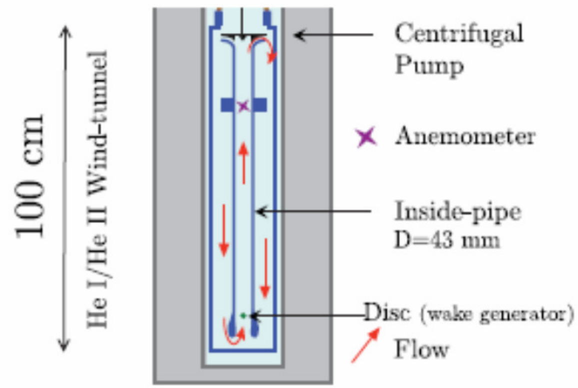

Fig. 1: (Color online) Wind tunnel (in blue) in the cryostat (in gray).

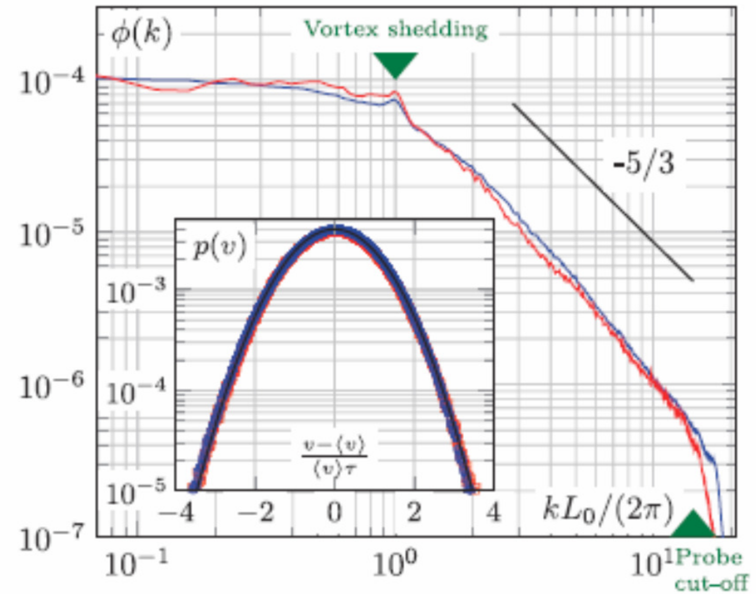

Fig. 2: (Color online) Experimental 1D velocity power spectrum above and below the superfluid transition. Red line: $T = 2.2\,\mathrm{K} > T_\lambda$ at $R_\lambda \approx 1640$. Blue line: $T = 1.56\,\mathrm{K} < T_\lambda$. Inset: velocity probability density distribution above and below the superfluid transition. Black line: Gaussian distribution.

J Salort, B Chabaud, E Lévêque, PE Roche **EPL** 97, 34006 (2012)

Large scales

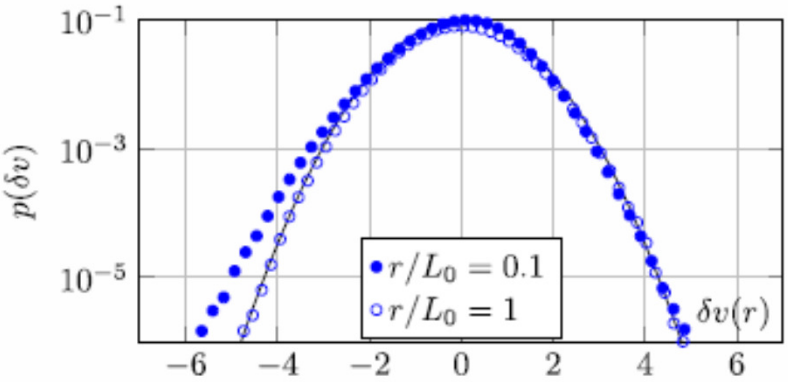

Fig. 3: (Color online) Experimental histogram of the longitudinal velocity increments at large and intermediate scales in a superfluid turbulent flow ($T = 1.56\,\mathrm{K}$). Solid black line: Gaussian PDF.

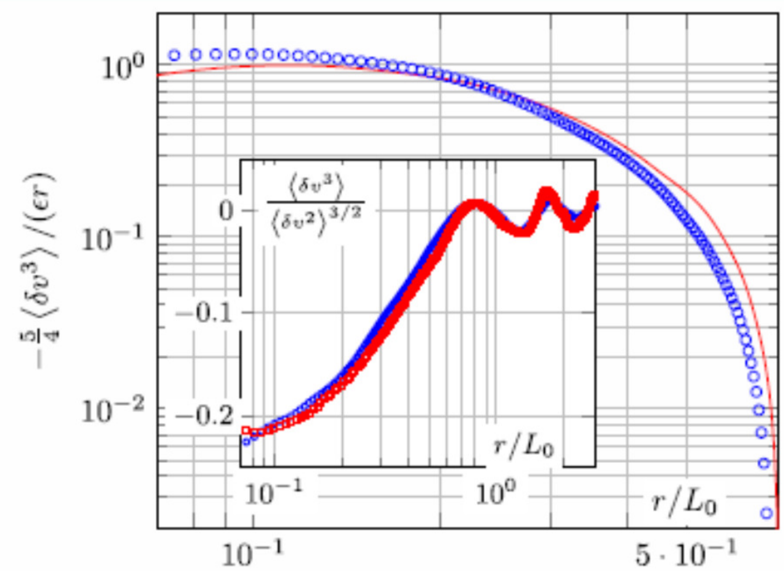

Fig. 4: (Color online) Experimental third-order velocity structure function compensated by the 4/5-law (eq. (9)) obtained in superfluid helium at $T = 1.56\,\mathrm{K}$ (blue circles) and in classical liquid helium at $T = 2.2\,\mathrm{K}$ (red squares). Inset: skewness of the distribution of longitudinal velocity increments (same color code). The smallest abscissa $r/L_0 = 7\times10^{-2}$ corresponds to the probe cut-off. The oscillation at large scales is related to the frequency of the vortex shedding.

in a similar fashion above and below the superfluid transition. More quantitatively, in classical homogeneous and isotropic turbulence, the 4/5-law states that

$$\langle\delta v(r)^3\rangle = -\frac{4}{5}\epsilon r, \qquad (9)$$

where ϵ stands for the mean dissipation rate of kinetic energy. This equation is only valid for inertial scales r, at which cascade dynamics prevails. It is often cited as the only exact result of classical fully developed turbulence, *i.e.* for asymptotically large Re. It is our motivation to test its validity in quantum turbulence. In our experimental setting $R_\lambda \approx 1640$ and, therefore, eq. (9) is expected to be "approached" in a finite inertial range of scales [24].

J Salort, B Chabaud, E Lévêque, PE Roche **EPL** 97, 34006 (2012)

Second sound

$$\ell = \frac{1}{\sqrt{L}}$$

L denotes the length of quantized vortices per unit volume, and is also known as the vortex line density [m^{-2}]

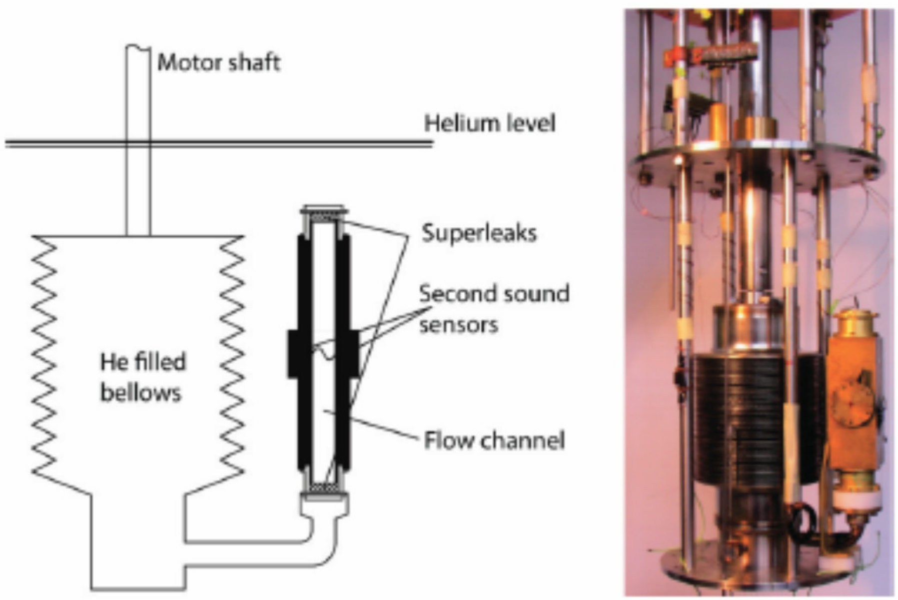

FIG. 1. (Color online) Schematic diagram and photograph of the bellows with the flow channel.

$$L = \frac{6\pi\,\Delta f_0}{B\kappa}\left(\frac{a_0}{a} - 1\right)$$

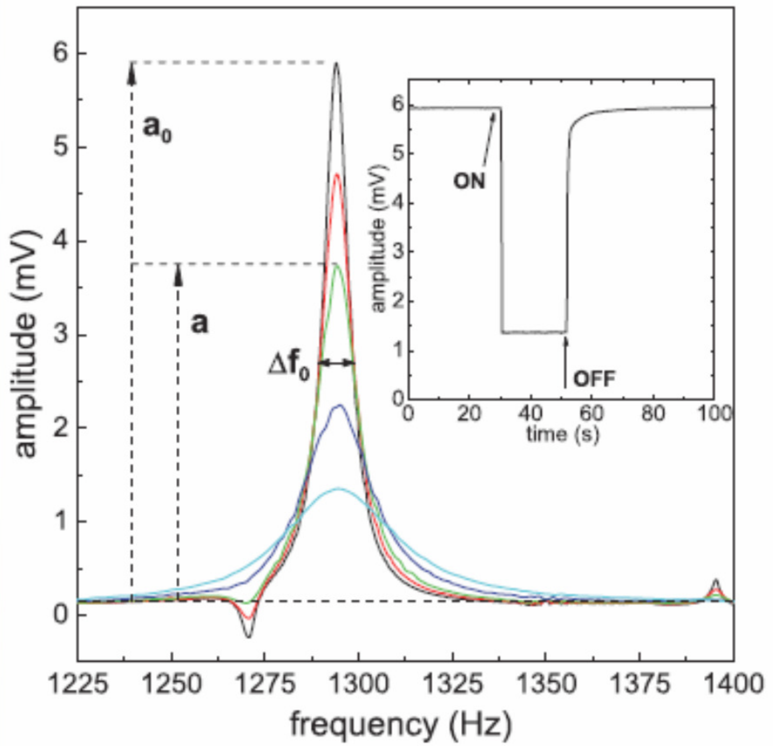

FIG. 2. (Color online) Second sound resonance curves (first mode) for different steady-state flow velocities in the 7-mm wide channel at $T = 1.35$ K. The tallest curve corresponds to the case of no flow in the channel, while others correspond to flow velocities of, from top to bottom, 1.73, 2.60, 4.33, and 6.07 cm/s. (Inset) The second sound amplitude at resonance monitored in time as a flow of steady velocity 6.07 cm/s is switched on and off (same flow velocity as most attenuated curve in main plot).

S Babuin, M Stammeier, E Varga, M Rotter, L Skrbek **Phys Rev B** 86, 134515 (2012)

Large scales

PHYSICS OF FLUIDS **27**, 065101 (2015)

Second-sound studies of coflow and counterflow of superfluid ^{4}He in channels

Emil Varga,[1] Simone Babuin,[2,a)] and L. Skrbek[1]
[1]*Faculty of Mathematics and Physics, Charles University, Ke Karlovu 3, 12116 Prague, Czech Republic*
[2]*Institute of Physics ASCR, Na Slovance 2, 180 00 Prague, Czech Republic*

(Received 16 January 2015; accepted 16 May 2015; published online 2 June 2015)

We report a comprehensive study of turbulent superfluid ^{4}He flow through a channel of square cross section. We study for the first time two distinct flow configurations with the same apparatus: *coflow* (normal and superfluid components move in the same direction), and *counterflow* (normal and superfluid components move in opposite directions). We realise also a variation of counterflow with the same relative velocity, but where the superfluid component moves while there is no net flow of the normal component through the channel, i.e., *pure superflow*. We use the second-sound attenuation technique to measure the density of quantised vortex lines in the temperature range 1.2 K $\lesssim$ T $\lesssim$ T$_\lambda \approx$ 2.18 K and for flow velocities from about 1 mm/s up to almost 1 m/s in fully developed turbulence. We find that both the steady-state and temporal decay of the turbulence significantly differ in the three flow configurations, yielding an interesting insight into two-fluid hydrodynamics. In both pure superflow and counterflow, the same scaling of vortex line density with counterflow velocity is observed, $L \propto V_{cf}^2$, with a pronounced temperature dependence; in coflow instead, the vortex line density scales with velocity as $L \propto V^{3/2}$ and is temperature independent; we provide theoretical explanations for these observations. Further, we develop a new promising technique to use different second-sound resonant modes to probe the spatial distribution of quantised vortices in the direction perpendicular to the flow. Preliminary measurements indicate that coflow is less homogeneous than counterflow/superflow, with a denser concentration of vortices between the centre of the channel and its walls. [http://dx.doi.org/10.1063/1.4921816]

Large scales

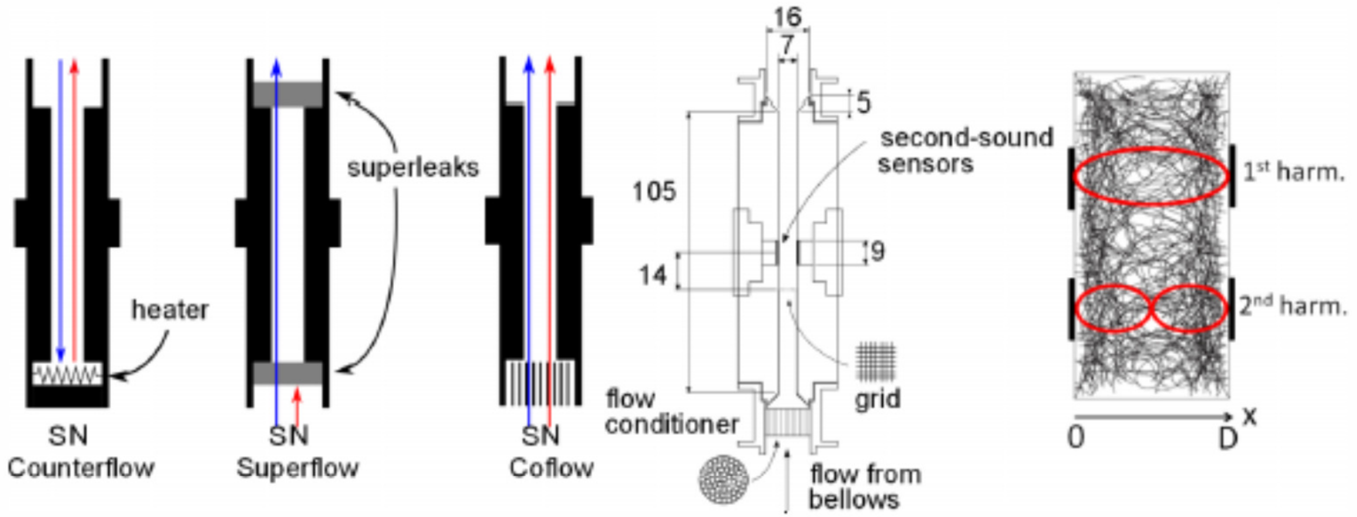

FIG. 1. Flow channels for the study of counterflow, pure superflow, and coflow. S and N stand for superfluid and normal components. The technical drawing is to scale with dimensions in mm and the channel cross section is square. Counterflow is produced thermally by a heater. Superflow and coflow are driven mechanically by a bellows. The superflow is produced by "superleak" filters blocking the normal component. For coflow, the superleaks are removed and the bottom one replaced by a flow conditioner. A grid can also been optionally added to intensify the turbulence. The turbulence is probed in the middle of the channel by second-sound sensors (technique details in the text). Second-sound, here excited and detected by mechanical vibration of a porous membrane, is a wave of fractional superfluid and normal fluid densities which is attenuated by the presence of quantum vortices. The sketch to the right illustrates how the first two second-sound resonant harmonics can be used to probe inhomogeneity in the vortex tangle (tangle image from numerical simulation of wall-bounded counterflow[17]). Sensitivity is higher where the standing wave amplitude is higher; therefore in this example, the second harmonic would provide a stronger signal than the first.

E Varga, S Babuin, L Skrbek **Phys Fluids** 27, 065101 (2015)

Large scales

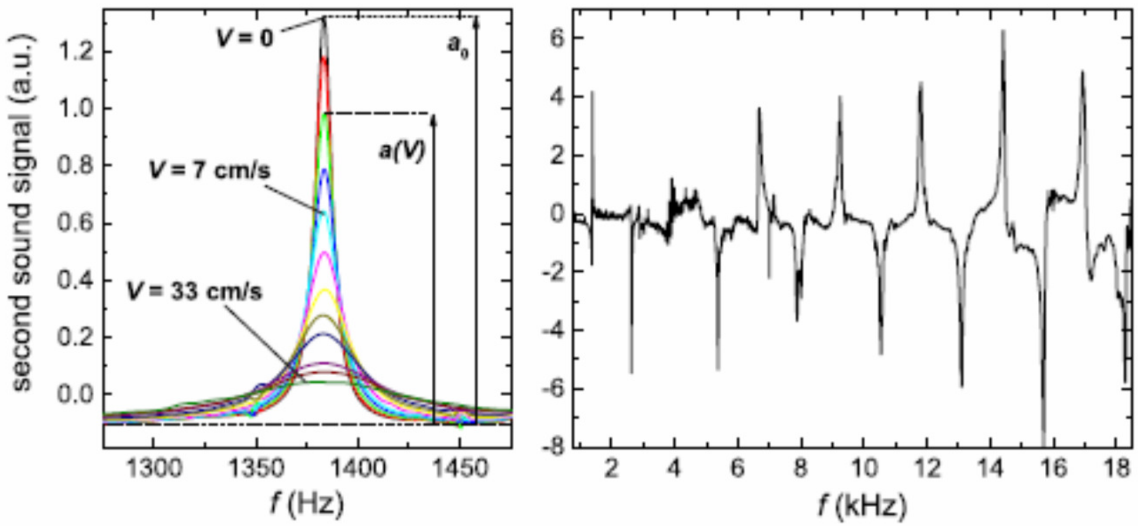

FIG. 2. (Left) The evolution of the second-sound first resonance mode with increasing steady-flow velocity V, in a coflow run at $T = 1.65$ K. The amplitude reduction relative to the $V = 0$ case enters the calculation of the vortex line density, L, in Eq. (1). (Right) An illustrative sample of the second-sound spectrum in our channel/second-sound resonator at higher frequency, without flow in the channel (at the same T as the first harmonic to the left, but different excitation amplitude and lock-in amplifier phase compensation — see text for more details). Higher resonance harmonics are almost exact integer multiples of the first one. For even harmonics, the oscillation of the detecting membrane is π out-of-phase with the driving membrane, causing the observed peak inversion.

$$L(V) = \frac{6\pi\Delta f_0}{B\kappa}\left(\frac{a_0}{a(V)} - 1\right)$$

E Varga, S Babuin, L Skrbek **Phys Fluids** 27, 065101 (2015)

Large scales

Counterflow

$$\boxed{\sqrt{L} = \gamma(T,G)\, v_{ns}(T,q)}$$

Coflow

$$\frac{\eta}{D} \sim \left(\frac{UD}{\nu}\right)^{-3/4}$$

$$\eta \sim \ell = \frac{1}{\sqrt{L}}$$

$$L \sim U^{3/2}$$

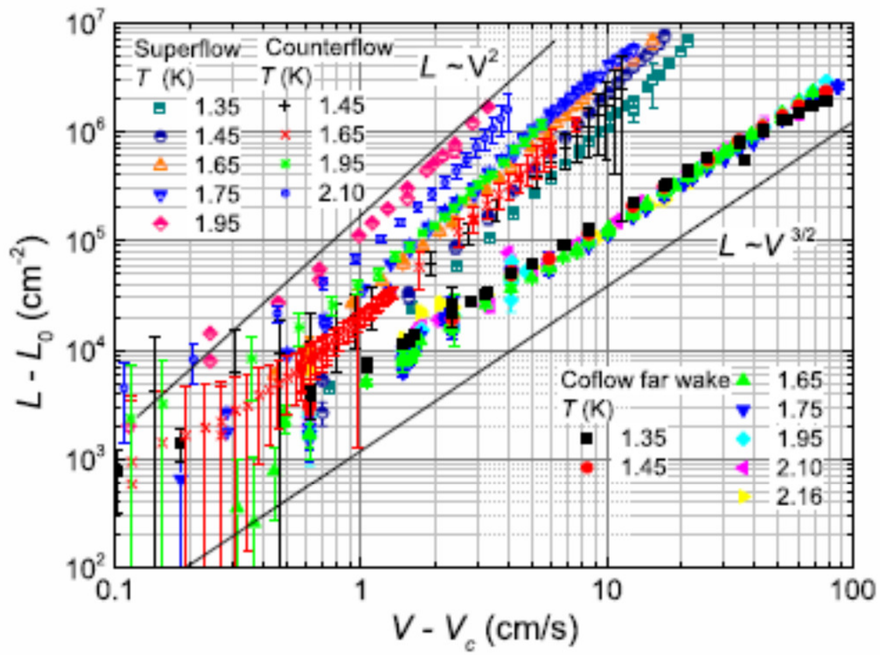

FIG. 3. Vortex line density versus mean flow velocity for superflow, counterflow, and coflow experiments. When the two helium components are forced to undergo relative motion (superflow and counterflow) compared to their natural coupling (coflow), the scaling and the temperature dependences are strongly affected. The residual line density in no flow conditions (L_0) and the critical velocity for turbulence onset (V_c) have been subtracted for correct log-log plotting (see text for details). The coflow has grid turbulence character, produced by the flow conditioner at the channel entrance. We call it "far wake" to distinguish it from the "near wake" case realised by adding a conventional grid near the sensors, results in Fig. 4. The velocity range corresponds roughly to a Reynolds number range $700 \leq Re \leq 3 \times 10^5$, definition based on the effective viscosity of He-II.[11]

E Varga, S Babuin, L Skrbek **Phys Fluids** 27, 065101 (2015)

Large scales

VOLUME 82, NUMBER 24 PHYSICAL REVIEW LETTERS 14 JUNE 1999

Decay of Grid Turbulence in a Finite Channel

Steven R. Stalp, L. Skrbek, and Russell J. Donnelly
Cryogenic Helium Turbulence Laboratory, Department of Physics, University of Oregon, Eugene, Oregon 97403
(Received 3 September 1998)

We develop a classical model for the decay of homogeneous and isotropic turbulence that takes into account the growth of the energy containing length scale and its saturation when it reaches the size of the containing vessel. The model describes our data on the decay of grid turbulence in helium II through 4 orders of magnitude in vorticity, as well as classical experiments on decaying turbulence. [S0031-9007(99)09342-4]

PACS numbers: 47.27.Gs, 47.37.+q, 67.40.Vs

$$\boxed{\omega(t) = \kappa L}$$

Superfluid vorticity

where κ is the circulation quantum [m²/s] and L denotes the length of quantized vortices per unit volume, also known as the vortex line density [m⁻²]

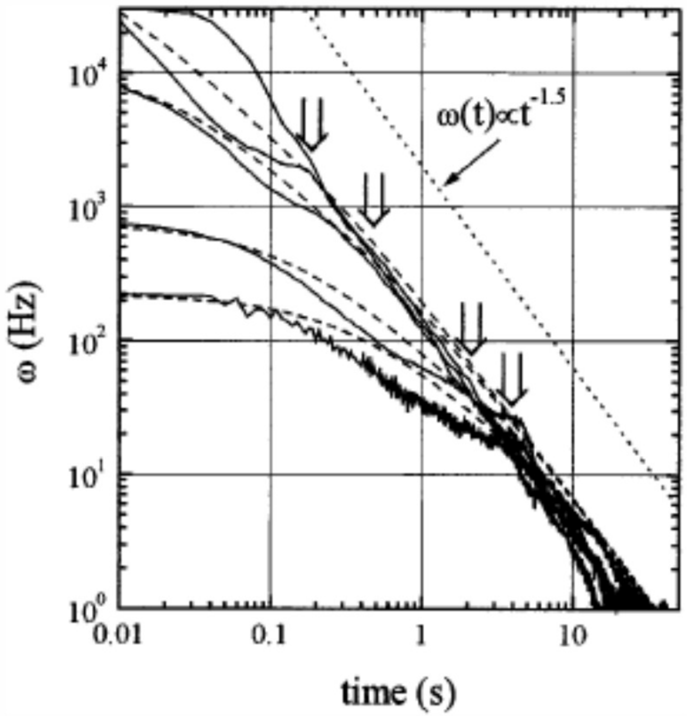

FIG. 2. Decay of vorticity for grid velocities of 5, 10, 50, 100, and 200 cm/s (top curve) at 1.5 K. Dashed lines represent model calculation.

SR Stalp, L Skrbek, RJ Donnelly
Phys Rev Lett 82, 4831 (1999)

Large scales

A Letters Journal Exploring the Frontiers of Physics

March 2007

EPL, **77** (2007) 66002
doi: 10.1209/0295-5075/77/66002

www.epljournal.org

Vortex density spectrum of quantum turbulence

P.-E. Roche[1], P. Diribarne[1], T. Didelot[1], O. Français[2,3], L. Rousseau[2] and H. Willaime[4]

[1] *Institut NÉEL, CNRS & Université J. Fourier - 25 avenue des Martyrs, BP166, F-38042 Grenoble Cedex 9, France*
[2] *Groupe ESIEE, Chambre de Commerce et d'Industrie de Paris - Cité Descartes, BP99, 2 boulevard Blaise Pascal, 93162 Noisy le Grand Cedex, France*
[3] *Conservatoire National des Arts et Métiers, Laboratoire de Physique - 2 rue Conté, 75003 Paris, France*
[4] *Ecole Supérieure de Physique et de Chimie Industrielles de la Ville de Paris - 10 rue Vauquelin, 75231 Paris Cedex 05, France*

received 25 October 2006; accepted in final form 29 January 2007
published online 28 February 2007

PACS 67.40.Vs – Vortices and turbulence
PACS 47.37.+q – Hydrodynamic aspects of superfluidity; quantum fluids
PACS 67.57.De – Quantum fluids and solids; liquid and solid helium: Superflow and hydrodynamics

Abstract – The fluctuations of the vortex density in a turbulent quantum fluid are deduced from local second-sound attenuation measurements. These measurements are performed with a micromachined open-cavity resonator inserted across a flow of turbulent He-II near 1.6 K. The frequency power spectrum of the measured vortex line density is compatible with a $(-5/3)$ power law. The physical interpretation is discussed.

Large scales

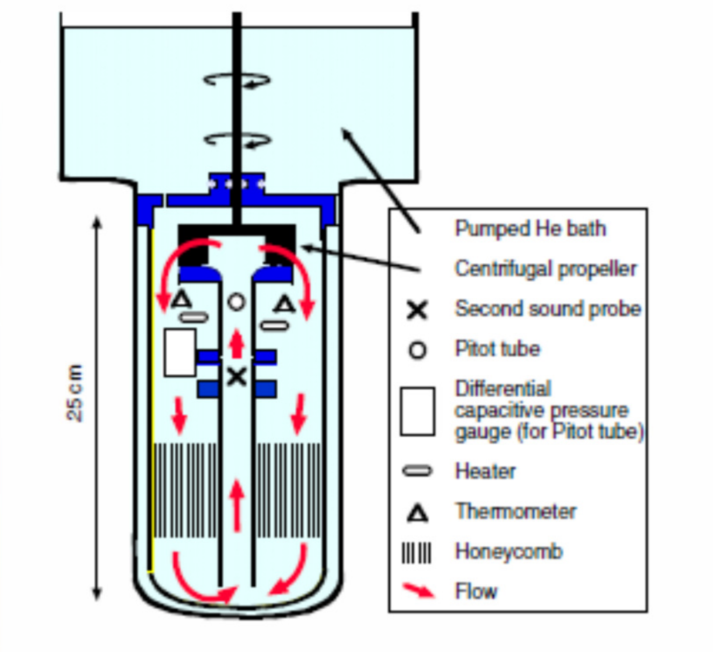

Fig. 1: Scheme of the flow loop with probes.

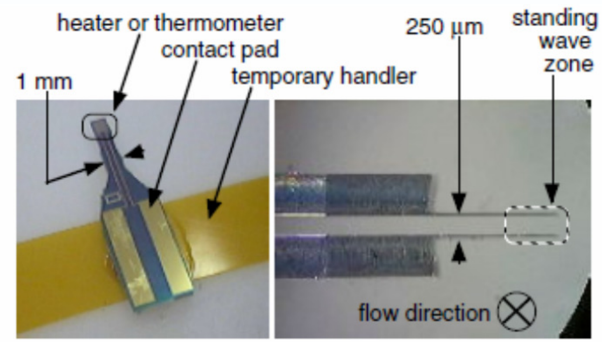

Fig. 2: Left figure: single silicon element before the probe assembling, with contact leads and heater layer (emitter) or thermometer layer (receiver). These layers are deposited over a $0.8\,\mathrm{mm} \times 0.8\,\mathrm{mm}$ surface. Right figure: side view of the tip of the assembled probe. The heater and thermometer are facing each other with a $250\,\mu\mathrm{m}$ gap between their $15\,\mu\mathrm{m}$ thick and $1.5\,\mathrm{mm}$ long support. The helium mainstream flows perpendicularly to the right-side figure.

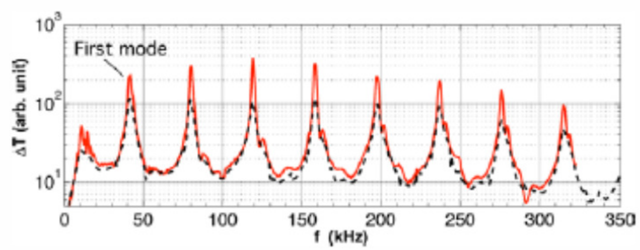

Fig. 3: The first modes of second-sound resonances of the probe, with flow (dashed line) and without (solid line).

PE Roche, P Diribarne, T Didelot, O Français, L Rousseau, H Willaime **EPL** 77, 66002 (2007)

Large scales

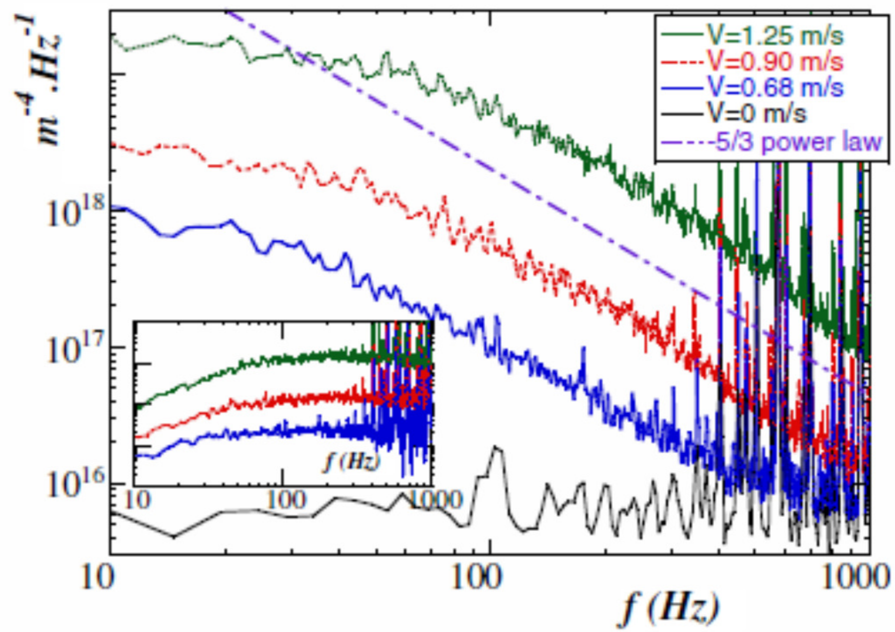

Fig. 4: Power spectrum density of the vortex line density $L_\perp$ for different mean flow velocities: from bottom to top 0, 0.68, 0.90 and 1.25 m/s. The straight line is a $(-5/3)$ power law. The insert is a $f^{-5/3}$ compensated spectrum for the 3 different mean flows after removal of a $5 \cdot 10^{15}\ \mathrm{m^{-4}\ Hz^{-1}}$ white-noise floor.

PE Roche, P Diribarne, T Didelot, O Français, L Rousseau, H Willaime **EPL** 77, 66002 (2007)

Large scales

How is the vortex line density L related to the flow vorticity?

A Letters Journal Exploring the Frontiers of Physics
February 2008
EPL, **81** (2008) 36002
www.epljournal.org
doi: 10.1209/0295-5075/81/36002

Vortex spectrum in superfluid turbulence: Interpretation of a recent experiment

P.-E. Roche[1] and C. F. Barenghi[2]

[1] *Institut NÉEL, CNRS/UJF - BP166, F-38042 Grenoble Cedex 9, France*
[2] *School of Mathematics, University of Newcastle - Newcastle upon Tyne, NE1 7RU, UK*

received 4 September 2007; accepted in final form 30 November 2007
published online 3 January 2008

PACS 67.40.Vs – Vortices and turbulence
PACS 47.37.+q – Hydrodynamic aspects of superfluidity: quantum fluids
PACS 67.57.De – Quantum fluids and solids; liquid and solid helium: Superflow and hydrodynamics

Abstract – We discuss a recent experiment in which the spectrum of the vortex line density fluctuations has been measured in superfluid turbulence. The observed frequency dependence of the spectrum, $f^{-5/3}$, disagrees with classical vorticity spectra if, following the literature, the vortex line density is interpreted as a measure of the vorticity or enstrophy. We argue that the disagreement is solved if the vortex line density field is decomposed into a polarised field (which carries most of the energy) and an isotropic field (which is responsible for the spectrum).

PRL **109**, 205304 (2012) PHYSICAL REVIEW LETTERS week ending 16 NOVEMBER 2012

Vortex-Density Fluctuations, Energy Spectra, and Vortical Regions in Superfluid Turbulence

Andrew W. Baggaley,[1,2,*] Jason Laurie,[3] and Carlo F. Barenghi[2]

[1] *School of Mathematics and Statistics, University of Glasgow, Glasgow G12 8QW, United Kingdom*
[2] *Joint Quantum Centre Durham-Newcastle, School of Mathematics and Statistics, Newcastle University, Newcastle upon Tyne NE1 7RU, United Kingdom*
[3] *Laboratoire de Physique, École Normale Supérieure de Lyon, 46 allée d'Italie, 69007 Lyon, France*
(Received 31 July 2012; published 14 November 2012)

Measurements of the energy spectrum and of the vortex-density fluctuation spectrum in superfluid turbulence seem to contradict each other. Using a numerical model, we show that at each instance of time the total vortex line density can be decomposed into two parts: one formed by metastable bundles of coherent vortices, and one in which the vortices are randomly oriented. We show that the former is responsible for the observed Kolmogorov energy spectrum, and the latter for the spectrum of the vortex line density fluctuations.

DOI: 10.1103/PhysRevLett.109.205304 PACS numbers: 67.25.dk, 47.27.Gs, 47.32.C−

Vortex tangle partly polarized (vortex bundles)

Large scales

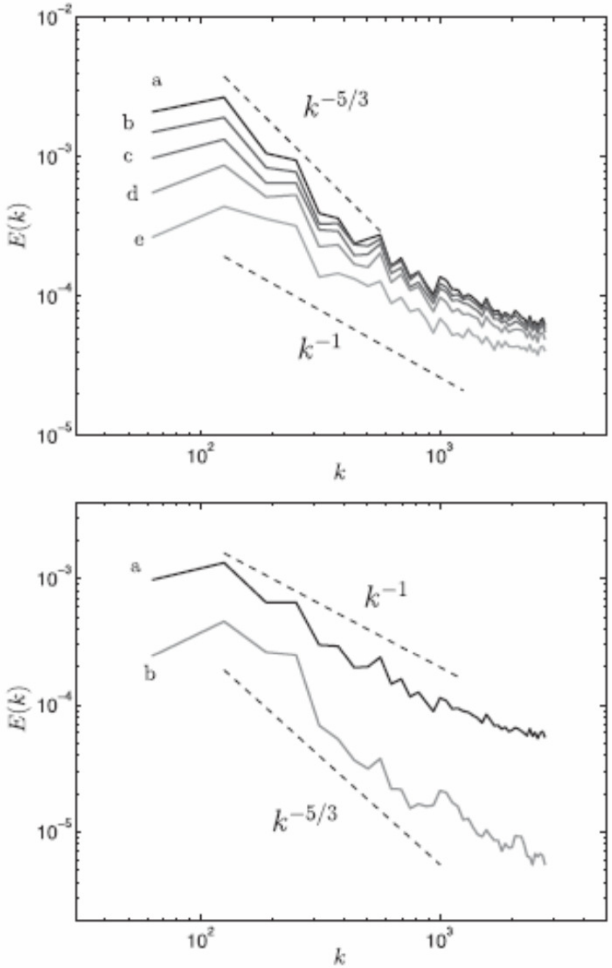

FIG. 4. Energy spectra $E(k)$ (arb. units) versus wave number k (cm^{-1}) corresponding to Fig. 3. Top: The upper solid line (a) is the energy spectrum corresponding to the flow induced by all vortex lines. Lower curves correspond to the flow induced by vortices with smoothed vorticity below the following thresholds: (b) $\omega < 1.7\omega_{\mathrm{rms}}$, (c) $1.4\omega_{\mathrm{rms}}$, (d) $1.2\omega_{\mathrm{rms}}$, and (e) ω_{rms}. Bottom: Energy spectra corresponding to vortex lines with smoothed vorticity, respectively, below (a) and above (b) the threshold $1.4\omega_{\mathrm{rms}}$. The dashed lines display the k^{-1} and the $k^{-5/3}$ scalings.

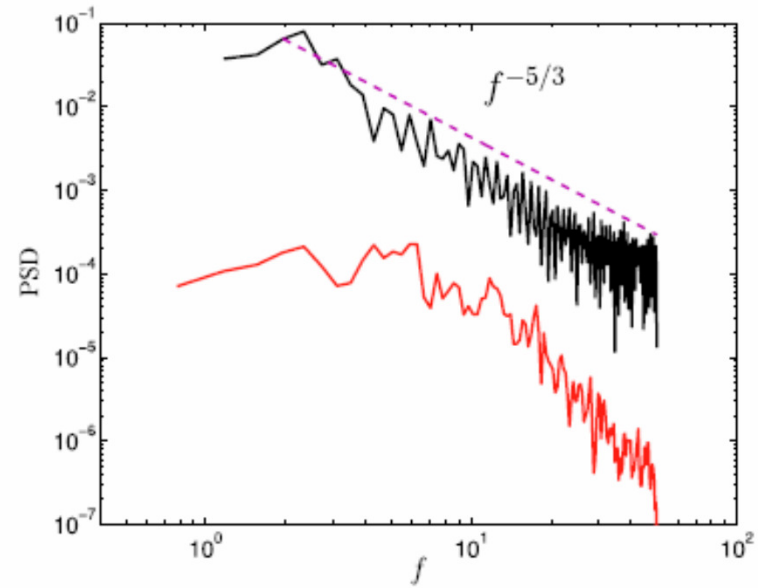

FIG. 2 (color online). Power spectral density (PSD) (arb. units) of fluctuations of the total vortex line density L (black upper solid line) and of the polarized vortex line density $L_{\parallel}$ (red lower solid line) versus frequency f (s^{-1}). The dashed (magenta) line shows the $f^{-5/3}$ scaling.

AW Baggaley, J Laurie, CF Barenghi
Phys Rev Lett 109, 205304 (2012)

Summary: large scales

2) Do large-scale quantum features of He II turbulent flows exist?

Different L scaling for counterflow and coflow

E Varga, S Babuin, L Skrbek **Phys Fluids** 27, 065101 (2015)

Counterflow

$$\boxed{\sqrt{L} = \gamma(T,G)\, v_{ns}(T,q)}$$

Coflow

$$\frac{\eta}{D} \sim \left(\frac{UD}{\nu}\right)^{-3/4}$$

$$\eta \sim \ell = \frac{1}{\sqrt{L}}$$

$$L \sim U^{3/2}$$

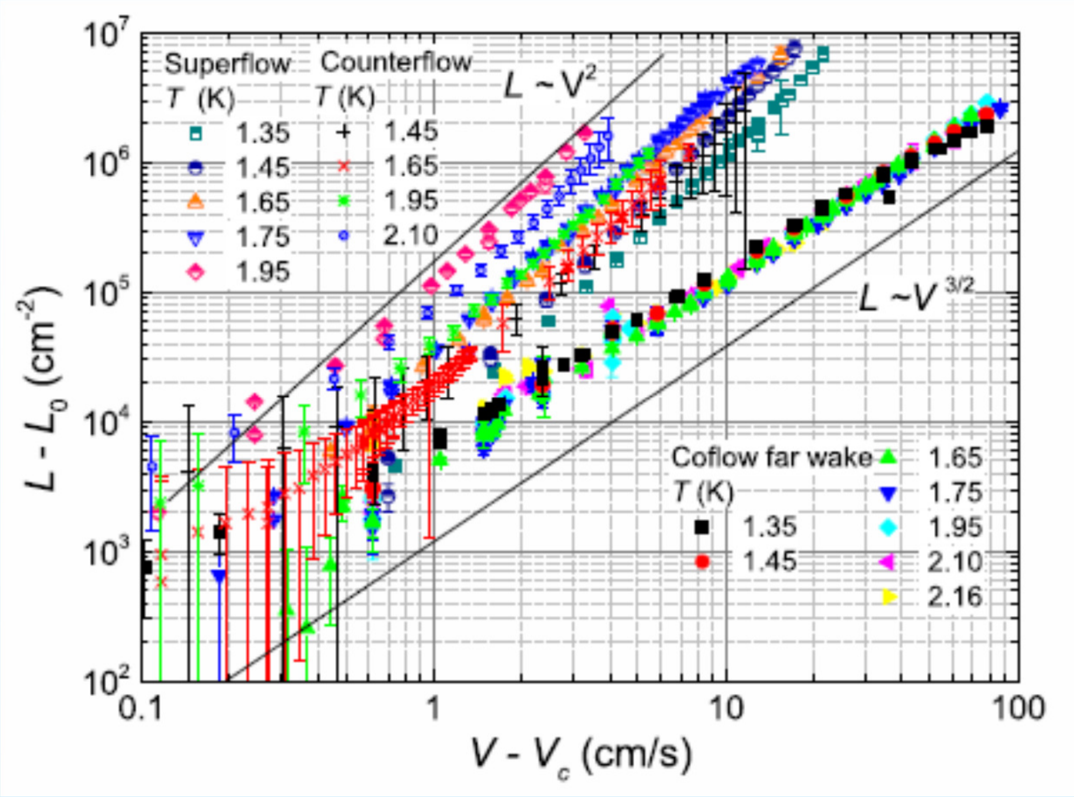

Summary: large scales

2) Do large-scale quantum features of He II turbulent flows exist?

Different L scaling for counterflow and coflow

E Varga, S Babuin, L Skrbek **Phys Fluids** 27, 065101 (2015)

Possible explanation: no Fourier law for He II flows

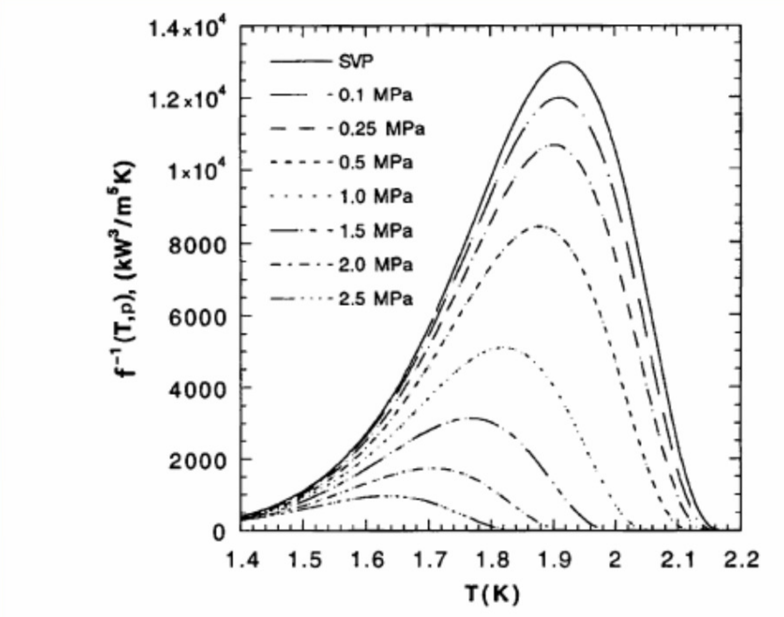

Fig. 7.3 Heat conductivity function for turbulent He II

$$\frac{dT}{dx} = -\frac{q}{k} \quad \text{Fourier law}$$

$$\frac{dT}{dx} = -f(T,p)\,q^3$$

$$k_{eff} = \frac{1}{f(T,p)\,q^2}$$

SW Van Sciver **Helium Cryogenics** Springer (2012)

MS Mongiovì, D Jou, M Sciacca **Phys Rep** 726, 1 (2018)

Summary: large scales

2) Do large-scale quantum features of He II turbulent flows exist?

L vs. vorticity spectra

PE Roche, P Diribarne, T Didelot, O Français, L Rousseau, H Willaime **EPL** 77, 66002 (2007)

Possible explanation:
tangle polarization
(quantized vortex bundles)

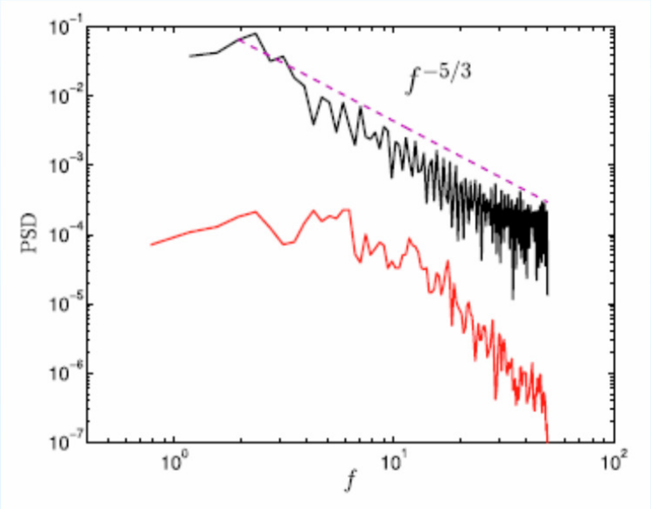

AW Baggaley, J Laurie, CF Barenghi
Phys Rev Lett 109, 205304 (2012)

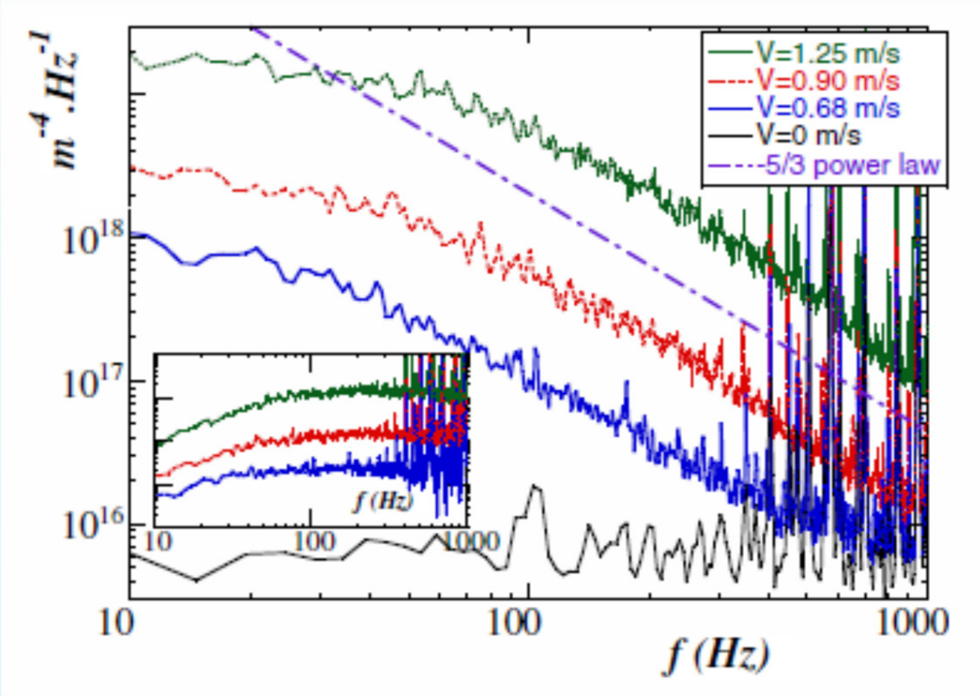

Flow visualization (with particles)

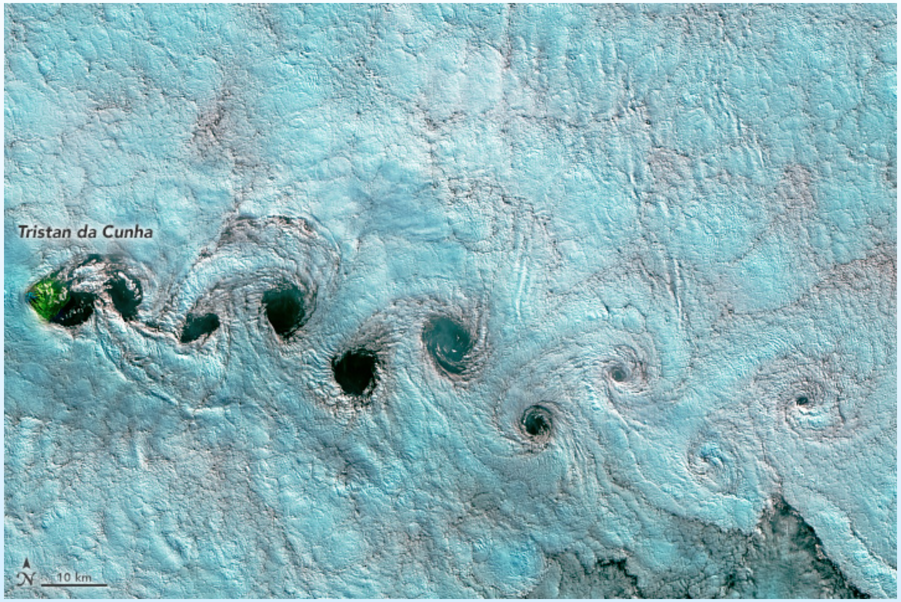

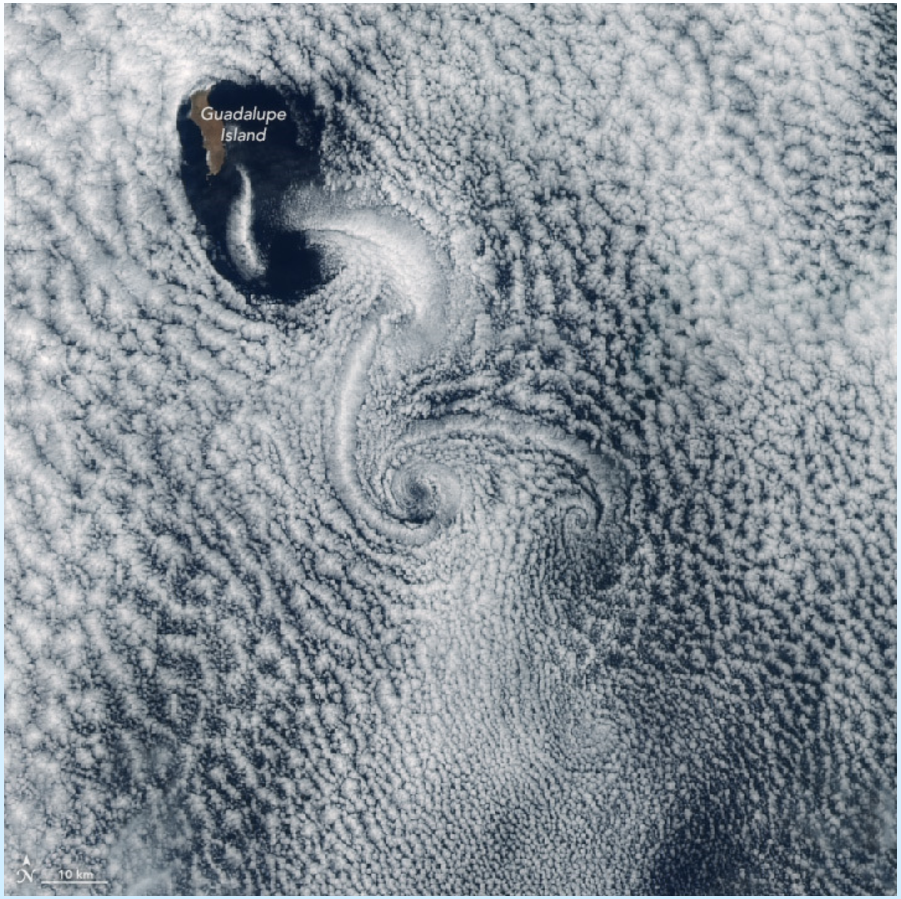

earthobservatory.nasa.gov/IOTD/view.php?id=90734

Visualization of He II flows

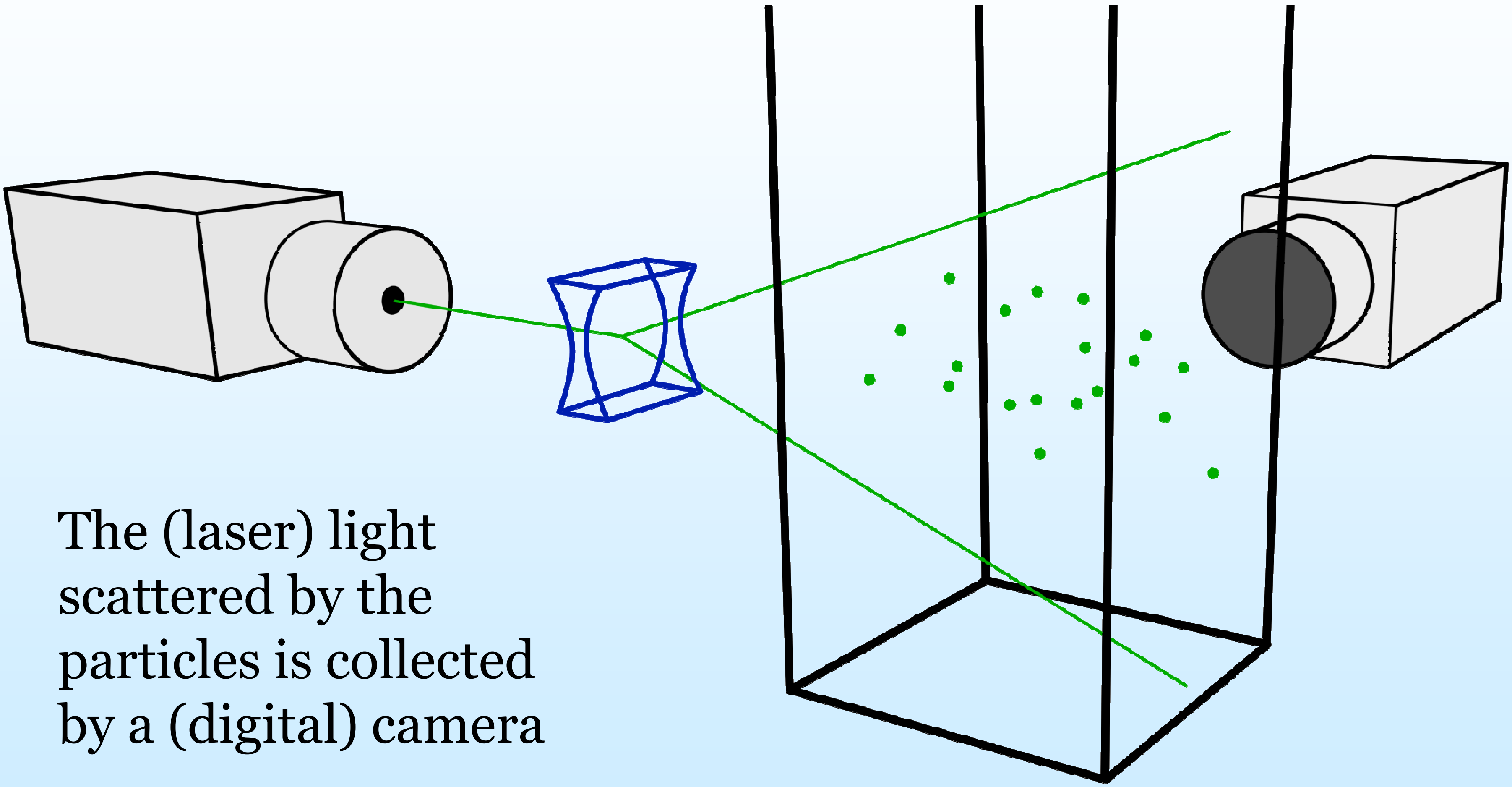

The (laser) light scattered by the particles is collected by a (digital) camera

Visualization of He II flows

Visualization of cryogenic flows is still in its infancy
The ways to optimise it are yet to be entirely investigated, due to a number of technical and fundamental reasons

- Optical access to the helium bath, to minimise heat input

- Choice of suitable particles, to trace low-temperature (quantum) flows

- Interaction of particles with quantized vortices, leading sometimes to particle trapping (and detrapping)

- Two large-scale velocity fields, in thermal counterflow

W Guo, M La Mantia, DP Lathrop, SW Van Sciver **Proc Natl Acad Sci USA** 111, 4653 (2014)

Visualization of He II flows

Phys Rev 108, 157 (1957)

Suspension of Particles in Liquid Helium

K. L. Chopra and J. B. Brown

Department of Physics, University of British Columbia, Vancouver, B.C., Canada

(Received July 17, 1957)

Using the suspension of particles to indicate the motion of the fluid, we have observed and measured acoustic streaming[3] in liquid He II. To the eye, the particle motion appears turbulent in He I, but along stream lines in He II. The velocity is surprisingly independent of temperature and is proportional to the square root of the driving pressure (sound intensity) to the lowest values measurable. Thus a tentative conclusion is that the flow in He II is probably turbulent. The details of these experiments will be published shortly.

Phys Rev Lett 14, 892 (1965)

MOTION OF SUSPENDED PARTICLES IN TURBULENT SUPERFLOW OF LIQUID HELIUM II

David Y. Chung and P. R. Critchlow

Department of Physics, University of British Columbia, Vancouver 8, British Columbia, Canada

(Received 8 February 1965; revised manuscript received 26 April 1965)

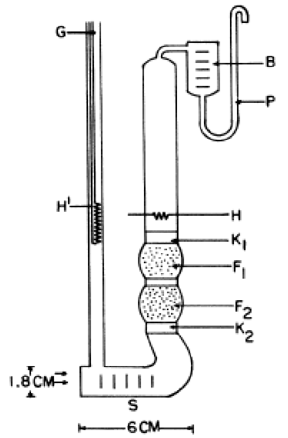

FIG. 1. The superfluid wind tunnel. (S), experimental region; (H) and (H'), heaters; (F_1) and (F_2), powder-packed superleaks; (K_1 and K_2) Kovar seals; (B), small beaker; and (P), a fountain pump.

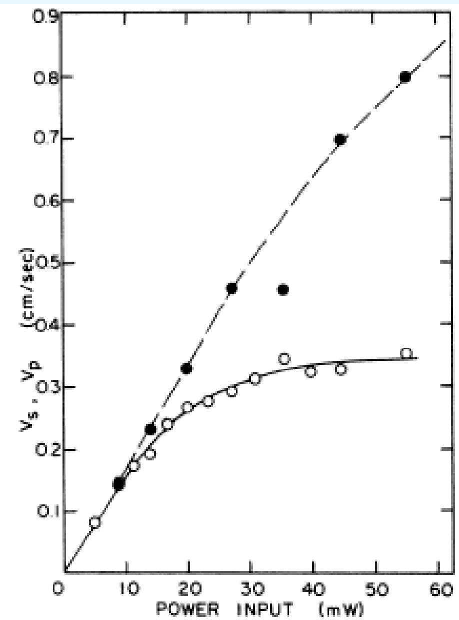

FIG. 2. A typical plot for average superfluid velocity (○) and particle velocity (●) versus power input.

Visualization of He II flows

Phys Rev Lett 14, 942 (1965)

FLOW VISUALIZATION IN He II: DIRECT OBSERVATION OF HELMHOLTZ FLOW*

T. A. Kitchens,† W. A. Steyert, and R. D. Taylor

University of California, Los Alamos Scientific Laboratory, Los Alamos, New Mexico

and

Paul P. Craig

Brookhaven National Laboratory, Upton, New York

(Received 6 May 1965)

(a)

(b)

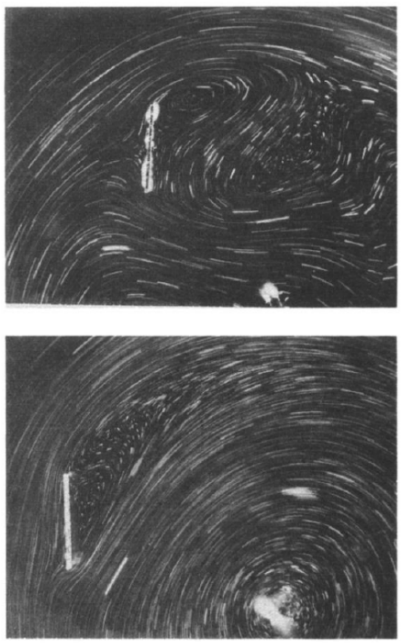

FIG. 2. A classical illustration of Helmholtz flow in a rotating water-glycerol mixture. The attack angle is 47° in Fig. 2(a) and 27° in Fig. 2(b). In both cases the Reynolds number Re = 80. The center of rotation is the light flare in the lower right.

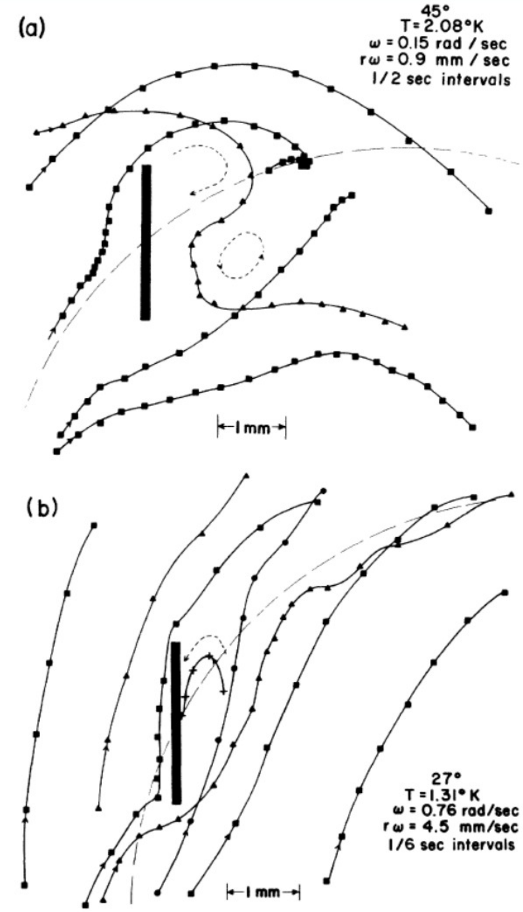

FIG. 1. (a) Typical trajectories of frozen particles of H-D about an airfoil immersed in clockwise-rotating He II. On the downstream side of the wing the flow is turbulent with discontinuities in the velocity streamlines, indicating the existence of Helmholtz flow. The wing attack angle is 45°. (b) Flow about a wing at 27° attack angle. Flow separation is not complete, and approaches much more closely to potential flow than Fig. 1(a).

Visualization of He II flows

Jpn J Appl Phys 26, Suppl. 26-3, 107 (1987)

Flow Visualization Study on Large-Scale Vortex Ring in He II

Masahide MURAKAMI, Masaya HANADA* and Tsutomu YAMAZAKI

Institute of Engineering Mechanics, Univ. of Tsukuba
Sakura, Ibaraki 305 Japan

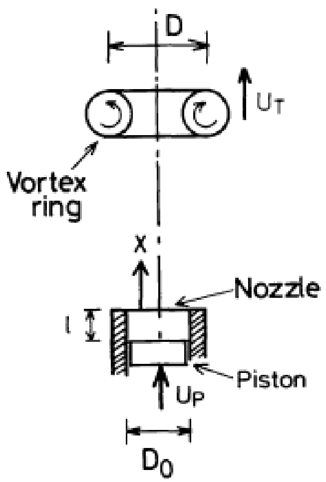

Fig. 1 Schematics of the vortex generator and a vortex ring.

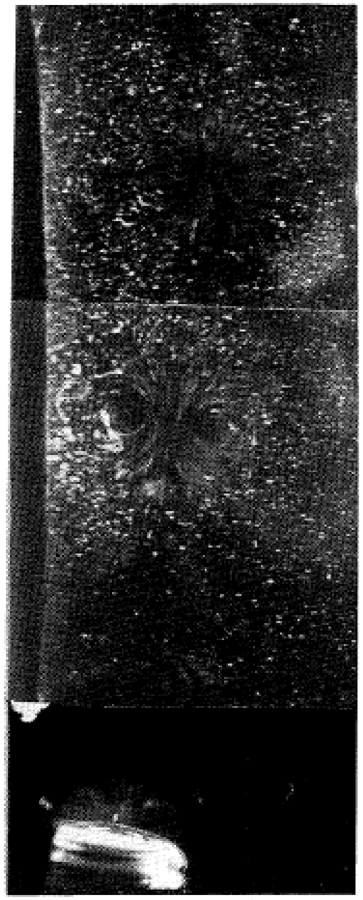

Fig. 2 Vortex rings at three stages, the initial, the developing and the fully developed ones, respectively. T_B=2.0 K, U_P=13 cm/s, l=8 mm.

Visualization of He II flows

Cryogenics 29, 438 (1989)

Flow visualization study of thermal counterflow jet in He II

M. Murakami and N. Ichikawa*

Institute of Engineering Mechanics, University of Tsukuba, Tsukuba, Ibaraki 305, Japan
*Mechanical Engineering Laboratory, MITI, Tsukuba, Ibaraki 305, Japan

Received 21 March 1988

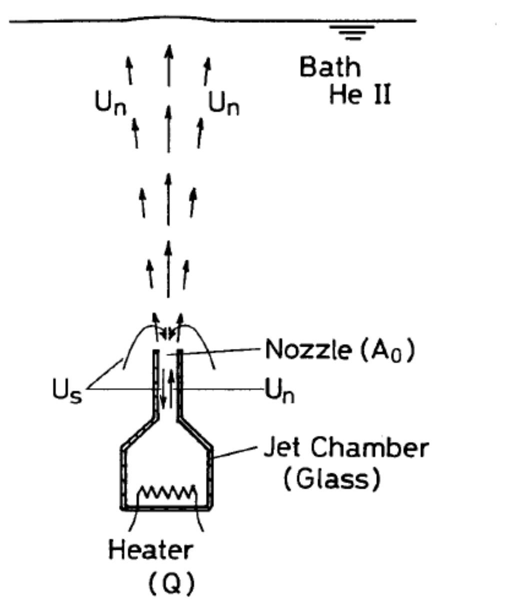

Figure 1 Schematic illustration of the thermal counterflow jet in He II

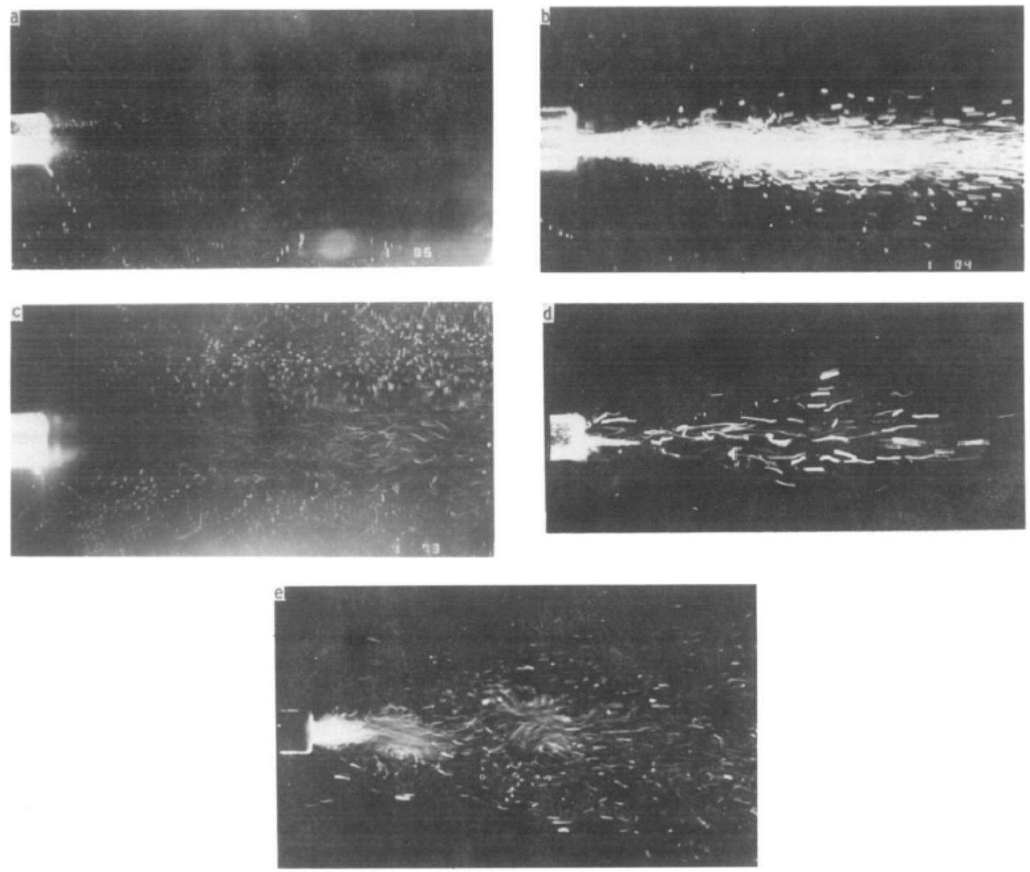

Figure 2 Flow visualization pictures of the thermal counterflow jet. (a) $T = 1.99$ K, $q = 1.06 \times 10^3$ W m^{-2}, $Re = 1600$, $Re_n = 500$, H_2–D_2 particles, 1/2 s multi-exposed; (b) $T = 2.12$ K, $q = 1.73 \times 10^4$ W m^{-2}, $Re = 12\,000$, $Re_n = 10\,000$, glass spheres, 1/4 s multi-exposed; (c) $T = 1.95$ K, $q = 1.77 \times 10^4$ W m^{-2}, Re = 30 000, $Re_n = 15\,000$, H_2–D_2 particles, 1/2 s successively multi-exposed; (d) $T = 1.63$ K, $q = 1.68 \times 10^4$ W m^{-2}, $Re = 100\,000$, $Re_n = 19\,000$, glass spheres, 1/8 s exposed; (e) $T = 1.90$ K, $q = 3.78 \times 10^4$ W m^{-2}, $Re = 81\,000$, $Re_n = 34\,000$, glass spheres, 1/8 s exposed

Visualization of He II flows

Physica B 193, 188 (1994)

Counterflow-induced macroscopic vortex rings in superfluid helium: visualization and numerical simulation

G. Stamm*, F. Bielert, W. Fiszdon[1], J. Piechna[2]

Max-Planck-Institut für Strömungsforschung, Bunsenstrasse 10, D-37073 Göttingen, Germany

Received 25 June 1993

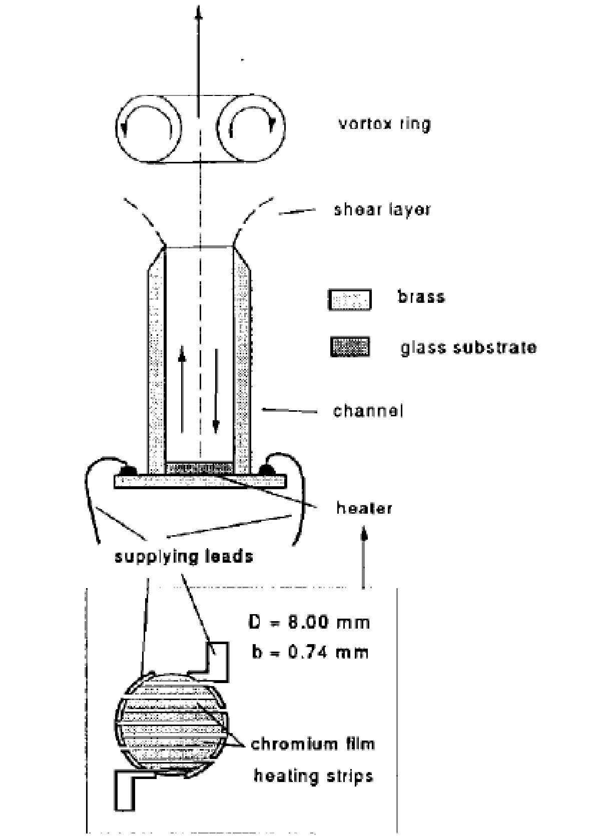

Fig. 1. Schematic view of the vortex ring generator. The meander-shaped heater is shown on the insert.

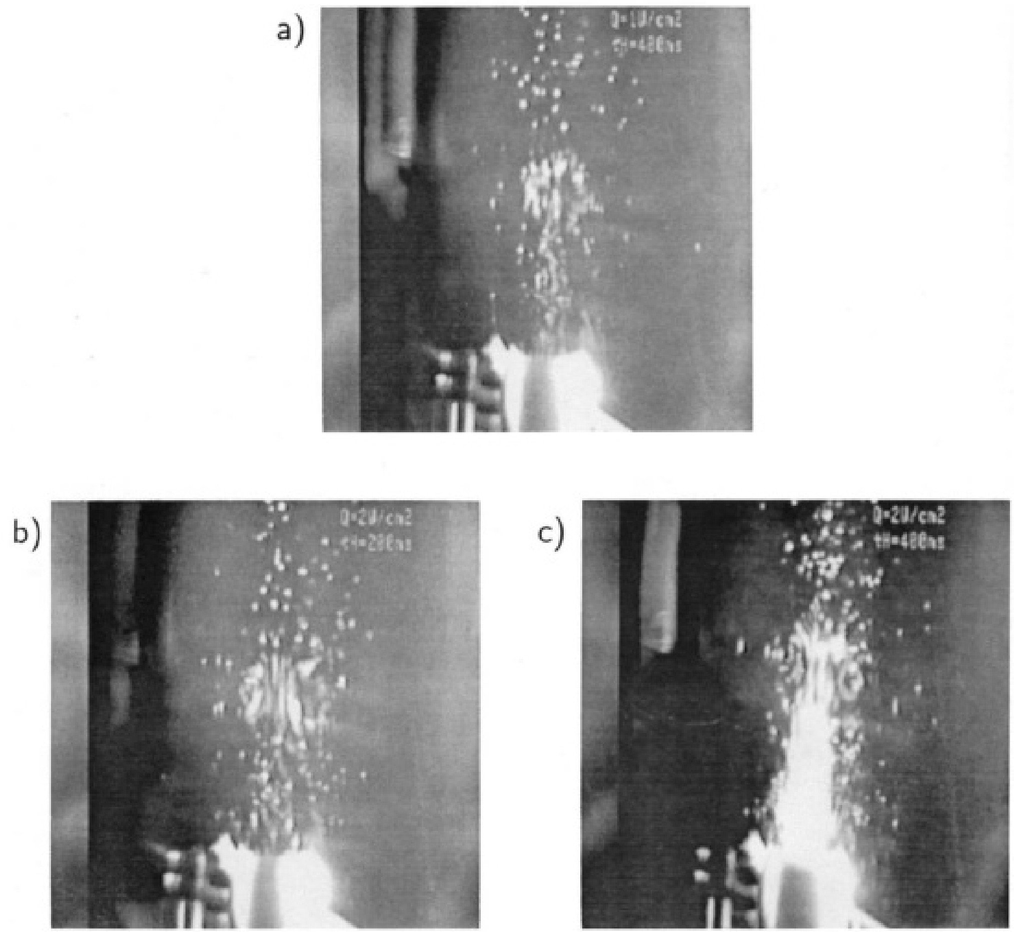

Fig. 3. Recorded pictures of the vortex ring for various parameter combinations for the generating heat pulses at a bath temperature of 1.85 K. The top half of the counterflow tube is shown in the middle bottom of each picture. (a) $Q = 1\ W/cm^2$, $t_H = 400$ ms; (b) $Q = 2\ W/cm^2$, $t_H = 200$ ms; (c) $Q = 2\ W/cm^2$, $t_H = 400$ ms.

Visualization of He II flows

T Zhang, SW Van Sciver **Nat Phys** 1, 36 (2005)

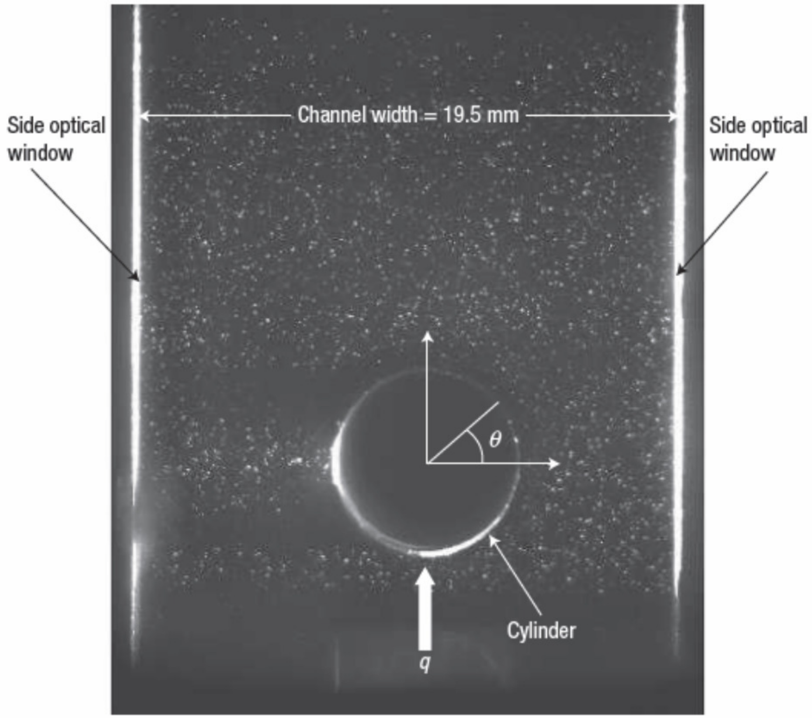

Figure 1 Particle seeding in a He(II) counterflow channel containing a 6.35 mm transparent cylinder. The particles are 1.7 μm diameter polymer micro-spheres[14] with a specific gravity of 1.1. In the video, the He(II) is at $T = 2.03$ K and $q = 11.2$ kW m^{-2} is applied upwards and co-axial to the channel. This flux corresponds to a superfluid vortex line density[18], L_0, of about 2.6×10^{10} m m^{-3}.

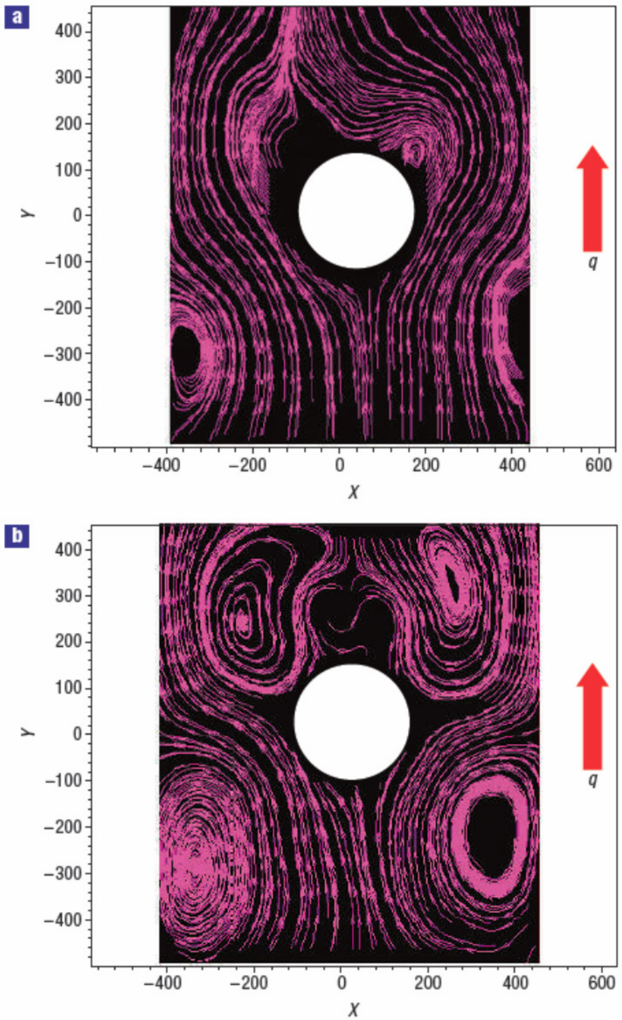

Figure 3 Computed streamlines for particle motion for the two heat flux cases in Fig. 2. a, $q = 4$ kW m^{-2} at $T = 1.6$ K corresponding to $Re_D = 41{,}000$ and $L_0 = 1 \times 10^{10}$ m m^{-3}. **b**, $q = 11.2$ kW m^{-2} at $T = 2.03$ K corresponding to $Re_D = 21{,}000$ and $L_0 = 2.6 \times 10^{10}$ m m^{-3}.

Visualization of He II flows

W Guo, M La Mantia, DP Lathrop, SW Van Sciver **Proc Natl Acad Sci USA** 111, 4653 (2014)

Visualization of two-fluid flows of superfluid helium-4

Wei Guo[a,b], Marco La Mantia[c], Daniel P. Lathrop[d], and Steven W. Van Sciver[a,b,1]

[a]Mechanical Engineering Department, Florida State University, Tallahassee, FL 32303; [b]National High Magnetic Field Laboratory, Florida State University, Tallahassee, FL 32310; [c]Department of Low Temperature Physics, Faculty of Mathematics and Physics, Charles University, 180 00 Prague, Czech Republic; and [d]Departments of Physics and Geology, Institute for Research in Electronics and Applied Physics, and Institute for Physics Science and Technology, University of Maryland, College Park, MD 20742

Edited by Katepalli R. Sreenivasan, New York University, New York, NY, and approved December 13, 2013 (received for review July 17, 2013)

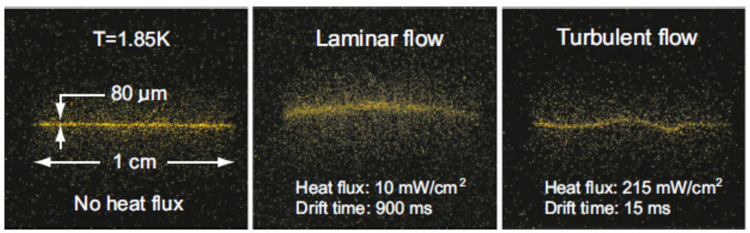

Fig. 4. Fluorescence images showing the motion of a thin line of He_2^* tracers in thermal counterflow. The tracer line is created via laser-field ionization by focusing a femtosecond laser pulse into superfluid helium. The drift time denotes the time between the creation and the imaging of the tracer line. The second image was taken in steady-state flow, whereas the third image was taken by the time the heater was turned off.

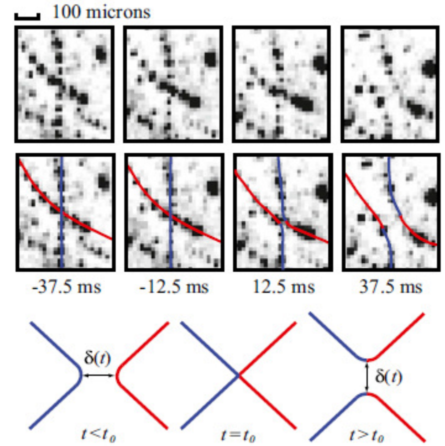

Fig. 2. Images at low ice concentration confirm vortex line reconnection and allow one to quantify the dynamics of the intervortex separation $\delta(t)$ (42).

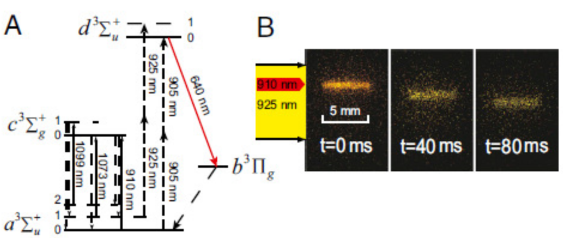

Fig. 3. (*A*) Schematic diagram showing the optical transitions for imaging the He_2^* triplet molecules. The levels, labeled 0, 1, 2 for each electronic state, are the vibrational levels of the corresponding state. (*B*) Averaged images of a line of tagged helium molecules via the tagging fluorescence method across a square channel (5 mm side width) in thermal counterflow with a heat flux of 640 mW/cm².

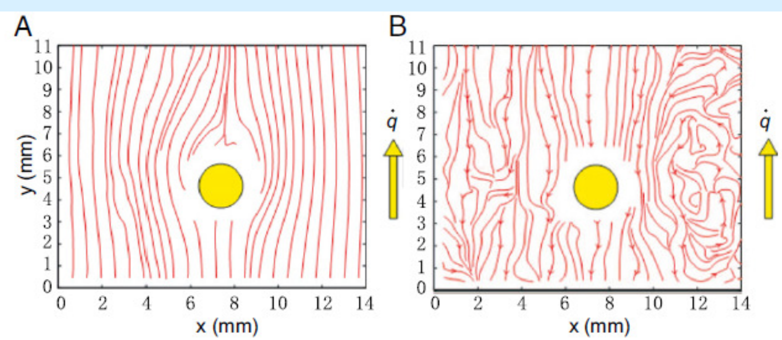

Fig. 6. Particle trajectories around a 2-mm cylinder obtained in counterflow by the PTV technique with hydrogen particles. (*A*) The particles that move with the normal fluid velocity. (*B*) The motion of particles that interact with quantized vortex lines ($q = 50$ mW/cm², $T = 1.93$ K, $v_n = 0.23$ cm/s, Reynolds number $Re = 485$).

Experimental apparatus

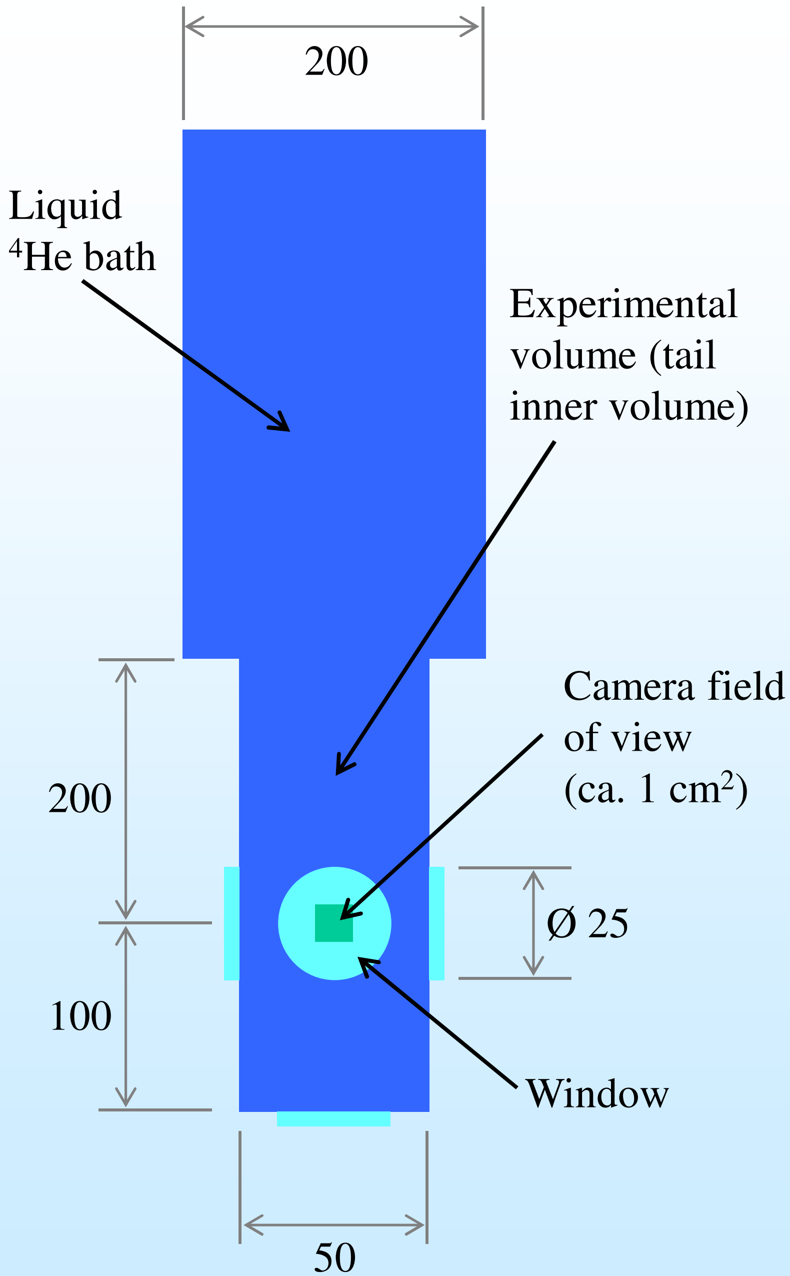

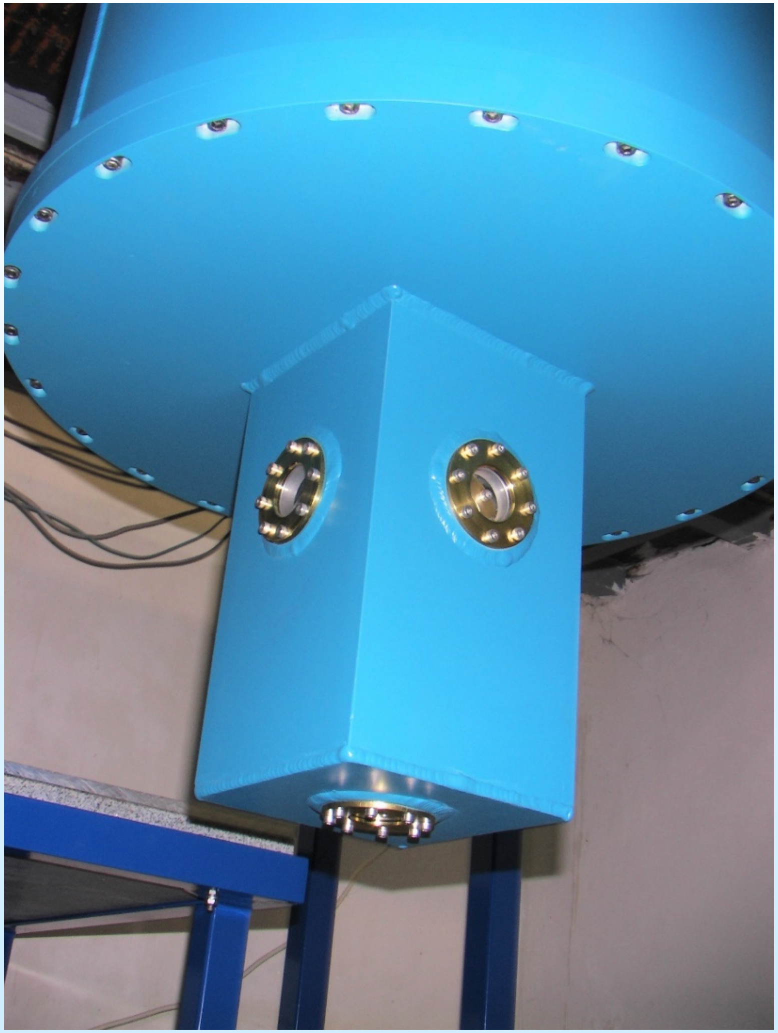

Cryostat optical tail

Experimental apparatus

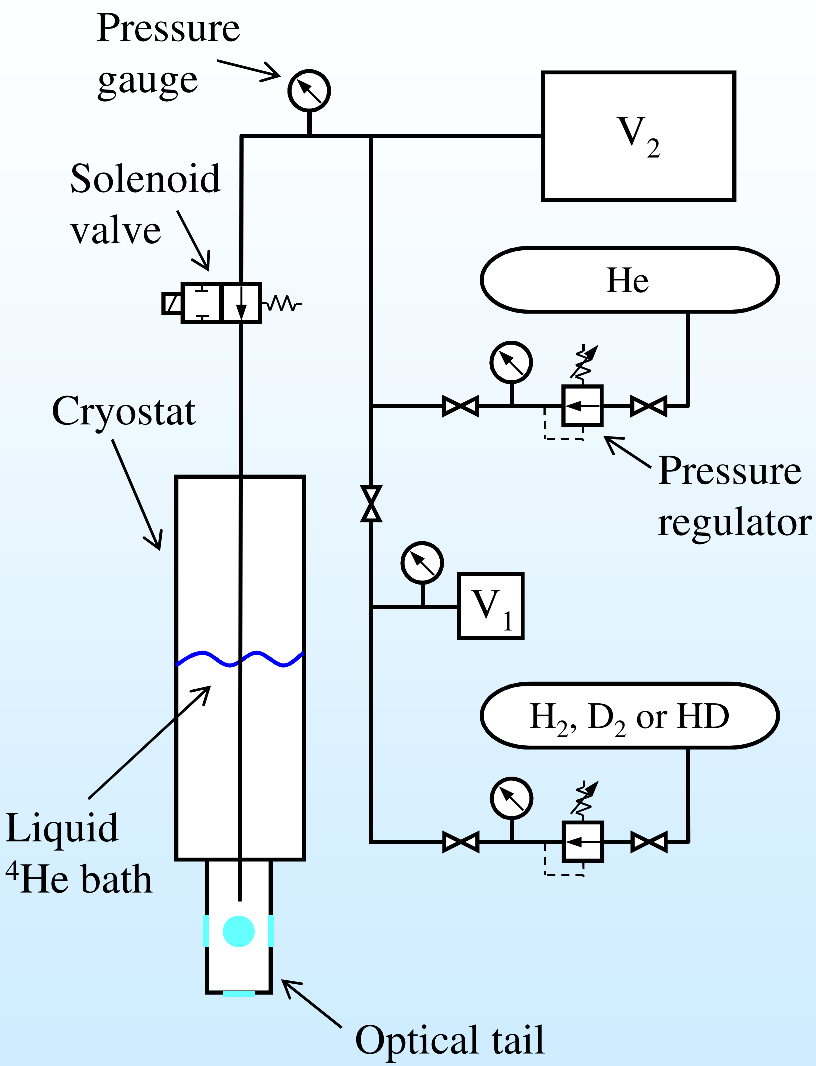

Seeding system

Helium II flows

$$j = \rho_n v_n + \rho_s v_s$$

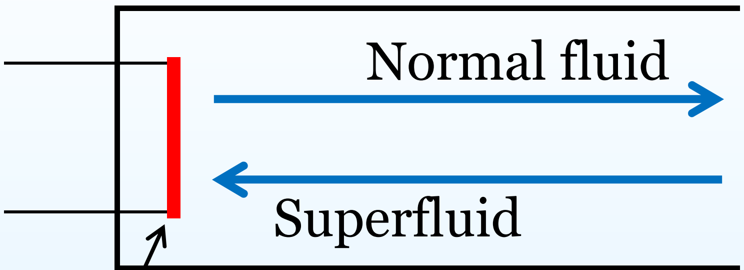

thermally driven flow
(e.g. heater)

Counterflow: $j = 0$

$$\rho_n v_n = -\rho_s v_s$$

(on average, at large scales)

Counterflow velocity v_{ns}

$$v_{ns} = v_n - v_s = \frac{q}{\rho S T}\left(1 + \frac{\rho_n}{\rho_s}\right) = \frac{q}{\rho_s S T}$$

mechanically driven flow
(e.g. piston)

Coflow: $j \neq 0$

$$v_n = v_s$$

(on average, at large scales)

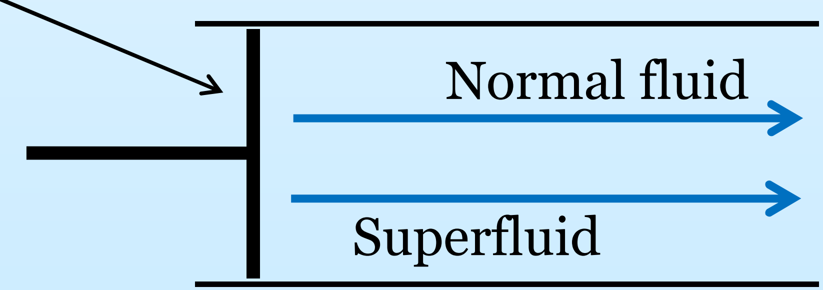

Coflow

Oscillating cylinder

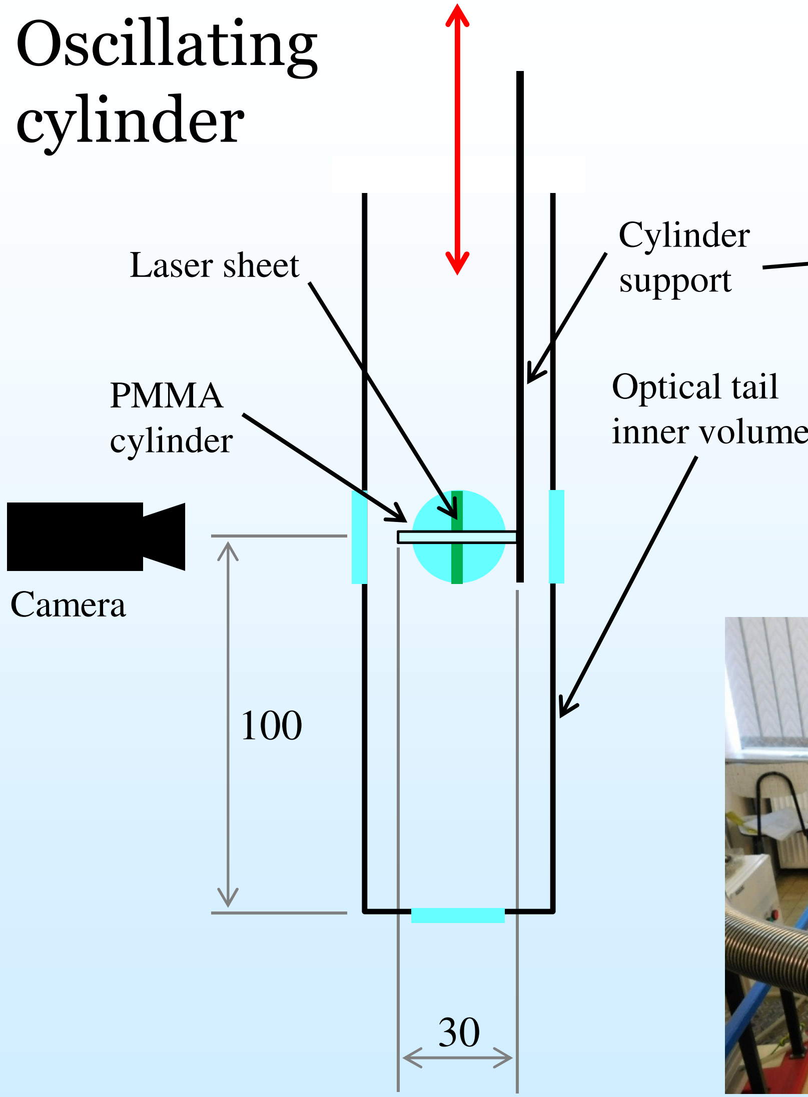

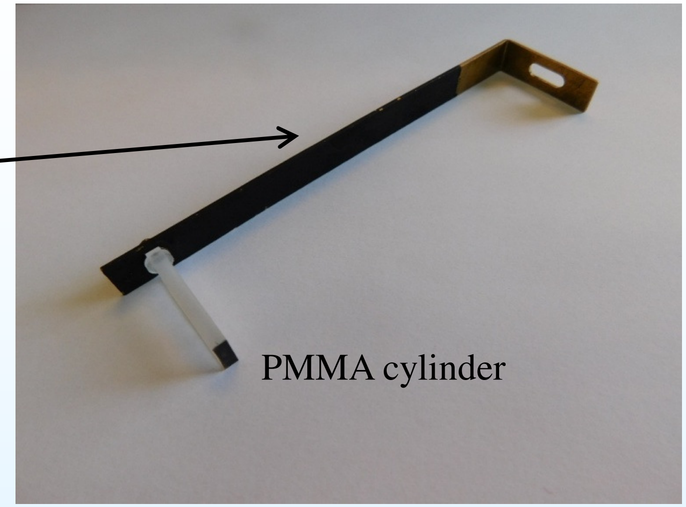

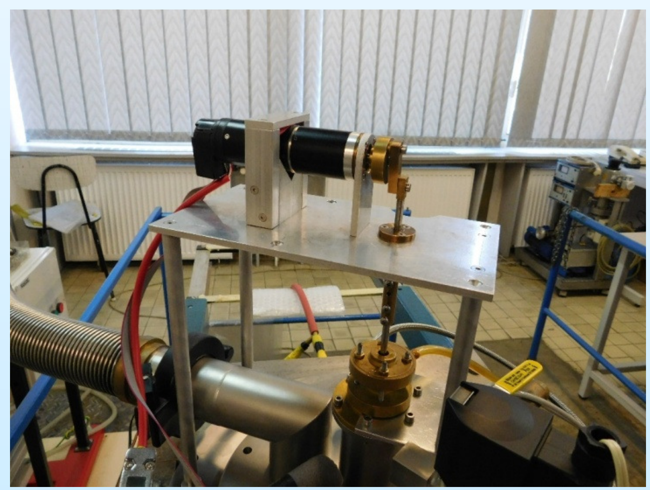

Motor
(on top of the cryostat)

- 30-mm long PMMA cylinder of rectangular cross section (3 mm high and 10 mm wide)
- vertical oscillations, perpendicular to the section width, in the middle of the cryostat optical tail, of 5 or 10 mm amplitude *a* and frequency *f* between 0.05 and 1.25 Hz

Oscillating cylinder

T = 1.3 K; f = 0.5 Hz; a = 10 mm; 100 fps (shown at 25 fps); 1 cycle; 34 mm (1280 px) wide and 21 mm (800 px) high field of view

Lagrangian pseudovorticity θ

Phase averaging: particle trajectories calculated during the same time interval in each cycle, i.e., tracks that have the same phase φ, are analysed together, in order to gather more information on the oscillatory motion.

We introduce the parameter θ, with the same dimensions as vorticity, which depends on the position r on a chosen grid and motion phase φ, and is defined as

$$\theta(r,\varphi) = \frac{1}{M} \sum_{|r-r_i|<R_M} \sum_{|\varphi-\varphi_i|<\Phi} \frac{\left[(r_i - r)\times v_i\right]_z}{|r_i - r|^2}$$

where M is the number of trajectory points,
φ_i indicates the phase of the i-th point,
r_i denotes its position and v_i is its velocity,
calculated (linearly) from the particle positions.
The chosen parameters are R_M = 200 px and Φ = 7.5 deg.

Oscillating cylinder

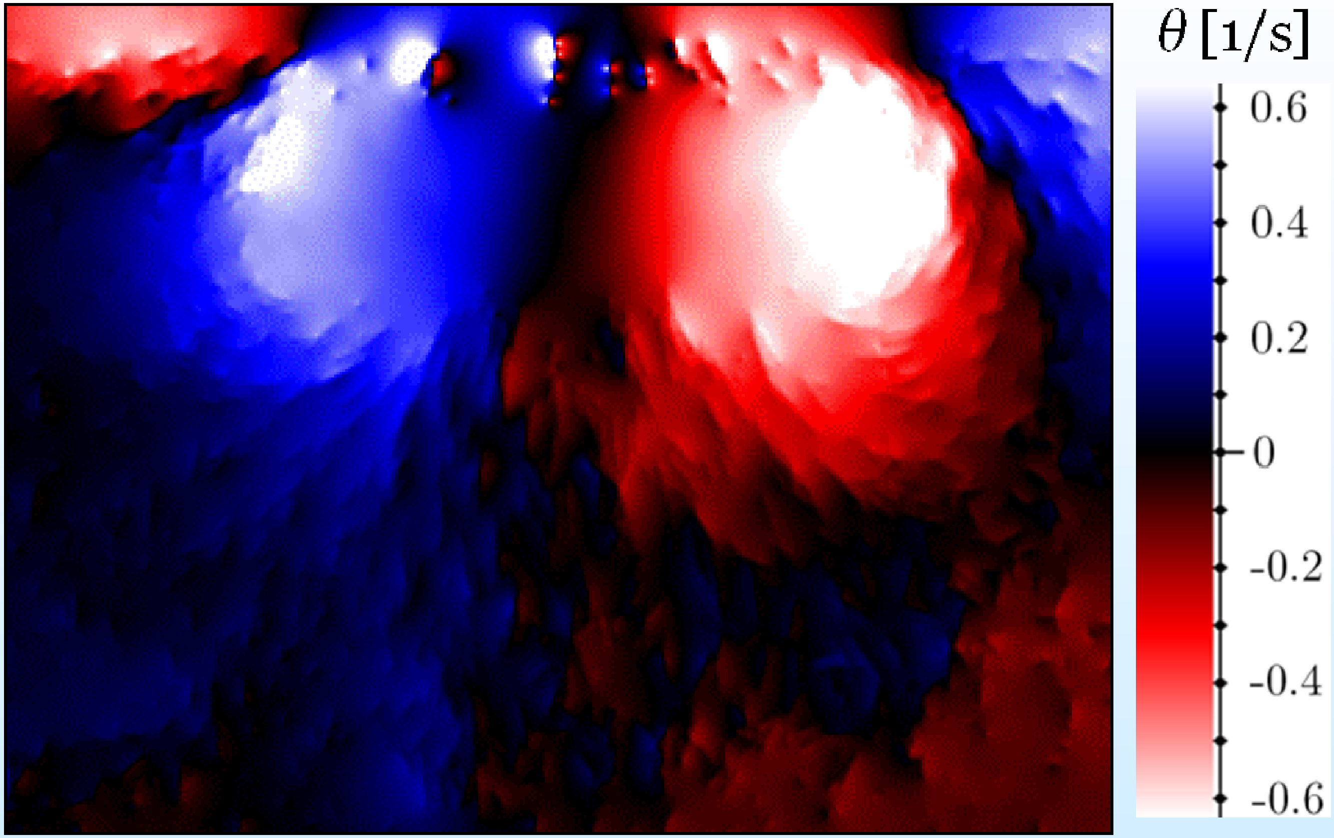

T = 1.3 K; f = 0.5 Hz; a = 10 mm; 12 fps (one image every 15 deg); 1 cycle; 21 mm (800 px) wide and 16 mm (600 px) high field of view

Experimental and quantum scales

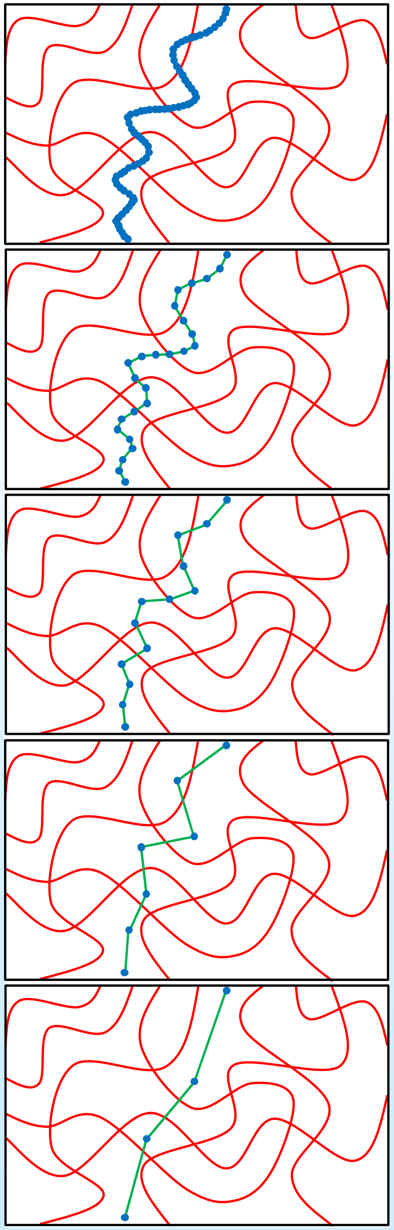

Physical (quantum) scales

• Quantum vortex core ≈ 10^{-10} m

• Mean distance between quantized vortices ≈ 10^{-4} m
(loosely related to the Kolmogorov dissipative scale of classical turbulent flows of viscous fluids)

• Outer flow scale ≈ 10^{-1} m
(of the order of the experimental volume size)

Experimental scales

• Particle size ≈ 10^{-5} m

• Distance travelled by particles between frames can be larger than the particle size and can be tuned (in various ways)

Experimental and quantum scales

Smallest length scale: particle size d, few μm; time t between frames, 0.01 s

Length scale probed by the particles: $\boxed{\ell_{exp} = 2\pi f a t \geq d}$

Flow length scale: mean distance between quantized vortices $\boxed{\ell_q}$ for He II ($\nu = \kappa/6$) and Kolmogorov length scale $\boxed{\eta}$ for He I ($\nu = \mu_n/\rho$)

Flow length scale

$$\ell_f = \ell_q = \eta = \left(\frac{\nu^2}{\langle \theta^2 \rangle} \right)^{1/4}$$

Flow time scale

$$t_f = \frac{\ell_f}{2\pi f a}$$

$$R = \frac{\ell_{exp}}{\ell_f} = \frac{t}{t_f} = 2\pi f a t \left(\frac{\nu^2}{\langle \theta^2 \rangle} \right)^{-1/4}$$

R is always larger than 0.01 and smaller than 100

Oscillating cylinder

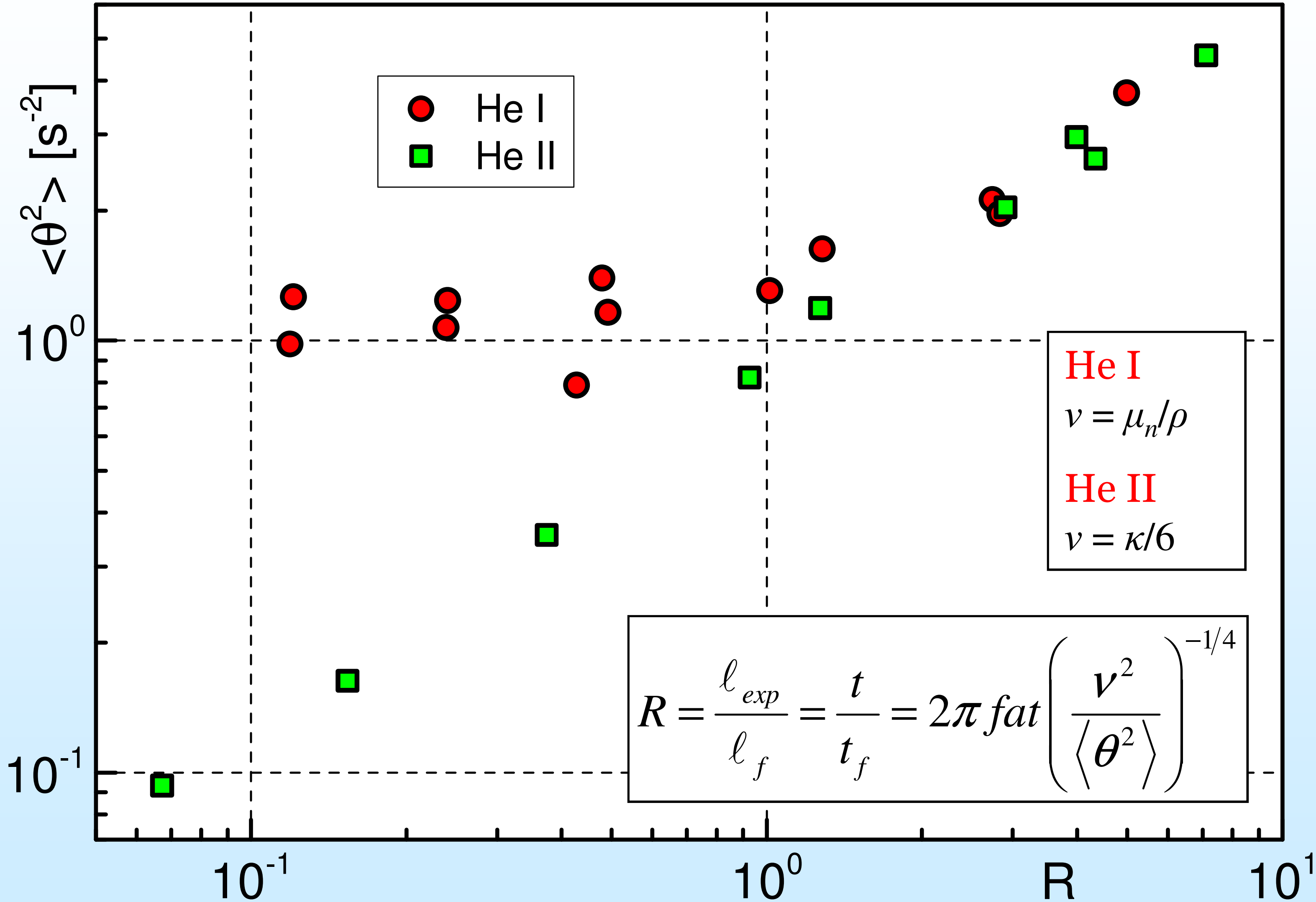

D Duda, P Švančara, M La Mantia, M Rotter, L Skrbek **Phys Rev B** 92, 064519 (2015)

Counterflow

Counterflow channel

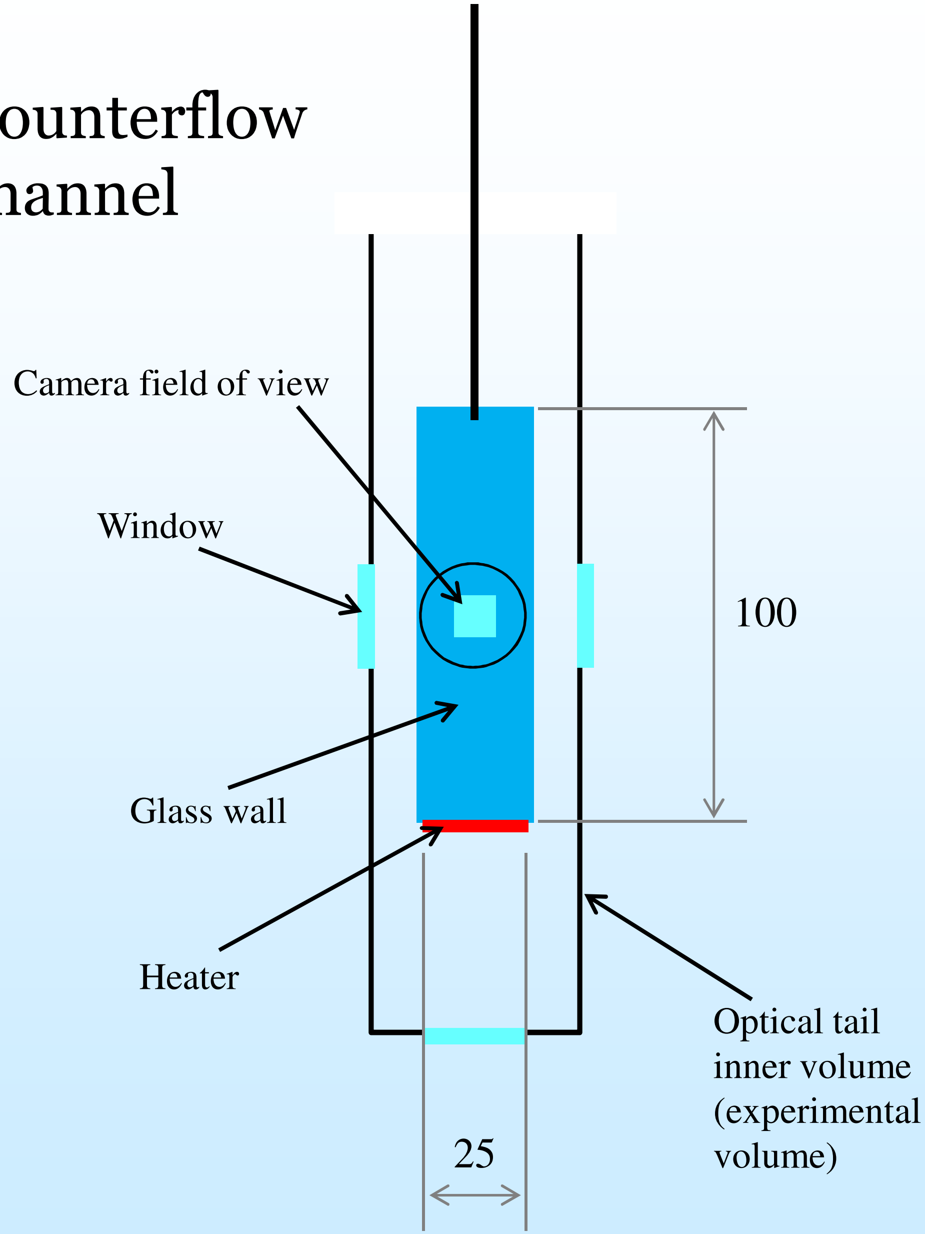

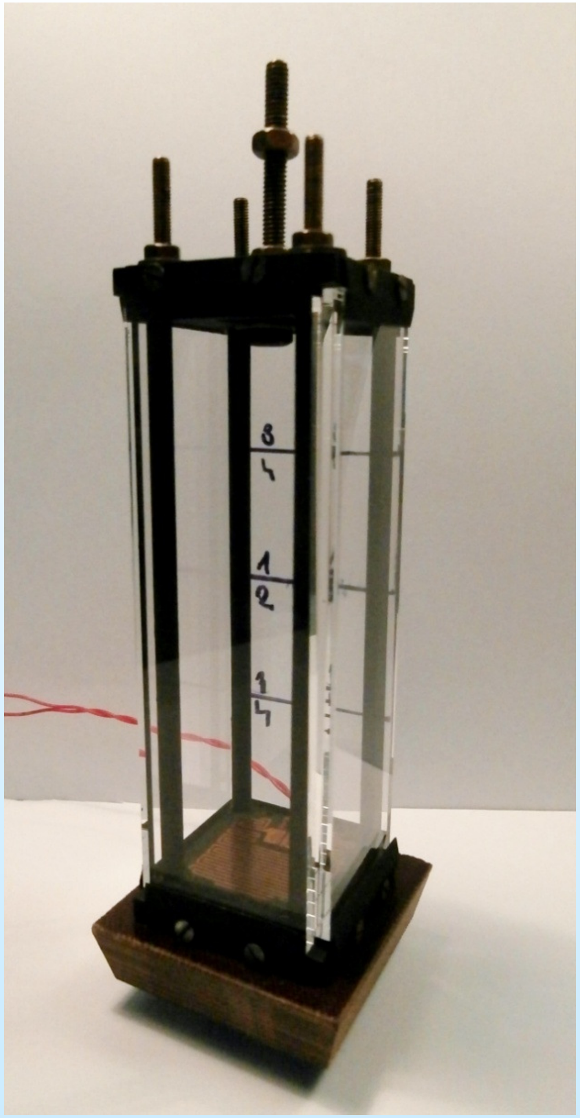

Counterflow

The movie shows micrometer-size solid deuterium particles at 1.66 K, with an applied heat flux of 492 W/m^2 (13 mm wide and 8 mm high field of view; movie taken at 100 fps).

Experimental and quantum scales

Smallest length scale: particle size d, few μm; time t between particle positions; mean particle velocity V_{abs} at the smallest t, few ms

Length scale probed by the particles: $\boxed{\ell_{exp} = V_{abs} t \geq d}$

Quantum length scale

$$\boxed{\ell_q = \frac{1}{\sqrt{L}} = \frac{1}{\gamma(T,G)\,v_{ns}(T,q)}}$$

Quantum time scale

$$\boxed{t_q = \frac{\ell_q}{V_{abs}}}$$

$$\boxed{R = \frac{\ell_{exp}}{\ell_q} = \frac{V_{abs} t}{\ell_q} = \frac{t}{t_q} = \left[\gamma(T,G)\,v_{ns}(T,q)\,V_{abs}\right] t}$$

R is always larger than 0.01 and smaller than 100

$$\mathrm{PDF}(v) \propto |v|^{-3} \text{ for large } v$$

Results: velocity PDFs

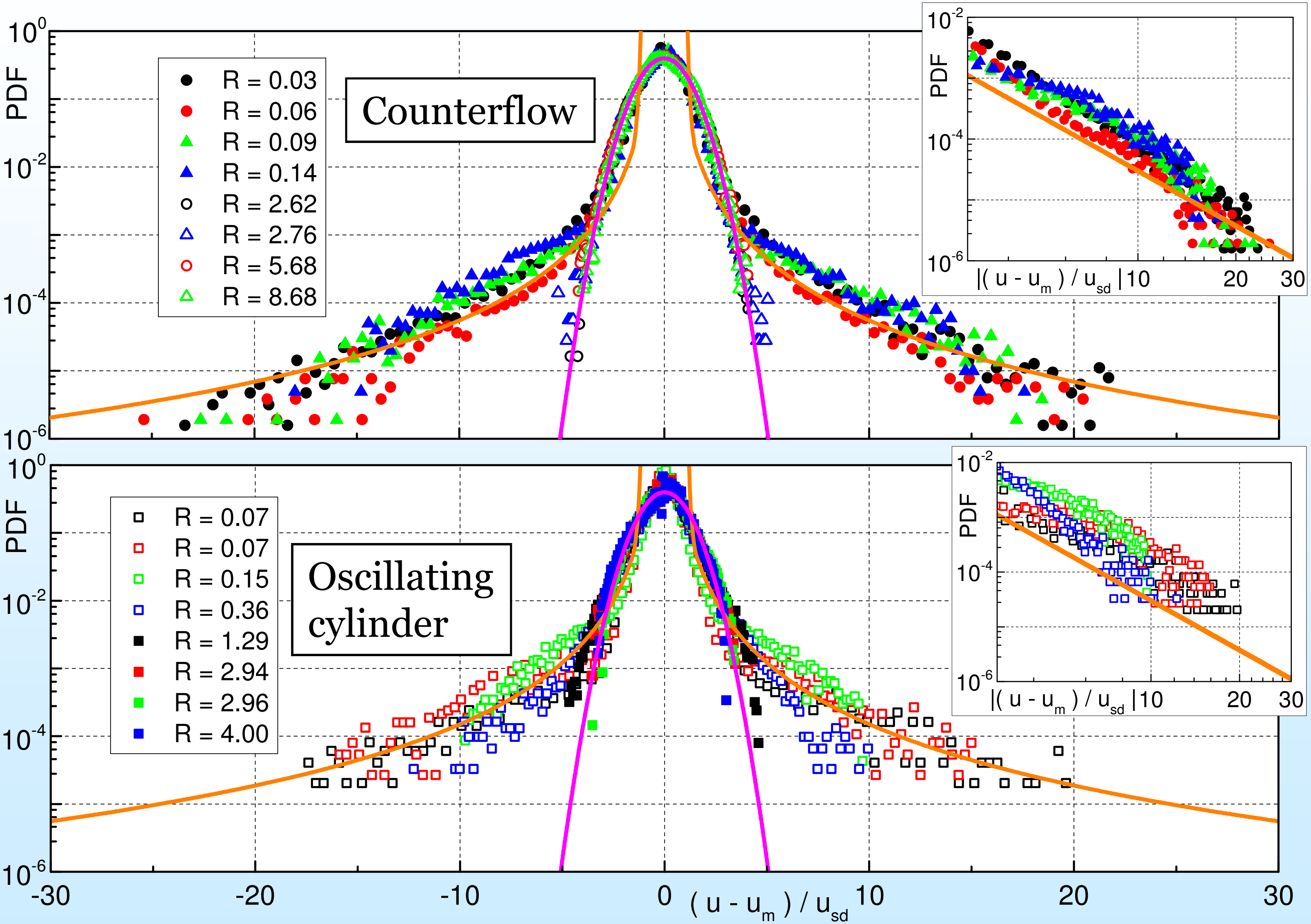

M La Mantia, P Švančara, D Duda, L Skrbek **Phys Rev B** 94, 184512 (2016)

Power-law tails

$$\boxed{v = \frac{\kappa}{2\pi r}}$$

fluid velocity around a straight vortex, with circulation κ, at a distance (radius) r from the vortex core

$$\boxed{\Pr_v(v) = |dr/dv| \Pr_r[r(v)]}$$

$$\boxed{\Pr_v(v)\,dv}$$

probability of observing a velocity between v and $v + dv$ at any radius

$$\boxed{\Pr_r(r)\,dr \propto r \propto v^{-1}}$$

probability of taking a measurement at a radius between r and $r + dr$

$$\boxed{\Pr_v(v) = |dr/dv| \Pr_r(r) \propto |v|^{-3}}$$

consistent with the experimental data

MP Rast, and JF Pinton **Phys Rev E** 79, 046314 (2009)
MS Paoletti, DP Lathrop **Annu Rev Condens Matter Phys** 2, 213 (2011)
AW Baggaley, CF Barenghi **Phys Rev E** 89, 033006 (2014)
M La Mantia, L Skrbek **Phys Rev B** 90, 014519 (2014)

Vortex reconnections

MS Paoletti, ME Fisher, KR Sreenivasan, DP Lathrop **Phys Rev Lett** 101, 154501 (2008)

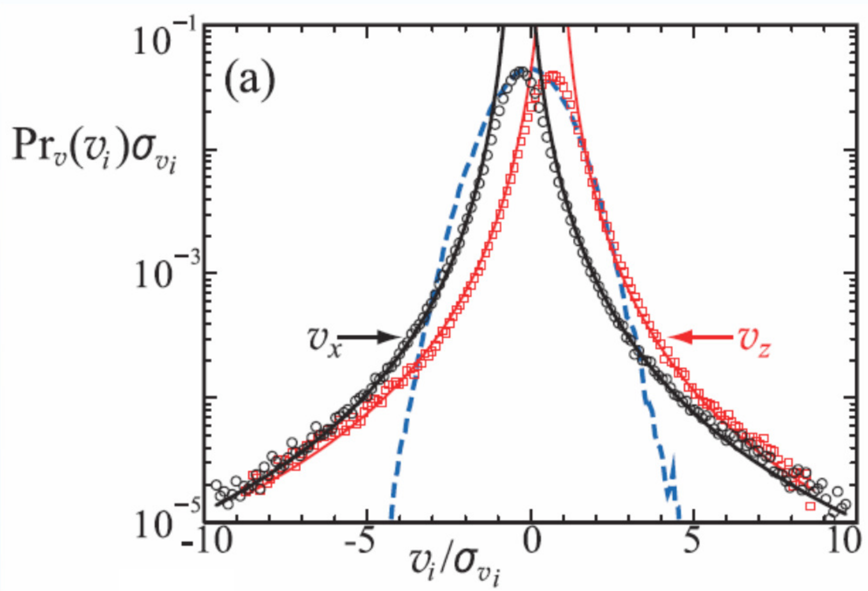

FIG. 3 (color). Local velocity and energy statistics derived from the data in Fig. 2 for all particle trajectories with $t > t_{\mathrm{off}}$ (computed from over 1.1×10^6 values of velocity). All distributions are scaled to give unit variance using $\sigma_{v_x} = 0.066$, $\sigma_{v_z} = 0.074$ cm/s, or $\sigma_E = 0.017$ (cm/s)^2. (a) Probability distribution function of v_x (black circles) and v_z (red squares). The solid lines are fits to $\mathrm{Pr}_v(v_i) = a|v_i - \bar{v}_i|^{-3}$, where i is either x (black) or z (red) and $\bar{v}_i$ is the mean value of v_i. For comparison, the dashed (blue) line shows the distribution for classical turbulence in water [32] computed from over 10^7 velocity values. The distribution is scaled using $\sigma_v = 0.25$ cm/s and with a peak value matched to the v_x data. The velocity statistics in water are close-to-Gaussian over five decades in probability.

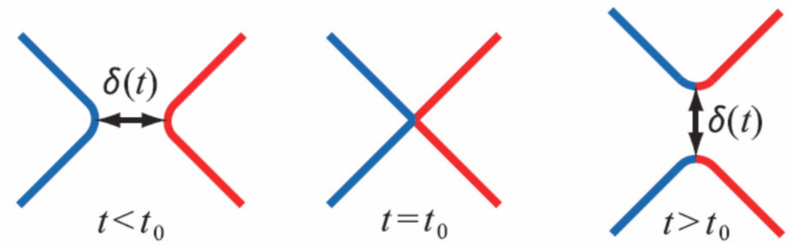

FIG. 1 (color). Depiction of one-dimensional topological vortices that reconnect by merging at the moment t_0 and then separate [25]; the minimum separation distance is $\delta(t)$, with $\delta(t_0) = 0$.

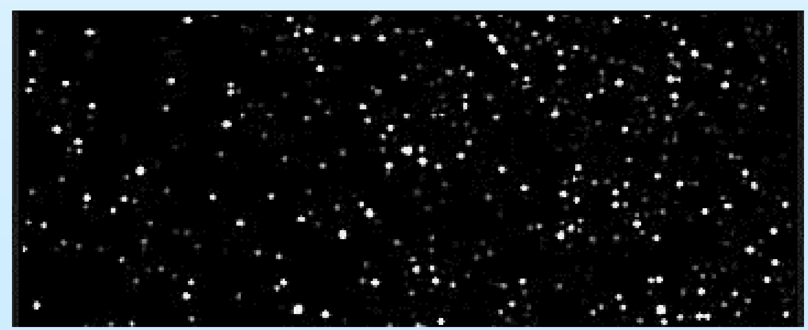

Vortex reconnections

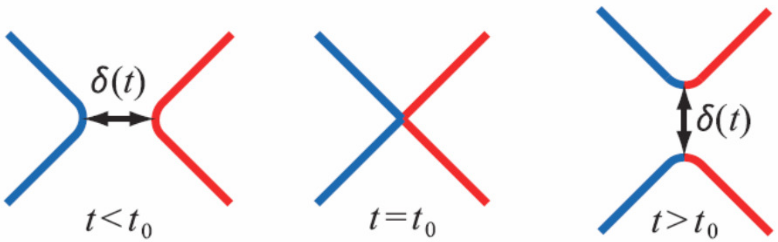

FIG. 1 (color). Depiction of one-dimensional topological vortices that reconnect by merging at the moment t_0 and then separate [25]; the minimum separation distance is $\delta(t)$, with $\delta(t_0) = 0$.

$$\boxed{\delta(t) = A\sqrt{\kappa|t-t_0|}}$$

$$\boxed{v(t) \propto |t-t_0|^{-1/2}}$$

$$\boxed{\Pr_v(v) = |dt/dv| \Pr_t[t(v)]}$$

$\boxed{\Pr_v(v)\,dv}$ probability of observing a velocity between v and $v + dv$ at any time

$\boxed{\Pr_t(t)\,dt}$ uniform probability of taking a measurement at a time between t and $t + dt$

$\boxed{\Pr_v(v) \propto |dt/dv| \propto |v|^{-3}}$ for large velocities (small times)

consistent with the experimental data: particles trapped onto vortices

MS Paoletti, ME Fisher, KR Sreenivasan, DP Lathrop **Phys Rev Lett** 101, 154501 (2008)
MS Paoletti, ME Fisher, DP Lathrop **Physica D** 239, 1367 (2010)

$$\mathrm{PDF}(v) \propto |v|^{-3} \text{ for large } v$$

Results: velocity PDFs

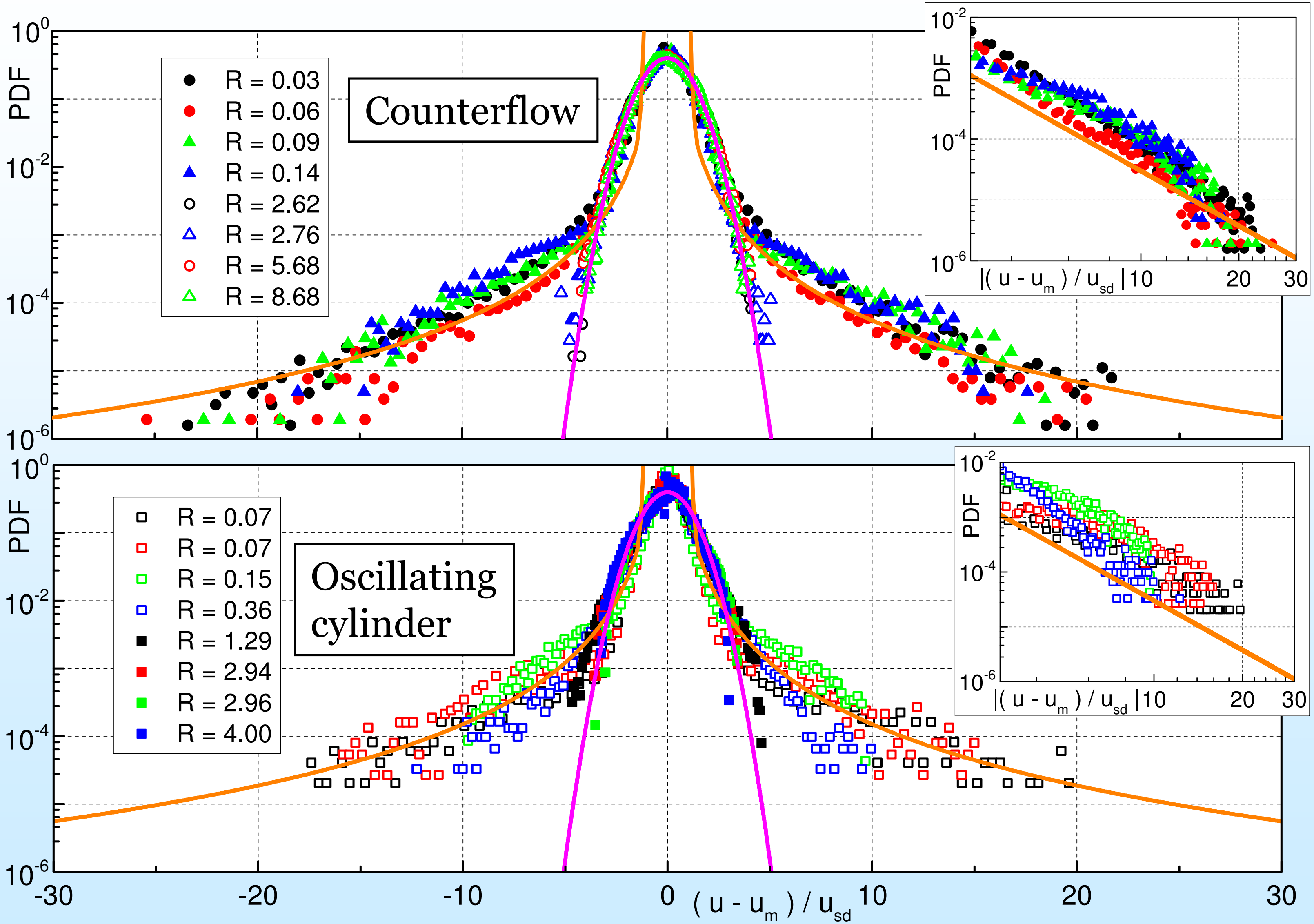

M La Mantia, P Švančara, D Duda, L Skrbek **Phys Rev B** 94, 184512 (2016)

Velocity PDF tails: upper limit

$$\boxed{F_{VT} = 2\frac{\rho_s \kappa^2}{4\pi}\ln\left(\frac{r_p}{\xi}\right)}$$

vortex tension force due to two vortex strands attached to a spherical particle

$$\boxed{F_S = 6\pi\mu_n r_p \left(u_f - u_p\right)}$$

Stokes drag force

for $u_f = 0$ (trapped particle) and for F_{VT} parallel to F_S
the velocity threshold for the trapped particle to break free is

$$\boxed{u_p = \frac{\rho_s \kappa^2}{12\pi^2 \mu_n r_p}\ln\left(\frac{r_p}{\xi}\right)}$$

consistent with the experimental data: particles trapped onto vortices probe the occurrence of quantized vortex reconnections

M La Mantia, P Švančara, D Duda, L Skrbek **Phys Rev B** 94, 184512 (2016)

$$\mathrm{PDF}(v) \propto |v|^{-3} \text{ for large } v$$

Results: velocity PDFs

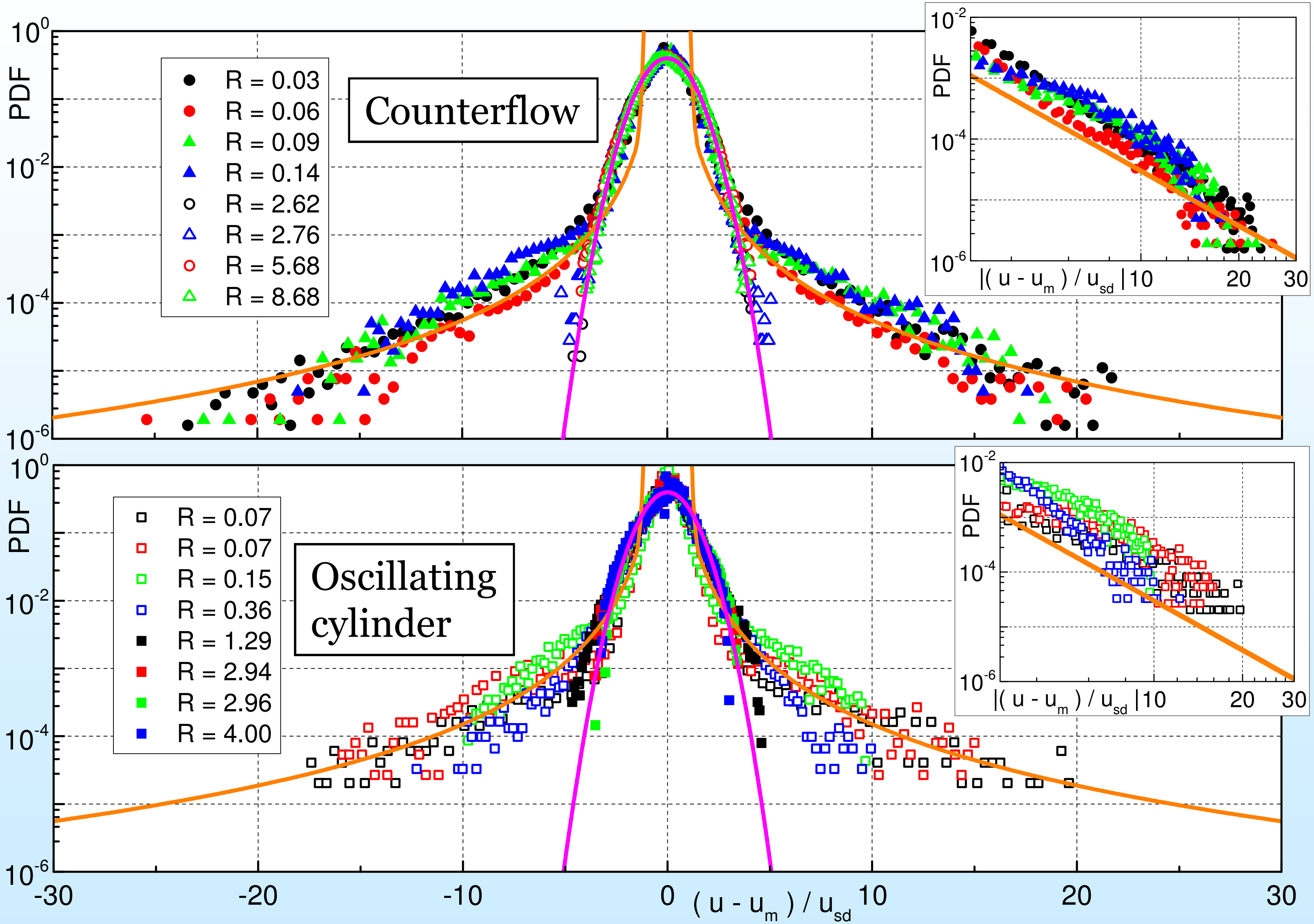

M La Mantia, P Švančara, D Duda, L Skrbek **Phys Rev B** 94, 184512 (2016)

Velocity PDF tails: lower limit

Particle equation of motion

$$\boxed{\rho_p \frac{du_p}{dt} = \rho_f \frac{Du_f}{Dt} + C\rho_f\left(\frac{Du_f}{Dt} - \frac{du_p}{dt}\right) + \ldots}$$

$$\boxed{\left(\rho_p + C\rho_f\right)\frac{du_p}{dt} = \rho_f\left(1+C\right)\frac{Du_f}{Dt} + \frac{F_S}{V_p} + \ldots}$$

If we assume that the only contribution to the fluid acceleration is due to the velocity field of a straight quantized vortex (perpendicular to the mean flow direction) and that the particle acceleration is null, we obtain …

YA Sergeev, CF Barenghi **J Low Temp Phys** 157, 429 (2009)
M La Mantia, L Skrbek **Phys Rev B** 90, 014519 (2014)
M La Mantia, P Švančara, D Duda, L Skrbek **Phys Rev B** 94, 184512 (2016)

Velocity PDF tails: lower limit

$$\boxed{\rho_s (1+C) V_p \frac{Du_s}{Dt} = F_S = 6\pi\mu_n r_p \left(u_f - u_p\right)}$$

$$\boxed{u_s = \frac{\kappa}{2\pi r}}$$

$$\boxed{\frac{Du_s}{Dt} = -\frac{\kappa^2}{4\pi^2 r^3}}$$

all particles (regardless of their density) are attracted to quantized vortices also in the absence of viscosity

$$\boxed{u_t = \frac{\rho_s \kappa^2}{12\pi^2 \mu_n r_p} = u_f - u_p}$$

velocity before trapping occurs, positive in the direction toward the vortex core

consistent with the experimental data: particles trapped onto vortices probe the occurrence of quantized vortex reconnections

M La Mantia, P Švančara, D Duda, L Skrbek **Phys Rev B** 94, 184512 (2016)

Vortex reconnections: kinetic energy

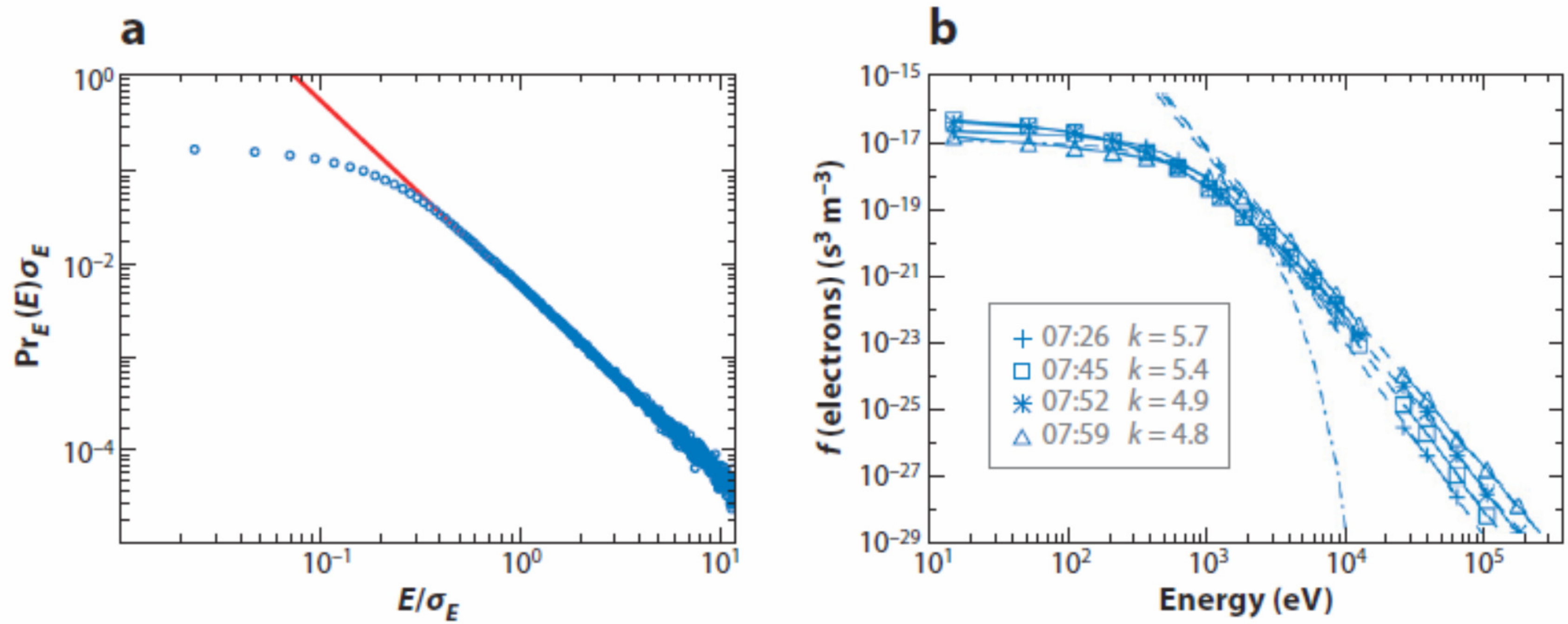

Figure 7

Distributions of the kinetic energy for (*a*) decaying counterflow turbulence in He II from Paoletti et al. (77), compared to (*b*) those of electrons (presumably) accelerated by magnetic reconnection in the diffusion region of Earth's magnetotail observed by Øieroset et al. (89). The solid lines are fits to (*a*) $\mathrm{Pr}_E = aE^{-2}$ and (*b*) $f = E^{-k}$, with k denoted in the legend.

MS Paoletti, DP Lathrop **Annu Rev Condens Matter Phys** 2, 213 (2011)
MS Paoletti, ME Fisher, KR Sreenivasan, DP Lathrop **Phys Rev Lett** 101, 154501 (2008)
M Øieroset, RP Lin, TD Phan, DE Larson, SD Bale **Phys Rev Lett** 89, 195001 (2002)

Vortex reconnections

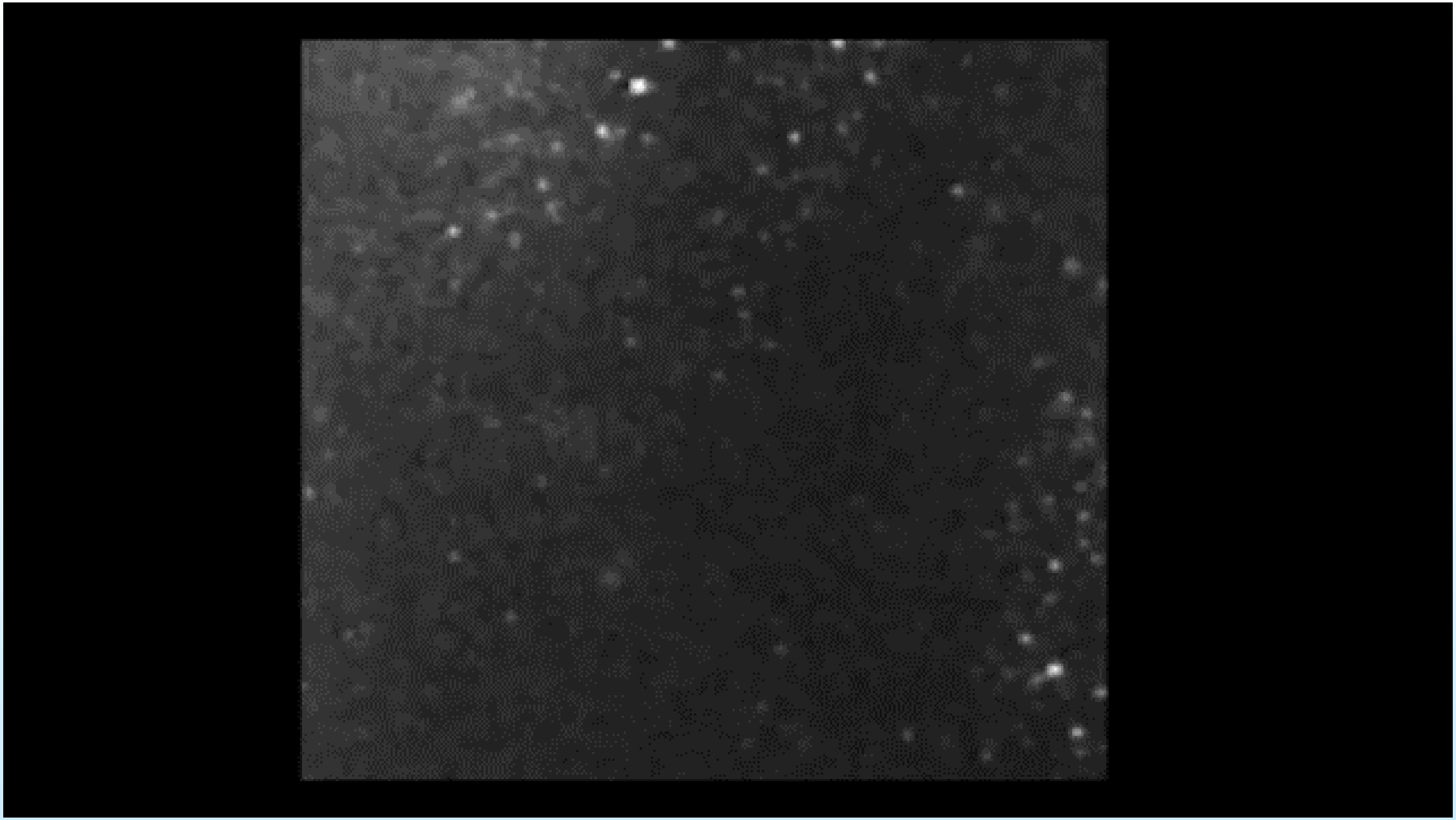

E Fonda, DP Meichle, NT Ouellette, S Hormoz, DP Lathrop **Proc Natl Acad Sci USA** 111, 4707 (2014)

Vortex reconnections

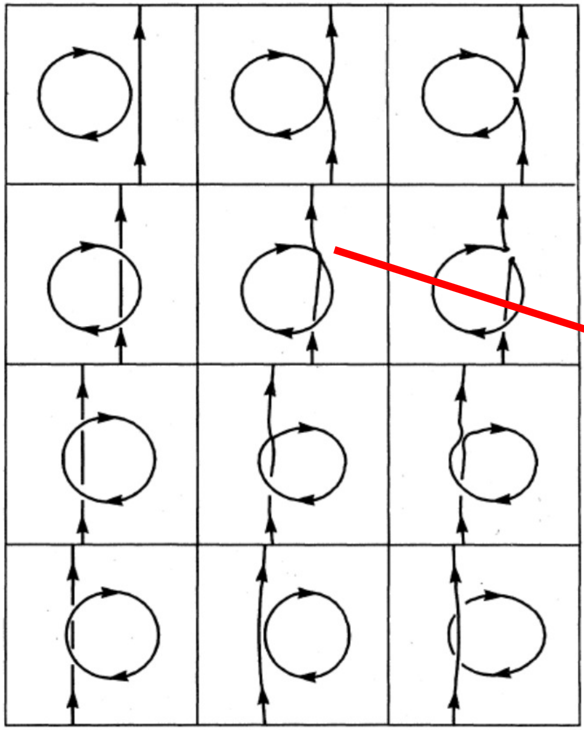

FIG. 16. Crossing encounters between a vortex ring and a line, viewed in the direction of ring propagation. Each row shows the initial configuration with the ring far away from the line, the configuration at the time of closest approach, and the state of the system some time after a microscopic reconnection has been made. The ring is tilted slightly so that the crossing takes place at one point on the line. The bottom row shows the only type of situation where a reconnection does not occur.

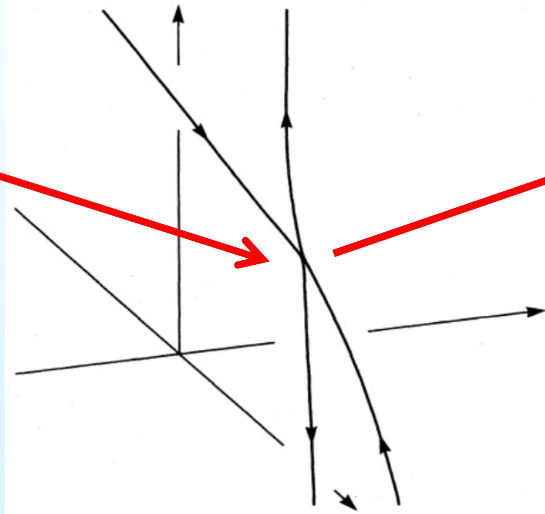

FIG. 17. Close-up perspective view of the line-line reconnection cusp for the situation illustrated in the second row of Fig. 16.

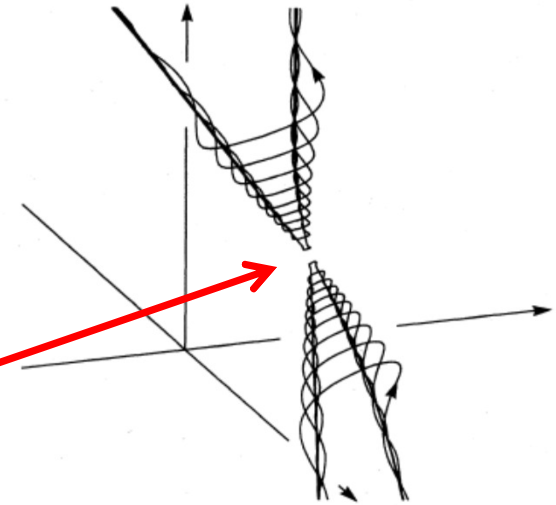

FIG. 18. Perspective view of the behavior after the lines of Fig. 17 are reconnected at the microscopic level.

KW Schwarz **Phys Rev B** 31, 5782 (1985)

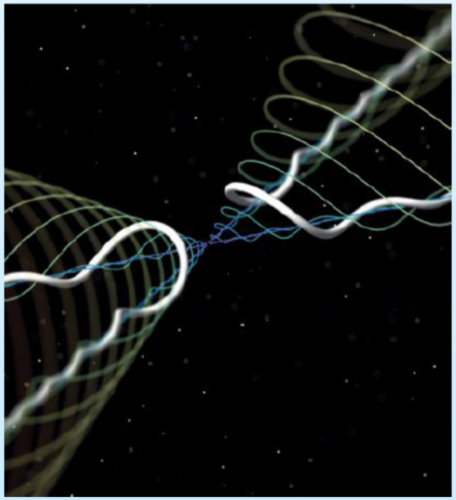

Courtesy of E Fonda

Vortex reconnections

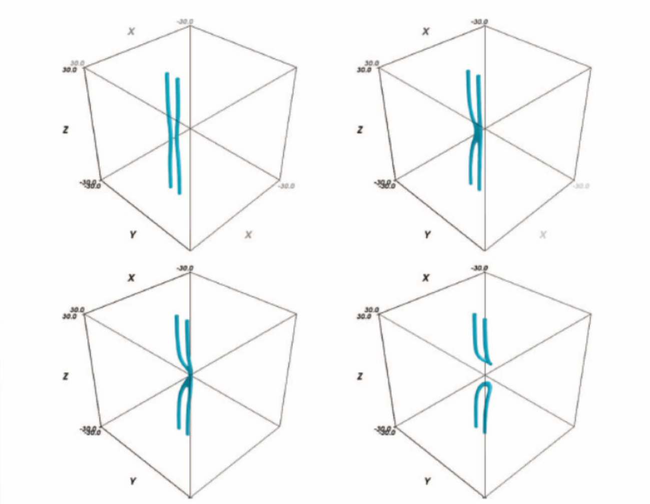

FIG. 3. Snapshots of the evolution of two anti-parallel vortices (angle between vortices $\beta = \pi$), initially slightly perturbed to enhance the Crow instability, at $t = 0$ (top left), $t = 20$ (top right), $t = 30$ (bottom left), and $t = 40$ (bottom right). Isosurfaces of $\rho = 0.2$ are plotted to visualize the vortex cores (enhanced online). [URL: http://dx.doi.org/10.1063/1.4772198.1]

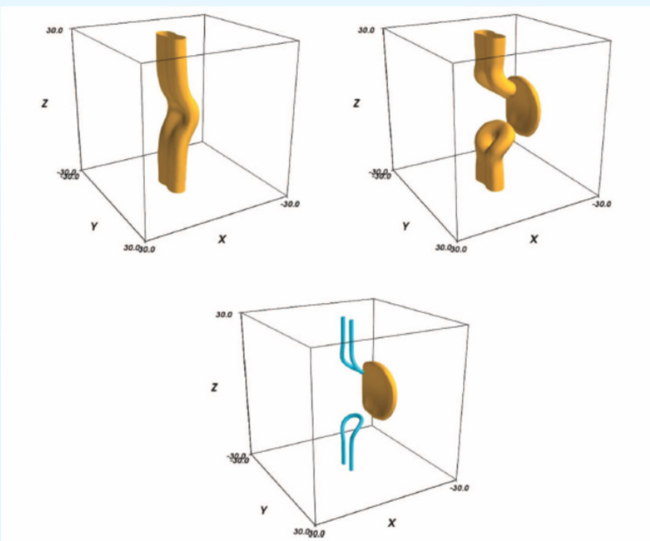

FIG. 8. Isosurfaces at $\rho = 0.94$ before (left, $t = 37$) and after (right and bottom, $t = 54$) reconnection for two anti-parallel vortices (angle between vortices $\beta = \pi$). Note the mushroom-shaped rarefaction wave which moves away.

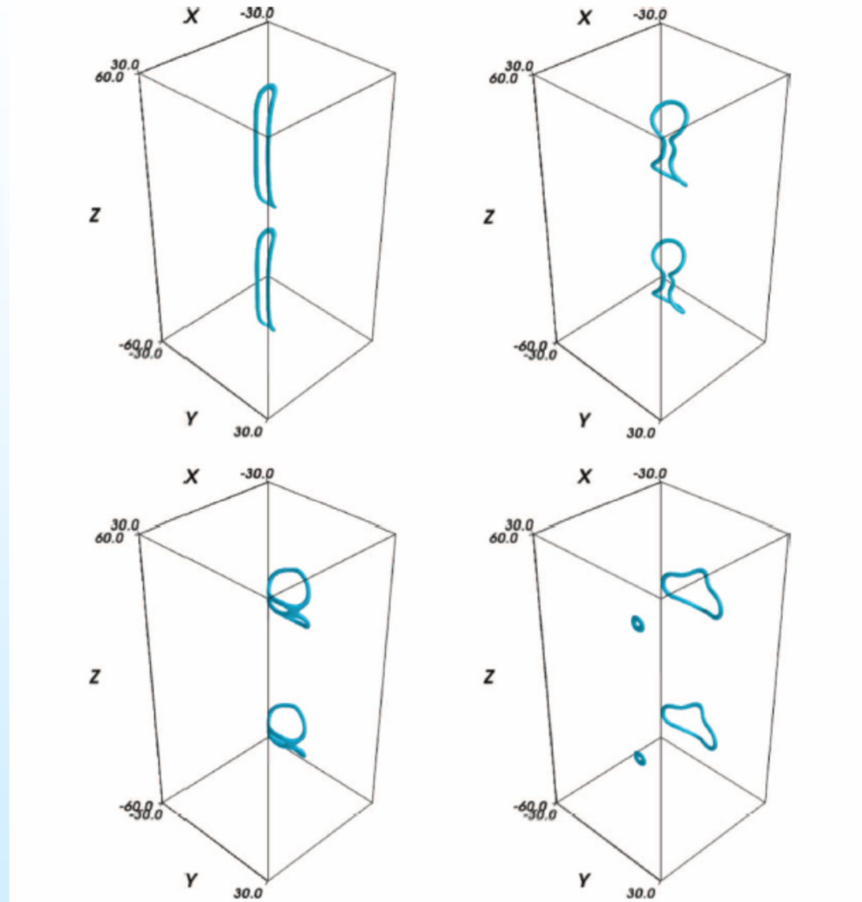

FIG. 11. Snapshots of the evolution of two anti-parallel vortices (angle $\beta = \pi$) initially slightly perturbed to enhance the Crow instability, at $t = 40$ (top left), $t = 80$ (top right), $t = 120$ (bottom left), and $t = 160$ (bottom right). Isosurfaces of $\rho = 0.2$ are plotted to visualize the vortex cores. The initial condition is the same as in Figure 3 but the computational box was extended to $-60 \le z \le 60$ to visualize the formation of vortex rings.

S Zuccher, M Caliari, AW Baggaley, CF Barenghi **Phys Fluids** 24, 125108 (2012)

Vortex reconnections

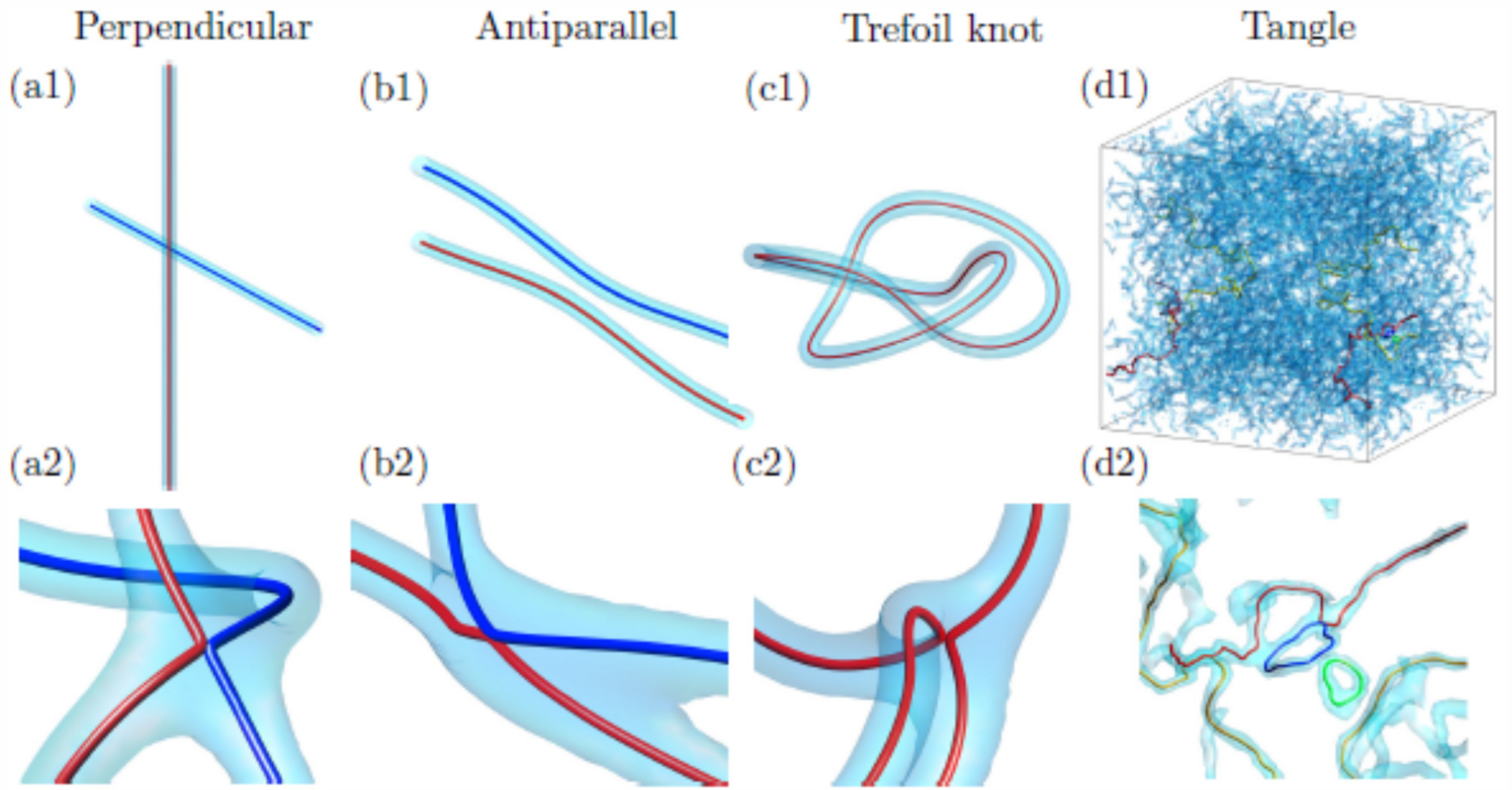

FIG. 1. Three-dimensional plot showing the reconnection events explored numerically. The initial configuration is displayed for (a1) the perpendicular vortex lines, (b1) the antiparallel lines, and (c1) the trefoil knot. (a2)–(c2) show a corresponding zoom at the moment of reconnection. Also shown are (d1) the turbulent tangle and (d2) a zoom in of where a reconnection takes place. Red and blue correspond to the reconnecting vortex filaments; the light blue isosurfaces render the density field at low values.

A Villois, D Proment, G Krstulovic **Phys Rev Fluids** 2, 044701 (2017)

Vortex reconnections

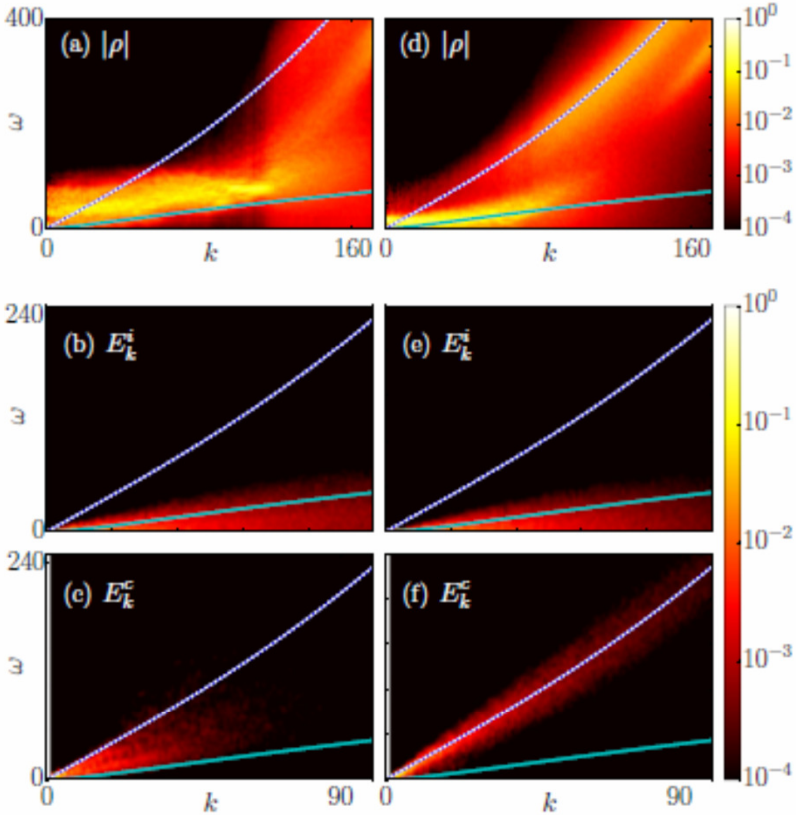

FIG. 4. Spatiotemporal power spectra for the 512^3 GPE run between $t = 0$ and 2 for (a) the mass density ρ, and zooms between $k = 0$ and 100 for (b) the incompressible and (c) compressible velocity. Same for late times ($t \in [8, 10]$) are shown in (d), (e), and (f). The solid (green) curve is the dispersion relation of Kelvin waves, while the dotted (white) curve corresponds to sound waves.

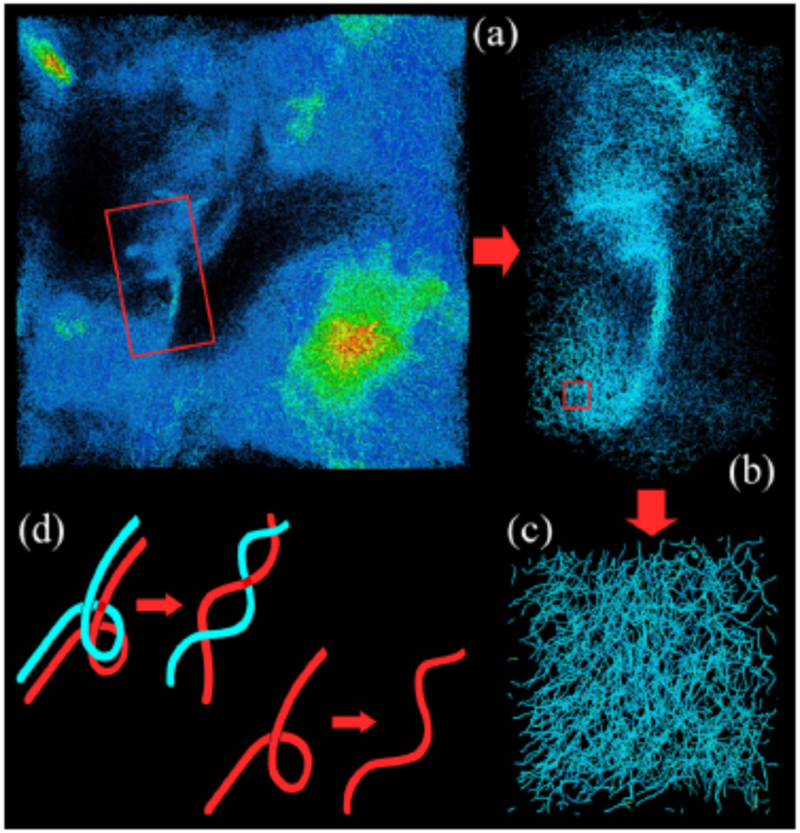

FIG. 5. Three-dimensional rendering of vortex lines at the onset of the decay in the 2048^4 GPE run of (a) a slice of the full box, and successive zooms in (b) and (c) into the regions indicated by the (red) rectangles. (d) Sketch of the transfer of helicity from writhe to twist in a bundle of vortices, and for an individual vortex.

P Clark di Leoni, PD Mininni, ME Brachet **Phys Rev A** 95, 053636 (2017)

Quantum vortex reconnections

- Mechanism of energy transfer

- The initial energy carried by the vortices is not solely employed to drive the vortex motions after reconnection but is also distributed to other processes

- Sound emission and excitation of Kelvin waves

- In the classical (viscous) case, generation of vortical structures smaller than the original ones follows instead reconnection

- Mostly numerical results

$$\mathrm{PDF}(v) \propto |v|^{-3} \text{ for large } v$$

Results: velocity PDFs

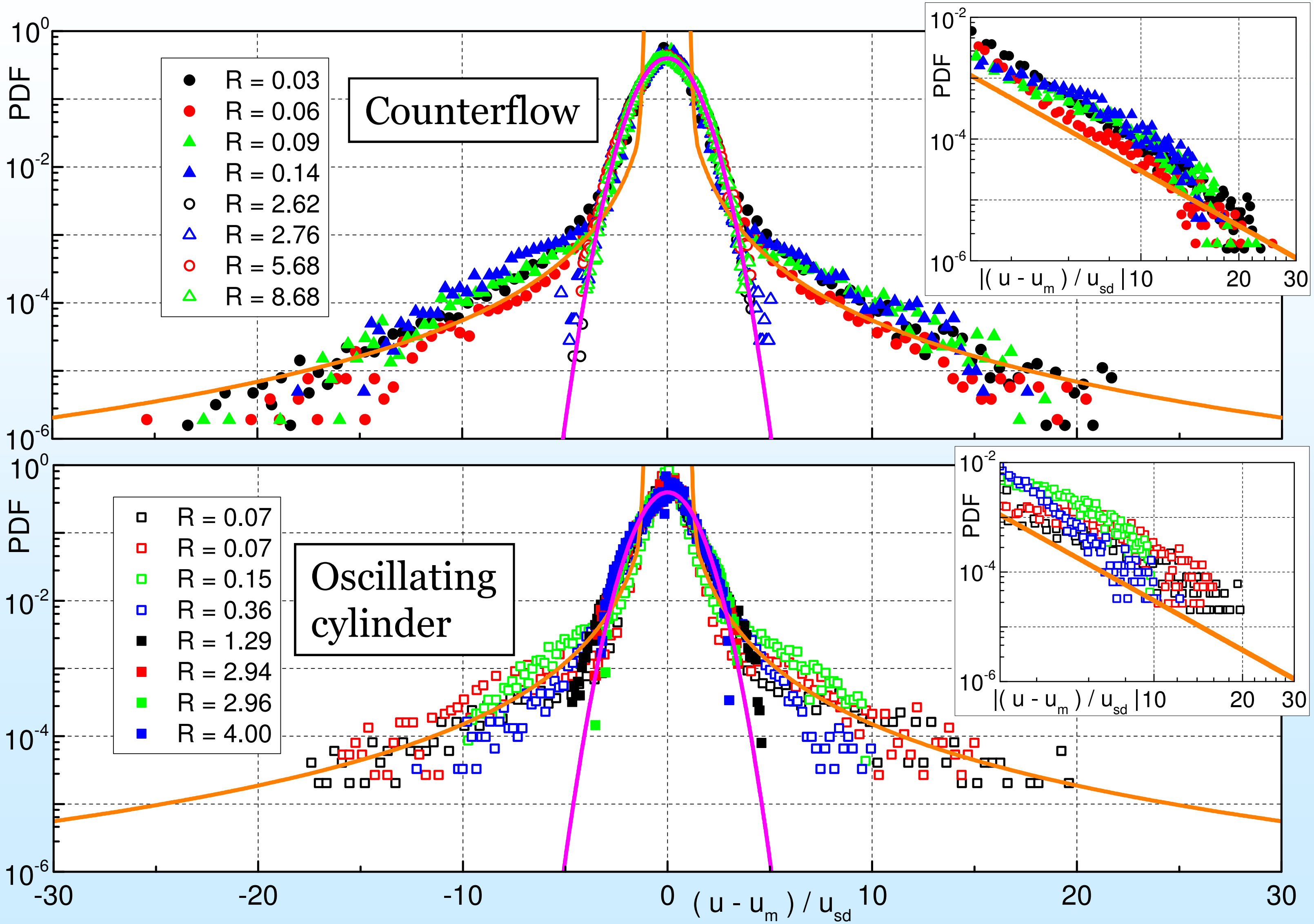

M La Mantia, P Švančara, D Duda, L Skrbek **Phys Rev B** 94, 184512 (2016)

Results: velocity flatness

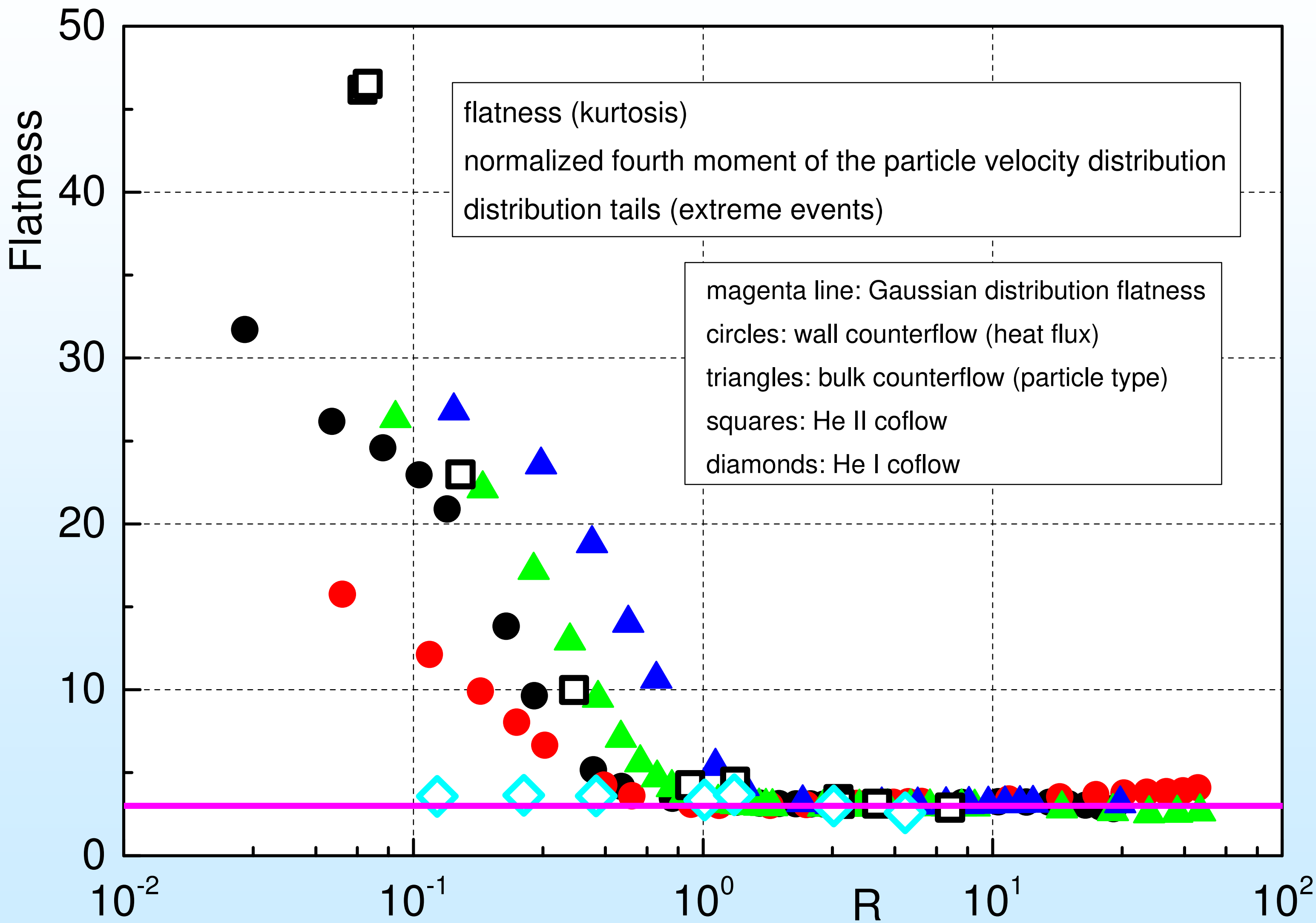

M La Mantia, P Švančara, D Duda, L Skrbek **Phys Rev B** 94, 184512 (2016)

Counterflow in the heater proximity

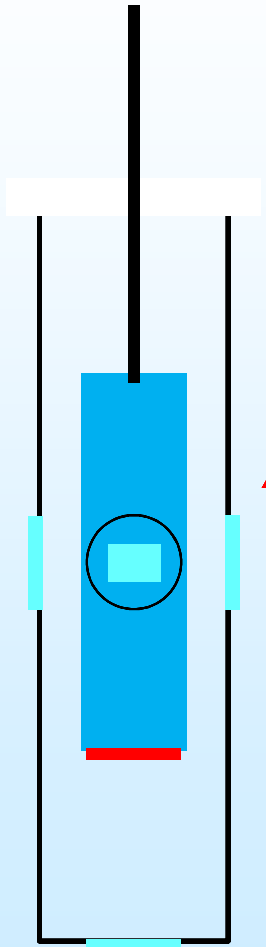

Bulk counterflow
13 mm wide and 8 mm high field of view,
6 mm away from both vertical walls
2 hydraulic diameters from the heater

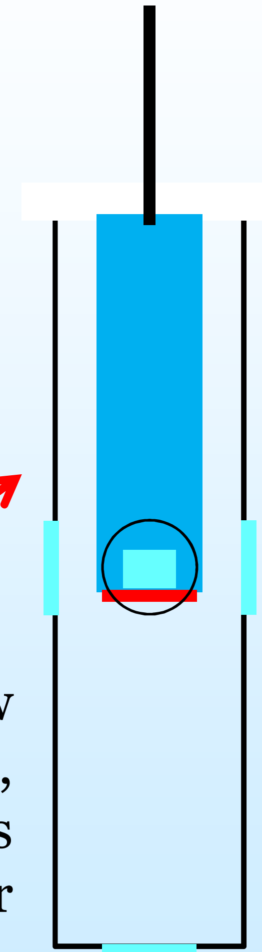

Bulk counterflow
13 mm wide and 8 mm high field of view,
6 mm away from both vertical walls
five times closer to the heater

Results: velocity PDFs

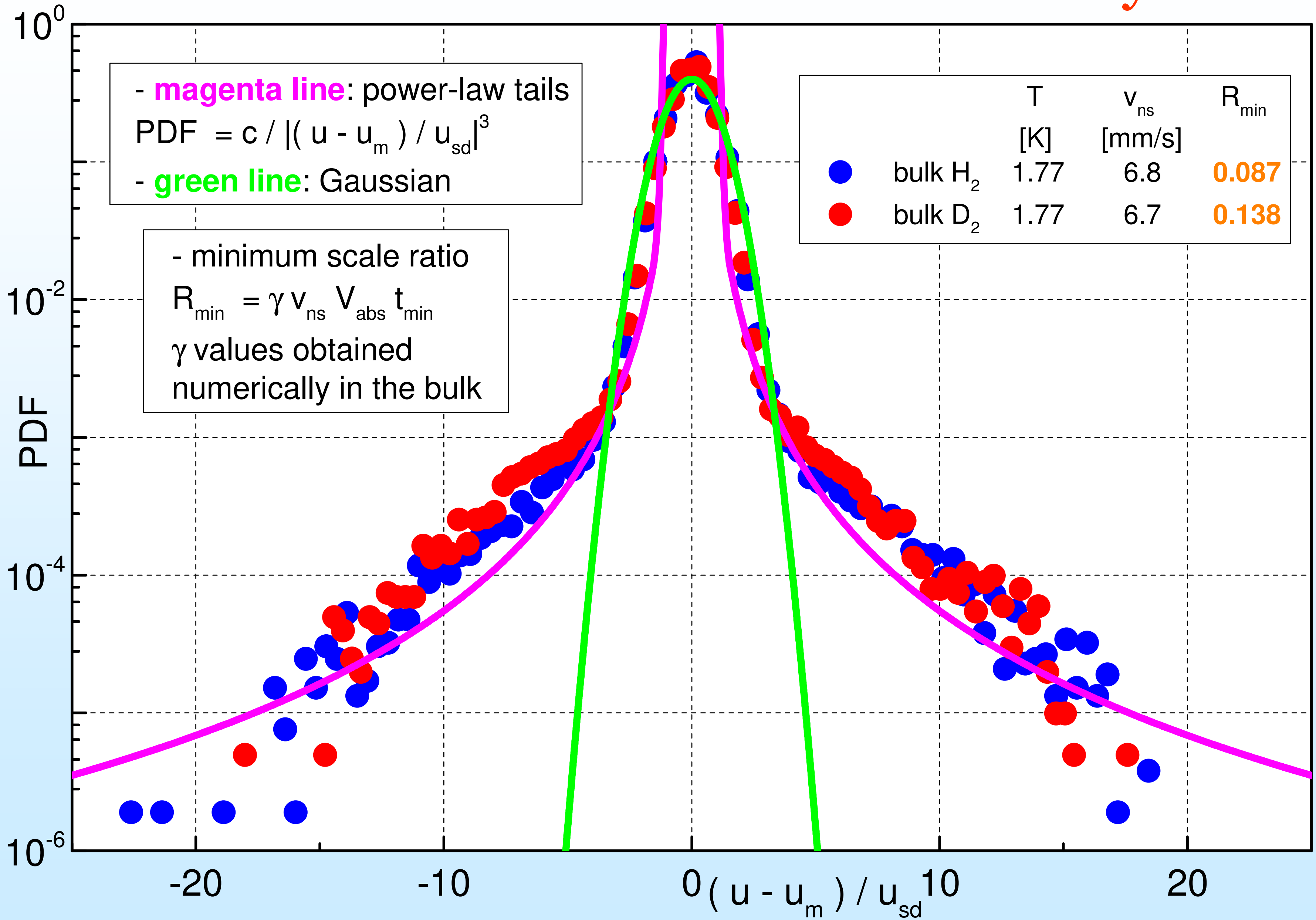

Results: velocity PDFs

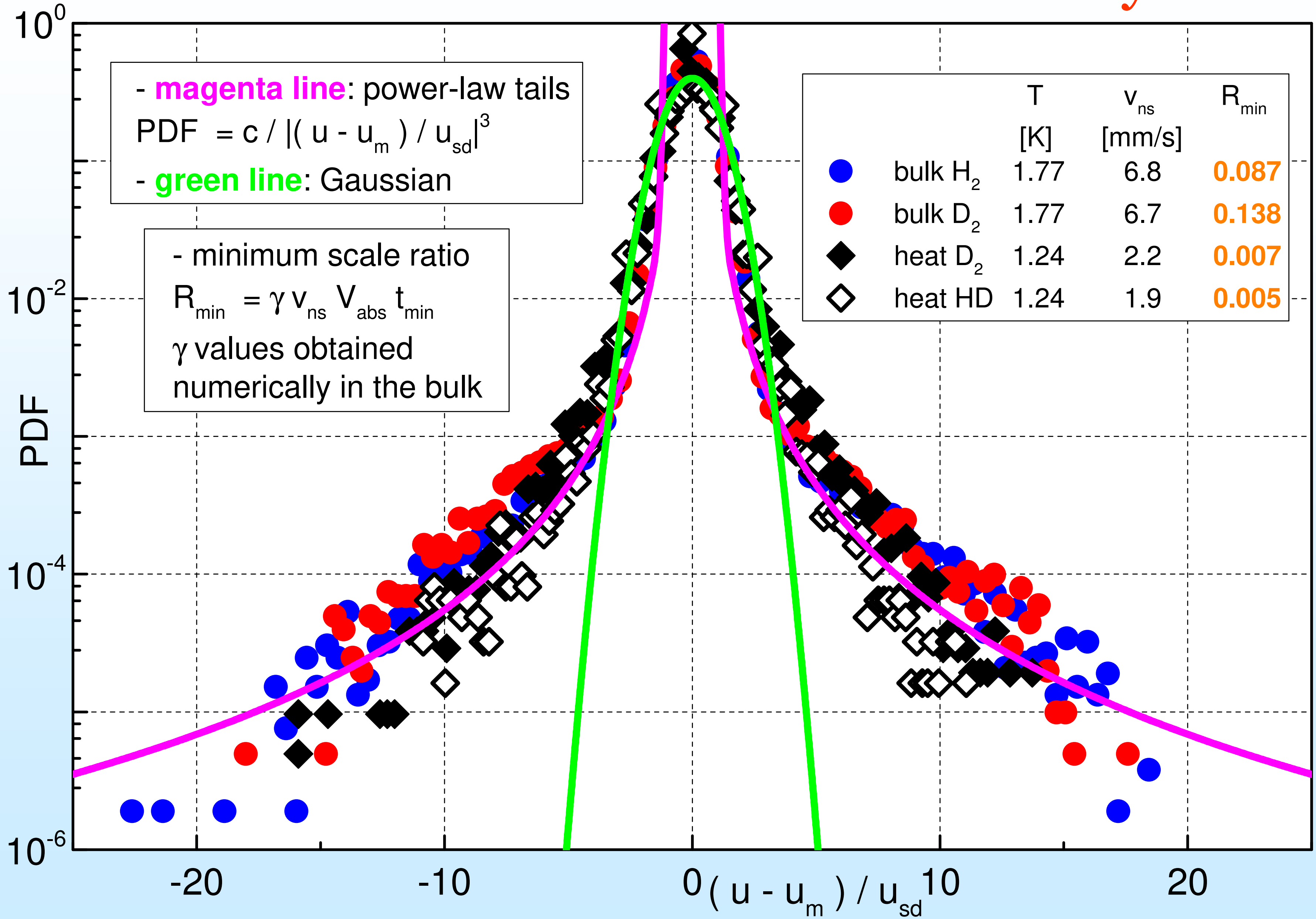

Results: velocity flatness

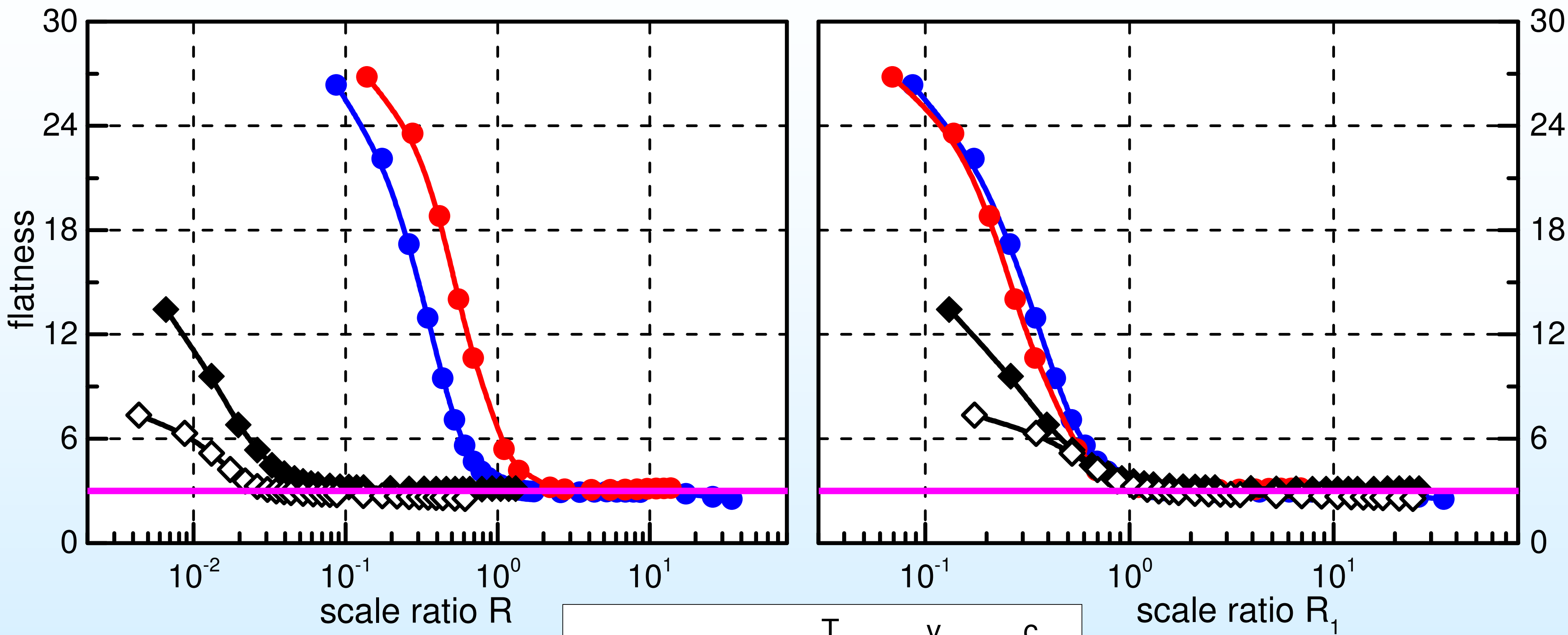

	T [K]	v_{ns} [mm/s]	c
bulk H_2	1.77	6.8	1
bulk D_2	1.77	6.7	0.5
heat D_2	1.24	2.2	20
heat HD	1.24	1.9	40

$$R = \gamma v_{ns} V_{abs} t$$

$$R_1 = c R$$

P Hrubcová, P Švančara, M La Mantia **Phys Rev B** 97, 064512 (2018)
P Švančara, P Hrubcová, M Rotter, M La Mantia **Phys Rev Fluids** 3, 114701 (2018)

He II wall-bounded flows

- The surface roughness may provide pinning and nucleation sites for the vortices, due to their atomic core size

- The tendency of quantum vortices to preferentially concentrate in regions of low fluid velocity, in the boundary proximity, can be related to the classical behaviour of the normal component of He II

- Boundary layers may then exist in He II flows, although their origin seems to be related more to the quantized vortex dynamics than to the fluid viscosity

- The experimental study of wall-bounded flows of He II is still in its infancy

M La Mantia **Phys Fluids** 29, 065102 (2017)
P Hrubcová, P Švančara, M La Mantia **Phys Rev B** 97, 064512 (2018)
P Švančara, P Hrubcová, M Rotter, M La Mantia **Phys Rev Fluids** 3, 114701 (2018)

Summary: flow visualization

Quantum turbulence, generated in thermally and mechanically driven flows of superfluid ^{4}He, has been probed experimentally, by visualization, at scales straddling about two orders of magnitude across the mean distance between quantized vortices, the flow characteristic scale.

• Quantum signature is apparent from the particle velocity (and velocity increment) distributions, at scales smaller than the flow quantum scale.

• Classical (viscous-like) signature is found from the particle velocity (and velocity increment) distributions, at scales larger than the flow quantum scale.

Summary: open problems

• Large-scale quantum features
Eulerian structure functions, intermittency
(visualization with excimer molecules)

• Study of He II wall-bounded flows is in its infancy
entrance length, fluid velocity profile, role of flow geometry

• Energy transport mechanisms
both below and above the mean distance between quantized vortices, i.e., dynamics of vortex reconnections and of large-scale vortical structures, respectively

Large-scale turbulent vortex ring

The movie shows micrometer-size solid deuterium particles at about 1.75 K; 25 mm wide and 22 mm high field of view; movie taken at 2000 fps, shown here at 200 fps; ring generated with a heat pulse of ca. 800 W/m².

Helium II

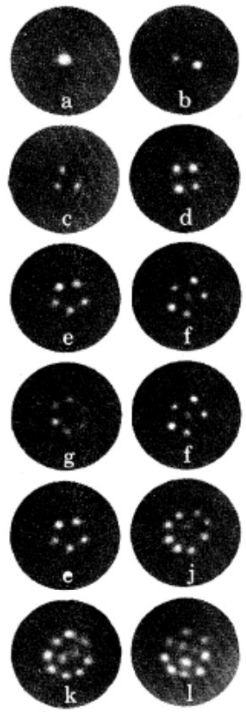

FIG. 2. Photographs of stable vortex arrays. Each photograph is a multiple exposure of 60 consecutive motion-picture frames. The length scale on the photographs is known to an accuracy of approximately 2%. The diameter of the dark circles corresponds to the 2-mm bucket diameter. The arrays were placed symmetrically within the circles. The actual location of the bucket relative to the arrays is not known. The angular volocities were (a) 0.30 sec^{-1}, (b) 0.30 sec^{-1}, (c) 0.40 sec^{-1}, (d) 0.37 sec^{-1}, (e) 0.45 sec^{-1}, (f) 0.47 sec^{-1}, (g) 0.47 sec^{-1}, (h) 0.45 sec^{-1}, (i) 0.86 sec^{-1}, (j) 0.55 sec^{-1}, (k) 0.58 sec^{-1}, and (l) 0.59 sec^{-1}. The two distinct configurations of six vortices appeared alternately at constant angular velocity.

Quantized vortices

Mutual friction force

Interaction of quantum vortex lines with the normal fluid component

$$\boxed{B\frac{\rho_n\rho_s}{\rho}\hat{\Omega}\times\left[\bar{\Omega}\times\left(\bar{v}_s-\bar{v}_n\right)\right]+B'\frac{\rho_n\rho_s}{\rho}\bar{\Omega}\times\left(\bar{v}_s-\bar{v}_n\right)}$$

Uniformly rotating bucket of He II

Vortices aligned with the rotation axis

Vortex lattice carries the flow vorticity

Feynman's rule

$$\boxed{n_0=\frac{curl\left(v_s\right)}{\kappa}=\frac{2\Omega}{\kappa}\approx 2000\Omega\ \frac{\text{lines}}{\text{cm}^2}}$$

EJ Yarmchuk, MJV Gordon, RE Packard **Phys Rev Lett** 43, 214 (1979)

Quantized vortices

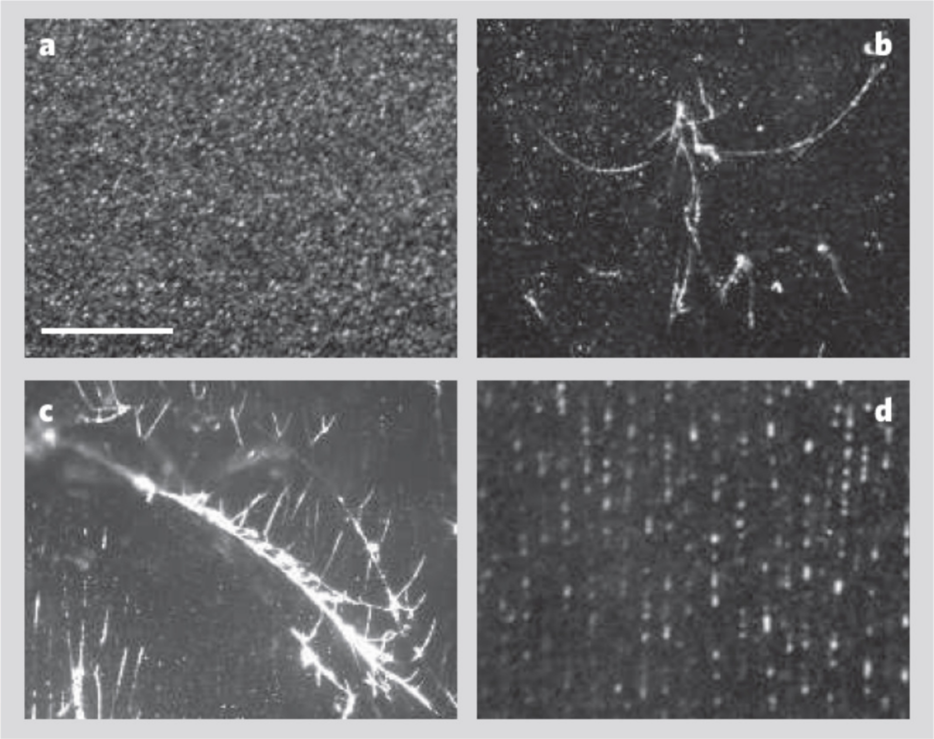

Figure 1 | Quantized vortex cores in liquid helium. a–d, Images of particles (light against dark background) obtained with a camera and 105-mm lens under different conditions: **a,** just above the transition temperature, when they are uniformly dispersed; **b, c,** on branching filaments at tens of millikelvin below the transition temperature; and **d,** regrouping along vertical lines for steady rotation about the vertical axis. In **b** and **c**, the particles on lines are evenly separated in small regions. Scale bar, 1 mm.

GP Bewley, DP Lathrop, KR Sreenivasan **Nature** 441, 588 (2006)